Theoretical Studies on the Properties and Dynamics of Electronic Excited States

by

Diptarka Hait

Submitted to the Department of Chemistry
in partial fulfillment of the requirements for the degree of

Bachelor of Science in Chemistry

at the

MASSACHUSETTS INSTITUTE OF TECHNOLOGY

June 2016

Author ..... Signature redacted .....
Department of Chemistry
May 6, 2016

Certified and Accepted by ..... Signature redacted
Troy Van Voorhis
Haslam and Dewey Professor of Chemistry
Thesis Supervisor
Undergraduate Officer, Department of Chemistry

Theoretical Studies on the Properties and Dynamics of Electronic Excited States

by

Diptarka Hait

Submitted to the Department of Chemistry
on May 6, 2016, in partial fulfillment of the
requirements for the degree of
Bachelor of Science in Chemistry

Abstract

Molecules are rarely found in electronic excited states under standard conditions but such states play a major role in chemical reactions. Computational prediction of properties of such states is hard with standard DFT protocols, as made evident by the failure of linear response TDDFT in predicting energies of charge-transfer excited states with semi-local functionals. Condensed phase dynamics of excited states are even more intractable on account of the computational cost scaling exponentially with the number of condensed phase particles under consideration. However, it is still possible to develop cheap but accurate approximations for properties and dynamics of excited states, and herein we describe some of the methods developed by us along those directions. We first demonstrate that restricted open shell Kohn-Sham (ROKS) calculations with semi-local hybrid functionals give good agreement with experimental absorption energies, emission energies, zero-zero transition energies and singlet-triplet gaps of CT states–unlike TDDFT, which significantly underestimates energy gaps. We then show that is possible to compute the effects of conical intersections on non-adiabatic dynamics of chemical systems by deriving perturbative memory kernels for the linear vibronic coupling model, and employing them to calculate the population dynamics of the Fe(II)-Fe(III) self-exchange reaction. Finally, we present a relationship between perturbation theory traces of the spin-boson model that allows us to obtain the exact solution with arbitrary initial harmonic bath state in the slow bath limit. We then attempt to generalize it to multiple states, and devise a similar trace relationship which makes it trivial to write down closed form expressions for populations and kernels to arbitrary order for any n level system.

Thesis Supervisor: Troy Van Voorhis
Title: Haslam and Dewey Professor of Chemistry

Acknowledgments

I have been fortunate enough to come into contact with an astoundingly large number of wonderful people throughout my time here at MIT, and this thesis is in many ways the culmination of their influence on me. Some of course have made a more direct impact than others, but probably none more so than Troy Van Voorhis, the best research advisor and teacher I could have ever hoped for. Troy has been a constant feature at all points of my MIT trajectory, with his insightful observations and bright smile never failing to give me hope no matter how much I was struggling with research or life outside of it. My transformation from a nervous, directionless freshman to a much more confident almost-graduate student owes a great deal to his mentorship, and I shall remain eternally grateful for that alone. It was an incredible privilege to work with him for the past three years, and I will be quite sad to move on elsewhere for graduate school, not the least because I have been spoilt by this wonderful experience.

I am also extremely grateful to Bob Field for introducing me to Quantum Mechanics, being a fantastic academic advisor and for giving me the confidence to do physical chemistry research back when I did not trust my own ability to do so. His mentorship has made me a much better scientist than I was coming into MIT, and I shall miss our spontaneous conversations a great deal.

I would like to thank Heather Kulik and Adam Willard for helpful discussions about science and graduate school which helped me converge on my future path. I am also grateful to Barton Zwiebach, Aram Harrow, Jeremy England, Tom Greytak, Moungi Bawendi, Keith Nelson and Patrick Lee for teaching me Chemical Physics.

I greatly enjoyed working with my co-workers in the Van Voorhis group: Tianyu Zhu and Dave McMahon for the OLED work, and Mike Mavros for quantum dynamics. Their presence made my life quite a bit brighter, and I benefited a great deal from their advice and figure making skills! I am also grateful for the enormous amount of help regarding thesis preparation that I got from Valerie Vaissier. In addition, I profited immensely from the advice and support I obtained from other fellow theorists over the years, namely Matt Welborn, Nathan Ricke, Helena Qi, Alex Kohn,

Zhou Lin, Nadav Geva, Hongzhou Ye, Kaitlyn Dwelle, James Shepard, Piotr de Silva, Evan Piephoff, Eric Alt, Chee-Kong Lee, Sucheol Shin and Liza Lee. Being in their presence offered me a valuable insight into the life of theoretical chemistry researchers that I could not have obtained elsewhere. In a similar vein, I would also like to thank Trevor Erickson, Brian Michael, Katie Shulenberger, Dan Banks, Sam Kazer, Sophie Bertram, Jay Prakadan, Frank Gao, Marty Gelenter, Dmitro Martynowych, Nicole Moody, Cole Perkinson, Timothy Sinclair, Jason Yoo and Crystal Chen for a first hand insight into graduate student life.

My non-pchem friends have provided me with a wonderfully stable support network over the years that has prevented me from drowning in work. In particular I would like to thank Lily Chen: my long suffering draft editor and best friend extraordinaire. We have had our fair share of disagreements about Game of Thrones, but I don't think my college experience would have been as enjoyable without her unquestioning support and interesting sense of humor. I also want to thank James Deng, my other editor-in-chief, Full Metal Alchemist watching partner and the only person willing to drag me out of work for a breath of fresh air. Scientific discussions with Tomo Soejima, Lane Gunderman, Harry Zhou and Yihui Quek proved to be fruitful throughout my time here, and often resulted in interesting ideas. I also extremely enjoyed hanging out with Ana Meek, Wai Lok Lai, Richard Chang, John Read, Ethan Klein, Aofei Liu, Natalie Burgos, Botong Ma, Yoa Clifton, Oom Pattarabanjird, Chris Hillenbrand and Songela Chen, and I will immensely miss all of them.

I was supported by the MIT UROP office for the majority of my time as a researcher. The OLED portion was entirely funded by Samsung (Grant No. 692030) and the quantum dynamics section by NSF (Grant No. CHE-1058219). I am deeply grateful to all three organizations for supporting my research.

Lastly I would like to thank my parents for always being willing to make sacrifices to ensure that I got the best educational opportunities, and for always providing a willing ear when I needed one.

Contents

List of Figures

List of Tables

Chapter 1

Introduction

> *The underlying physical laws necessary for the mathematical theory of a large part of physics and the whole of chemistry are thus completely known, and the difficulty is only that the exact application of these laws leads to equations much too complicated to be soluble. It therefore becomes desirable that approximate practical methods of applying quantum mechanics should be developed, which can lead to an explanation of the main features of complex atomic systems without too much computation.*
>
> Paul Dirac, 6th April 1929[6].

Almost a century has passed since Dirac's observation that the advances in quantum mechanics had in principle reduced chemistry to an applied mathematics problem, with no new experimental evidence been found to the contrary in the intervening years. Yet the majority of chemistry has not yet been "solved" numerically and theory did not really play a major role in advancing the science for most of the last century, which is a somewhat curious state of affairs for an exactly "solved" problem. Dirac had correctly noted that the problem was the "exactness" itself, as the exact methods for solving many-body problems in quantum mechanics were far too expensive for realistic chemical systems on account of the large numbers of electrons and nuclei present. The computational cost for such methods typically scaled exponentially with the number of particles involved[7], making them intractable for all but the smallest

of molecules even with modern computers.

Therefore, approximations remain the only way forward for doing quantum chemistry, as Dirac had correctly observed. Yet there is also very good reason to be cautious of approximations when it comes to applications in chemistry. Chemical bonds typically have strengths of the order of 1 eV$\approx 10^{-2}$ hartree and thermal energy at room temperature is around 10^{-3} hartree, while system energies are often easily 10^2 hartrees or greater in magnitude, indicating that a very high level of accuracy is needed in order to have qualitatively accurate methods, to say nothing of quantitative accuracy. Such approximations were unfeasible for all but the smallest of systems (with at most ten light atoms) prior to the wide availability of computing power from the 1980s and even molecular orbital theory (or as quantum chemists call it, Hartee-Fock[8]) was simultaneously both too expensive and too inaccurate for most purposes. Semi-empirical methods therefore tended to be much more useful than *ab-initio* approaches for most systems of chemical interest for the majority of the last century.

The arrival of the computing age and the advances made by Kohn-Sham Density Functional Theory (DFT) [9, 10] has led to a significant shift in the situation, as had the widespread availability of "black-box" quantum chemistry programs. DFT in fact is extremely accurate for closed shell organic molecules in their electronic ground-state, and it is rarely necessary to apply more accurate techniques that have a computational cost exceeding the $O(N^4)$ scaling of DFT (where N is the number of electrons). It is now in fact possible for even non-specialists to run DFT calculations for moderately sized systems, leading to widespread use of theoretical methods to augment experimental discoveries[2–4].

Excited states however offer pose a larger challenge for conventional black box DFT approaches like Linear Response Time Dependent Density Functional Theory (LR-TDDFT). LR-TDDFT has classically been employed to study excited states on account of it being formally exact, courtesy the Runge-Gross theorem[11]. However, it fails to treat charge-transfer properly with widely used semi-local functionals[12–14] like B3LYP or PBE0 on account of incorrect description of long-range exchange inter-

actions. Such issues were seldom a problem for ground state calculations with mostly localized electrons, but prove to be a major challenge for studying excited states, especially as systems of interest to experimentalists like organic photovoltaics and LEDs involve charge-transfer states. This issue however may be alleviated by non-linear response approaches like ΔSCF[15] and Restricted Open-Shell Kohn Sham(ROKS)[16], which can treat excited states at the cheap mean-field level but can still recover correct behavior of charge transfer states. We in fact have demonstrated this point in the next chapter, where we show that ROKS can calculate properties of candidate materials for OLED use, while conventional semi-local LR-TDDFT fails due to CT character of excited states.

Dynamics between electronic excited states however pose a much larger challenge, especially in condensed phases where there are too many atoms for *ab-initio* atomistic approaches, whether mean-field or not. This is problematic because nearly all chemical reactions involve some role of electronic excited states, making it important to have theoretical methods that can predict the properties and dynamics of such states in order to gain a better understanding of how reactions proceed at the molecular level. We thus attempt to sidestep the need for atomistic dynamics calculations by mapping chemical systems into approximate model Hamiltonians like the spin-boson model[17] and related systems, and then obtain exact chemical dynamics for such model systems. Certain physical properties of the real chemical system are lost in the mapping to the simple model, but the effectiveness of methods like Marcus theory[18] demonstrate that this is an approximation worth making in order to incorporate effects of the condensed phase. Thus in chapter 3, we attempt to develop methods for studying condensed phase dynamics between electronic excited states using this approach, and attempt to apply this formalism to study other processes like electron transfer. In particular, we are greatly interested in systems with non-adiabatic surface crossings[19] and strong coupling between electronic states, and we demonstrate that we have developed methods capable of accurately modeling the dynamics for such systems under certain limits.

We have thus been able to demonstrate the efficacy of a suite of cheap approxima-

tions that can be employed to calculate both the stationary properties and dynamics of excited states. In future, we plan to build on these methods in order to develop more generalized accurate variants with similar cost, that can be employed to theoretically study interesting chemical systems and processes involving excited states. These should help development of new materials by providing a computational screen that would enable experimentalists to determine whether candidate molecules are likely to fulfill targeted roles, and thus eliminate waste that would have otherwise been resulted from synthesis and experimental testing of properties for hopeless structures. Our ultimate hope is that our methods will not only contribute to a quantitative understanding of chemical processes in the atomic scale, but also lead to a more efficient approach to chemistry where computation can be employed to assist chemical intuition in designing new materials with interesting properties that can be used to solve the myriad problems our species faces.

Chapter 2

Energies of Charge Transfer Excited States from Mean Field Approaches

2.1 Introduction

Extensively π conjugated organic molecules with distinct charge donor and acceptor subunits are known to exhibit interesting optoelectronic[20, 21] properties on account of the high charge-transfer (CT) behavior of their first few excited electronic states, and thus can be used in fields like non-linear optics[22], organic photovoltaics[23] or organic field-effect transistors[24]. The spatial separation of the transferred electron (effectively in the ground state LUMO localized on the acceptor) and the resulting hole (effectively in the ground state HOMO localized on the donor) also minimizes the exchange interaction between the two singly occupied orbitals in excited CT states, resulting in a reduced energy gap between singlet and triplet states[25–30]. This permits such molecules to exhibit Thermally Activated Delayed Fluorescence (TADF)[31, 32] where the "dark" first excited triplet (T_1) state indirectly fluoresces back into the singlet ground (S_0) state via thermally activated reverse intersystem crossing to the "bright" first excited singlet (S_1) state (as depicted in Fig 2-1). Molecules exhibiting TADF are considered to be useful for OLED applications, as they can significantly increase energy efficiency by harvesting some of the energy that is normally wasted in generating non-radiative triplet excitons[33–37].

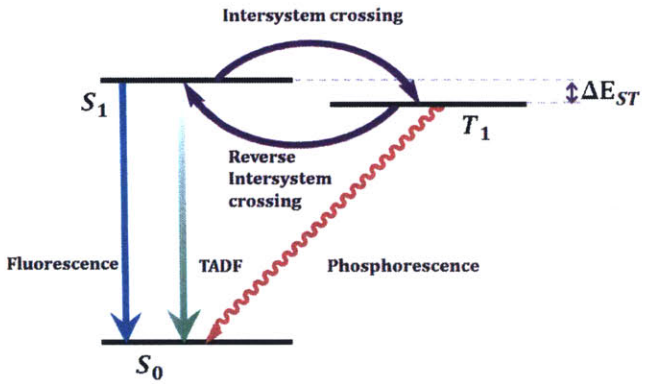

Figure 2-1: Simplified Jablonski diagram for TADF molecules. Phosphorescence is spin forbidden and hence much slower than fluorescence, but reverse intersystem crossing is permitted as ΔE_{ST} is small. This allows $T_1 \rightarrow S_1$ transition, permitting indirect fluorescence of T_1.

TADF is however only possible at appreciable rates if the energy gap (ΔE_{ST}) between the S_1 and T_1 states is smaller than or comparable to $k_B T$. OLED applications also frequently require emitted radiation of a particular color, thereby constraining suitable values of emission energy (E_{emit}) to a narrow interval. It is therefore useful to have computational protocols for prediction of photophysical properties like $E_{\mathrm{emit}}, \Delta E_{ST}$, quantum yields etc., of molecules with CT excited states[38, 39], as it allows screening of molecules for use in TADF based OLEDs. Unfortunately, many of the molecules of interest are too large (>100 atoms) to be studied with high-level *ab-initio* wavefunction based methods like CASPT2[40, 41] or coupled-cluster[8], which are known to give quite accurate results for small organic molecules[42, 43]. As a result, Density Functional Theory (DFT)[9, 10, 44] based approaches are the only viable post Hartree-Fock[8] computational tools for studying such molecules.

Consequently, a large amount of effort has gone into developing DFT based protocols for estimation of photophysical properties of potential OLED molecules. One of the earliest protocols was devised by Adachi and coworkers[28, 35], who attempted to obtain estimates for ΔE_{ST} from the difference between S_1 and T_1 energies obtained at S_0 optimized geometries with Linear Response Time-Dependent Density Functional Theory (LR-TDDFT)[11, 45], employing semi-local hybrid functionals like B3LYP[46] or PBE0[47]. This approach however, was only effective for molecules with relatively

low CT character[3, 35], as semi-local LR-TDDFT systematically underestimates the energy of CT states in general[12–14, 48]. A later method proposed by Adachi and coworkers[1] tried to determine the ideal TDDFT functional for each structure by empirically calculating an "optimal" percentage of exact-exchange from ground-state calculations that estimated the extent of CT. Any semi-local hybrid functional employing close to the calculated exact-exchange percentage was postulated to be effective for TDDFT studies.

An alternative approach would be to use range-separated hybrid functionals[49, 50] that were developed for the purpose of performing TDDFT on CT states. This was also tested by Adachi and coworkers[1], who however reported that range-separated functionals like CAM-B3LYP[51] or LC-ωPBE[52] tended to overestimate absorption energies (E_{abs}) for common TADF molecules, indicating that the range separation parameters for such molecules were not optimal for the length-scale of charge transfer in such systems. This was not particularly surprising, as such parameters are often strongly system dependent[53, 54], although it is possible to "tune" them for individual systems[55]. Recently, Penfold[29] and Brédas et al. [30] independently used tuned range separated functionals to investigate TADF molecules, and discovered that such an approach gave ΔE_{ST} values that are fairly consistent with experimental data.

There also exist time-independent excited state DFT techniques like ΔSCF[15], which offer alternate routes for studying CT excited states. Such methods generally do not rely on linear response theory and can therefore be expected to not share the deficiencies of semi-local LR-TDDFT with regards to CT states. In particular, it is possible to use a Restricted Open Shell Kohn-Sham (ROKS) [16, 56–58] approach to obtain energies of the S_1 state, which offers a new way to estimate emission wavelengths. Additionally, the Hohenberg-Kohn theorem[9] indicates that ground-state spin density functional theory (SDFT) should be able to estimate the energy of the first excited triplet (T_1) state, as it is the ground-state within the subspace of all triplet electronic states. This indicates that a combination of ROKS and SDFT could also be employed to calculate ΔE_{ST}, thereby implying that such a combination could

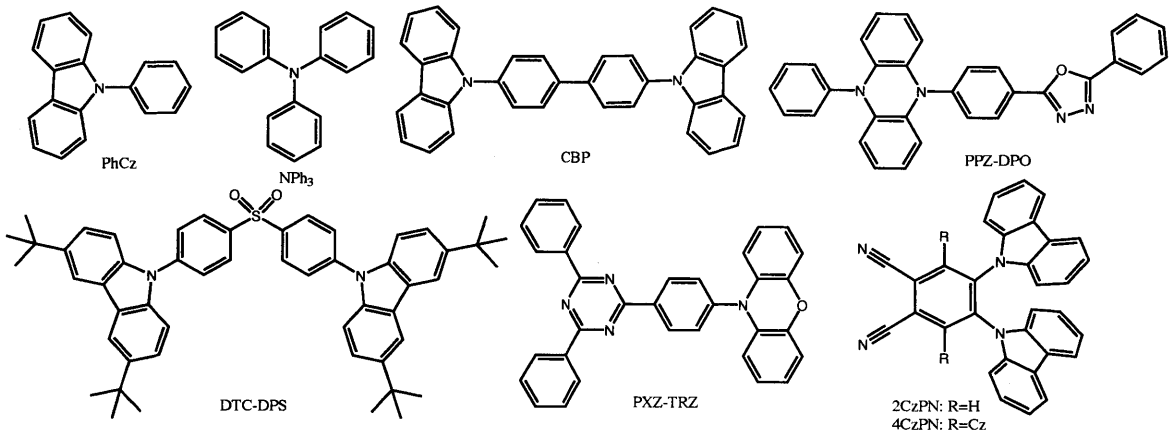

Figure 2-2: Representative members of the test-set. Experimental data obtained from Adachi et al.[1–4]. Structures of all the molecules in the test-set can be found in the SI.

be useful as a fast and reliable computational screen for potential TADF molecules.

In this chapter, we address these questions by devising two computational protocols that use a combination of ROKS and SDFT to estimate photophysical properties like E_{abs}, E_{emit}, E_{0-0} (as described in the central panel in Fig.2-3) and ΔE_{ST}. Consequently, these protocols were compared with two TDDFT derived protocols against a test-set of 27 TADF compounds (Fig.2-2) with available experimental data[1–4]. This revealed that while it was possible to use cancellation of errors to obtain some useful results from TDDFT, such approaches in general do not lead to accurate estimations of all desired parameters. On the other hand, semi-local hybrid functional based ROKS/SDFT based approaches led to very accurate predictions of E_{emit}, ΔE_{ST} etc., without having to resort to cancellation of errors or parameter optimization. Overall, it appears that ROKS with semi-local hybrid functionals provides a reliable and fast alternative to estimating properties of CT states, and can thus be used as a screen for potential TADF molecules.

2.2 Computational Details

All the calculations were done with the Q-Chem 4.2 Package[59], employing the PBE[60],B3LYP[46], PBE0[47] and LC-ωPBE[52] (with $\omega = 0.3$ bohr^{-1}) function-

als. Most calculations employed the 6-31G* basis[61] set, although some B3LYP calculations were repeated with the larger cc-pVTZ[62] basis to investigate the basis set dependence of the paratmeters measured. The Tamm-Dancoff approximation (TDA)[63–65] was not invoked in TDDFT calculations. Solvent effects were not taken into consideration in this study, nor was the effect of zero-point energy of molecular vibrations taken into account.

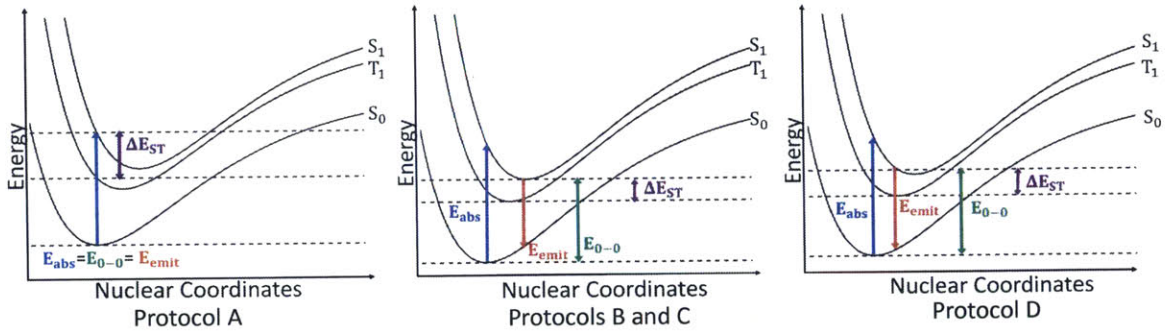

Figure 2-3: Photophysical parameters measured by the Protocols. The arrows only indicate energy gaps, and not nuclear coordinates of transitions.

The protocols themselves were as follows:

1. **Protocol A**: S_0 geometry is optimized using ground-state DFT, and TDDFT is then employed to find the energies of the S_1 and T_1 states at this geometry. The resulting vertical absorption energy E_{abs} is then assumed to be a reasonable estimate for both E_{emit} and E_{0-0} (Fig.2-3, left panel). ΔE_{ST} is assumed to be the difference between S_1 and T_1 energies at the equilibrium S_0 geometry. This is the computationally cheapest of all the protocols, as it involves only one ground-state geometry optimization. However, it compromises the physics as real TADF molecules have non-zero experimental Stokes shifts, and is not at all likely to be effective when the exact functional is employed.

2. **Protocol B**: S_0 geometry is optimized using ground-state DFT, while both S_1 and T_1 geometries are optimized by TDDFT. TDDFT is then employed to find E_{abs} and E_{emit} as the vertical transition energy between the S_0 and S_1 surfaces, starting from the equilibrium S_0 and S_1 geometries respectively. E_{0-0} is obtained from the difference in the equilibrium S_1 and S_0 energies (found by TDDFT and ground-state DFT respectively) and ΔE_{ST} is given by the

difference between equilibrium S_1 and T_1 energies (found by TDDFT). Unlike Protocol A, this Protocol does not compromise the physics, as the calculated parameters correspond exactly with experimentally measured ones.

3. **Protocol C**: S_0 geometry is optimized by ground state DFT while the T_1 geometry is optimized with Restricted Open-Shell DFT (RO-DFT). The equilibrium S_1 geometry is obtained via ROKS. The energy differences are then found in the same manner as Protocol B, except that ROKS and RO-DFT are used instead of TDDFT to calculate S_1 and T_1 energies respectively. RO-DFT is preferred over unrestricted open-shell DFT for accessing T_1 energies in order to avoid systematic errors in ΔE_{ST}, as discussed in the results section. Like Protocol B, the parameters calculated with this Protocol also correspond exactly to experimentally measured ones.

4. **Protocol D**: S_0 geometry is optimized by ground state DFT while the T_1 geometry is optimized with RO-DFT. It was assumed that the equilibrium S_1 geometry is fairly well approximated by the T_1 geometry (which is definitely the case for molecules with large CT character where ΔE_{ST} is small), and the energy differences were then found in the same manner as Protocol C. Overall, only two geometry optimizations (both of which were formally in the ground-state) were employed, making this significantly cheaper than Protocol C.

The accuracy of the different protocols were compared by applying them to a set of relevant TADF chromophores, some of which are shown in Fig. 2-2. The experimental results were collected from work by from Adachi et al.[1–4] A complete listing of the molecules in the set and the associated experimental absorption and emission energies and singlet-triplet gaps is provided in the supporting information.

2.3 Results and discussion

The errors associated with Protocols A & B are given in Table 1, while the errors for Protocol C & D can be found in Table 2. Because of the wide spectrum of

Parameter Measured	PBE RMSE (ME)	B3LYP RMSE (ME)	PBE0 RMSE (ME)	LC-ωPBE RMSE (ME)
E_{abs} (Protocols A and B)	1.38 (−1.31)	0.57 (−0.45)	0.43 (−0.28)	0.74 (0.72)
E_{em} (Protocol A)	0.81 (−0.75)	0.25 (0.11)	0.35 (0.28)	1.29 (1.28)
E_{em} (Protocol B)	1.48 (−1.45)	0.65 (−0.62)	0.49 (−0.44)	0.66 (0.63)
$E_{\text{0-0}}$(Protocol A)	1.00 (−0.95)	0.26 (−0.10)	0.23 (0.07)	1.04 (1.03)
$E_{\text{0-0}}$(Protocol B)	1.30 (−1.25)	0.52 (−0.46)	0.37 (−0.28)	0.82 (0.81)
$\log(\Delta E_{\text{ST}})$ (Protocol A)	0.92 (−0.74)	0.68 (−0.37)	0.45 (−0.09)	0.76 (0.71)
$\log(\Delta E_{\text{ST}})$ (Protocol B)	1.45 (−1.34)	1.04 (−0.85)	0.85 (−0.60)	0.74 (0.69)

Table 2.1: Errors associated with Energy estimates from TDDFT derived protocols (RMSE= Root Mean Squared Error, ME= Mean Error). Errors in $E_{\text{abs}}, E_{\text{emit}}$ and $E_{\text{0-0}}$ have unit eV. Both protocols calculate absorption energy in the same manner, and thus have same errors associated with that parameter.

values for the experimental ΔE_{ST} associated with the test-set, we report the errors in $\log(\Delta E_{\text{ST}})$ instead of errors in ΔE_{ST}.

2.3.1 TDDFT Results: Protocols A & B

Protocol A fares quite badly in estimating E_{abs}, with all the functionals. This is unsurprising for semi-local PBE, B3LYP and PBE0 calculations in light of the large CT nature of the S_1 state[12–14, 48]–which leads to systematic underestimation of S_1 energy. Even the long-range corrected LC-ωPBE is not successful in estimating E_{abs}, although it systematically overestimates energy unlike the other three. This behavior indicates the length-scale of charge-transfer for the test-set molecules is smaller than $\frac{1}{\omega}$ and is consistent with what was reported earlier by Adachi et al.[1] However, the spurious TDDFT red-shift of energies in the B3LYP and PBE0 calculations were comparable to the Stokes shift for many of the molecules, resulting in a cancellation of errors that permitted $E_{\text{abs}}^{\text{TDDFT}}$ to be a fairly accurate estimate of $E_{\text{0-0}}^{\text{Expt}}$. With B3LYP, it was also possible to get reasonable estimates of $E_{\text{emit}}^{\text{Expt}}$ by using $E_{\text{abs}}^{\text{TDDFT}}$, although PBE0 significantly overestimated this parameter (possibly on account of using a greater percentage of exact-exchange than B3LYP). The energy-shifts for PBE were too large for a similar cancellation of errors to occur there and LC-ωPBE overestimated energies, making such a cancellation impossible.

This cancellation of errors however is not applicable to the ΔE_{ST} estimates, and Protocol A does not perform particularly well on that front. PBE and B3LYP both have large systematic errors as TDDFT artificially increases the extent of CT in the S_1 and T_1 states in a bid to lower their energies. This spuriously increased CT character leads to a smaller than expected energy gap, causing underestimation of ΔE_{ST}. PBE0 however has a smaller systematic error in ΔE_{ST}, possibly on account of the larger proportion of exact-exchange being employed in the functional (a trend that can also been seen in the decreased errors on going from PBE to B3LYP). LC-ωPBE on the other hand, significantly overestimates ΔE_{ST}, which is consistent with the CT length-scale being smaller than $\frac{1}{\omega}$. Consequently, single-functional Protocol A calculations cannot generally be used to get accurate ideas about ΔE_{ST} and E_{emit} simultaneously. The former is predicted best with PBE0 and the latter by B3LYP. However, Protocol A does not require excited-state geometry optimizations and is thus attractive as a preliminary screen for OLED materials, even if two calculations with different functionals are required.

Protocol B has no cancellation of errors to fall back upon, and thus consistently underestimates E_{emit} and E_{0-0} with PBE, B3LYP and PBE0. The ΔE_{ST} estimates are also considerably underestimated (by nearly an order of magnitude), and are in fact much worse than Protocol A estimates. This is a consequence of TDDFT further enhancing the CT character of S_1/T_1 states by distorting the equilibrium geometry in an attempt to spuriously lower the energy. LC-ωPBE again overestimates parameters significantly, for the same reason as earlier. Despite Protocol B being the most computationally expensive of the protocols tested (as it requires three geometry optimizations, two of which were in the excited state), it proves to be the least effective in predicting energies. This behavior is consistent with earlier studies[1], and only serves to reinforce the notion that TDDFT with traditional functionals is unsuitable for predicting energies of CT states.

Parameter Measured	PBE RMSE (ME)	B3LYP RMSE (ME)	PBE0 RMSE (ME)	LC-ωPBE RMSE (ME)
E_{abs} (Protocols C and D)	0.69 (−0.64)	0.18 (−0.06)	0.28 (0.11)	0.82 (0.75)
E_{em} (Protocol C)	0.53 (−0.49)	0.19 (0.00)	0.20 (0.10)	0.79 (0.45)
E_{em} (Protocol D)	0.52 (−0.48)	0.22 (0.02)	0.23 (0.11)	0.85 (0.79)
$E_{0\text{-}0}$(Protocol C)	0.56 (−0.54)	0.14 (0.02)	0.17 (0.11)	0.70 (0.66)
$E_{0\text{-}0}$(Protocol D)	0.55 (−0.52)	0.23 (0.10)	0.27 (0.19)	1.09 (1.03)
$\log(\Delta E_{ST})$ (Protocol C)	0.73 (−0.55)	0.35 (−0.20)	0.27 (−0.07)	0.58 (−0.06)
$\log(\Delta E_{ST})$ (Protocol D)	0.49 (−0.34)	0.35 (−0.03)	0.32 (0.04)	0.64 (0.25)

Table 2.2: Errors associated with Energy estimates from ROKS derived protocols (ME= Mean Error, RMSE= Root Mean Squared Error). Errors in E_{abs}, E_{emit} and $E_{0\text{-}0}$ have unit eV. Both protocols calculate absorption energy in the same manner, and thus have same errors associated with that parameter.

2.3.2 ROKS Results: Protocols C & D

Protocols C and D attempt to circumvent the red-shifting of energies by using ROKS and Restricted Open-Shell DFT (RO-DFT) instead of TDDFT to access the S_1 and T_1 surfaces. While it is possible to use Unrestricted Open-Shell DFT (UO-DFT) to access T_1 energies instead, we chose to use RO-DFT as ROKS is a restricted method, and thus using UO-DFT triplet energies could lead to a systematic error in ΔE_{ST} from the extra stabilization recovered by the unrestricted calculation. Nonetheless, we compared UO-DFT and RO-DFT calculation results for the case of the B3LYP functional and found that the numbers are not significantly different (the UO-DFT numbers are given in SI), further suggesting that performing RO-DFT was sufficient.

Though Protocol C is not a particularly cheap protocol (it requires three geometry optimizations, although only one of them is in the excited state), it gives quite accurate estimates of E_{abs}, E_{emit} and E_{0-0} with B3LYP and PBE0. The near zero mean errors of B3LYP calculations are of particular interest, as they indicate there is no systematic bias unlike Protocol B with B3LYP. Interestingly, PBE0 mean errors are consistently greater than B3LYP errors by approx 0.1 eV, possibly on account of PBE0 blue-shifting the energies more due to greater exact-exchange. PBE still underestimates energies, but the deviation is still much less than Protocol B (by approximately 0.5 eV) or even Protocol A. LC-ωPBE still overestimates energies, and

the deviations here are comparable to the TDDFT deviations, suggesting that these are more a consequence of the functional than the method.

The trends in ΔE_{ST}'s obtained from Protocol C are somewhat more interesting. B3LYP and PBE0 have the smallest RMS errors, which coupled with their relatively small mean errors indicate that these two are best suited for calculating ΔE_{ST} (PBE0 being somewhat better than B3LYP). Like in TDDFT calculations, PBE significantly underestimates ΔE_{ST}, although the errors are smaller. On the other hand, LC-ωPBE has an extremely small mean error along with a fairly large RMS error, indicating that a lot of noise is associated with calculations based on this functional, but not much of a bias–which stands in direct contrast to the large Protocol A and B mean errors. This indicates that the ROKS/RO-DFT combination does not add a systematic bias to ΔE_{ST} for LC-ωPBE calculations, unlike TDDFT–although ΔE_{ST} calculations are still fairly inaccurate because this functional causes a large blue-shift of the S_1 and T_1 energies, which leads to a lot of noise. Overall, Protocol C is found to give very accurate energies with B3LYP and PBE0 and should be the method of choice if sufficient computational resources for S_1 geometry optimization are available. It is also possible to reduce the S_1 optimization cost by using T_1 optimized geometries as the starting guess, as those are expected to be closer to equilibrium S_1 geometry than S_0 geometries or ground-state forcefield fits for TADF molecules.

Protocol D aimed to attain accuracy comparable to Protocol C at a lesser computational cost by approximating the equilibrium S_1 geometry with the equilibrium T_1 geometry. This approach is reasonable for systems exhibiting TADF, as ΔE_{ST} is very small in these cases, indicating that the S_1 and T_1 surfaces are near parallel. Overall, Protocol D E_{emit} estimates are quite close to Protocol C estimates, and thus correspond well to experimental values for B3LYP and PBE0 functionals. PBE calculations also give E_{0-0} similar to Protocol C, although the other three functionals overestimate this parameter relative to Protocol C (although the shift is only of the order of 0.1 eV on average for PBE0 and B3LYP).

This deficiency is somewhat compensated by the lack of apparent systematic bias in ΔE_{ST} calculated with PBE0 and B3LYP. PBE underestimates ΔE_{ST} as in all

previous calculations, while LC-ωPBE overestimates ΔE_{ST} on average–unlike in Protocol C. Overall, all the functionals overestimate ΔE_{ST} with Protocol D, relative to Protocol C as Protocol D slightly overestimates S_1 energy as it is evaluated close to, but not at the minima. However, this slight blue shift of ΔE_{ST} improves the mean accuracy of both PBE0 and B3LYP–and allows Protocol D with these two functionals to be either better than or as effective as Protocol C in estimating E_{emit} and ΔE_{ST}, the two parameters of greatest interest for OLED screening. Protocol D with B3LYP/PBE0 is therefore the method we recommend be used first, with Protocol C only being used for the cases where D predicts large ΔE_{ST} (> 0.5 eV), indicating smaller than expected CT character that causes our assumption about similarities in equilibrium S_1 and T_1 geometries to break down.

2.3.3 Basis Set Effects

Several B3LYP single-point calculations were repeated with the larger cc-pVTZ[62] basis (using the 6-31G*[61] optimized geometries). It was found that neither the calculated parameters nor the associated errors were significantly altered, indicating that calculations with the smaller 6-31G* basis were sufficient.

2.4 Conclusions

In this paper we evaluated four computational protocols for calculating energies associated with CT states, in order to determine a method that gives accurate estimates of parameters like ΔE_{ST} and E_{emit} with minimal computational expense. We tested these protocols with four functionals (PBE, B3LYP, PBE0, LC-ωPBE) against a test-set of 27 compounds and determined TDDFT with all four functionals gave poor results, although fortuitous cancellation of errors can oftentimes give acceptable estimates for E_{emit} (with B3LYP) or ΔE_{ST} (with PBE0). We further discovered that protocols based on ROKS/RO-DFT with B3LYP and PBE0 were well suited for this problem, as they led to quite accurate predictions for TADF molecules, without having to do any form of tuning or fitting. Protocol D in particular seems to be very

well suited for studying molecules with large CT character, as it requires only two ground-state geometry optimizations and yet gives accuracy comparable to methods that rely on computationally expensive excited state optimizations. We believe that other SCF excited state methods like ΔSCF[15] and CDFT[66] will also give similar accuracy to ROKS, and overall such methods are better suited for studying CT states than TDDFT.

Our results however neglected the impact of the surroundings on the photophysics of these TADF molecules, mainly because the effects of the surrounding molecules are difficult to account for. This study only performed calculations on molecules that were experimentally studied in non-polar solvents like cyclohexane ($\epsilon_r = 2.02$[67]) or toluene ($\epsilon_r = 2.38$[67]), in part because the small dielectric constants should have a proportionately small effect on the photophysics. In future it would be interesting to examine how these protocols could be extended to deal accurately with the effects of the surroundings – for example, to tell the difference between the stokes shift in solution versus in a film. We are also currently unable to predict quantum yields from first principles, which is another important parameter to be considered for practical applications. Our future work therefore shall focus on properly accounting for solvent effects on photophysical properties and *ab-initio* quantum yield prediction, in order to enable more efficient design of organic semiconductors involving CT states.

Chapter 3

Dynamics of Excited States

3.1 Introduction

Previously we discussed how mean-field quantum chemistry approaches might be employed to calculate equilibrium properties of electronic excited states. However, such stationary states seldom exist in nature as electronic excited states are rather prone to relaxation back to the ground state or conversion to other excited states. In TADF for instance, we effectively have a five state problem with thermal interconversion between S_1 and the three T_1 states, all of which are also capable of relaxation back to the S_0 state. The overall energy efficiency of the system depends not only on the thermal reverse intersystem crossing rate, but also the relative rates of radiative versus non-radiative pathways for relaxation. Common photochemical processes such as DNA/RNA relaxation[68, 69] also involve excited state relaxation and interconversion mechanisms, and an understanding of these processes is therefore essential for studying photochemistry. The same formalism can also easily be generalized to study dynamics of electron-transfer processes like photosynthesis, with the reaction itself essentially being interconversion between the electronic state of the reactants and the electronic state of the products. It is also important to note that a kinetic understanding is not sufficient in many of these cases due to the short time-scales involved, as quantum oscillations often play a much larger role than the exponential decay predicted by kinetic models in that limit. Kinetics parameters may also be

calculated from a dynamical model, but the reverse is not possible, indicating that the more general dynamical model ought to be preferable. The dynamics of electronic excited states are thus of interest to us, and it would therefore be immensely useful to have protocols for accurate computation of the dynamics of electronic states.

Unfortunately, this is significantly more complex than computing stationary properties as most phenomenon of interest like photochemistry and electron-transfer occur in condensed phases. Previously we avoided incorporating solvent effects in our calculation of stationary properties, as that was supported by experimental evidence[1–4]. However it was observed by Marcus [18, 70, 71] and others [72, 73] that reorganization of the condensed phase was crucial for the dynamics, making it now essential to include the condensed phase in our models. However the condensed phase (roughly) has Avogadro's number of atoms while the cost for building the exact-propagator naively scales exponentially with the number of degrees of freedom under consideration, making a direct numerical solution to the time-dependent Schroedinger equation an impractical idea for any realistic condensed phase system.

Multiple approaches for performing *ab-initio* molecular dynamics have been developed after the pioneering work of Carr and Parinello[74], but such approaches mostly explore dynamics of nuclear degrees of freedom within a particular electronic state, as opposed to computing transitions between different electronic states, which is orthogonal to what we are interested in. Tully's surface hopping algorithm [75] permits transitions between electronic states, but it cannot recover Marcus theory at the outer-sphere electron transfer limit, giving an incorrect scaling with the electronic coupling [76] . This is on account of incorrect decoherence effects stemming from it being a mixed quantum-classical approach, as opposed to a purely quantum one. Overall, it is relatively easy to calculate energy surfaces for electronic states with accurate (or at least formally exact) quantum chemistry methods, as seen in the previous chapter. It is however extremely difficult to do dynamics on these surfaces to an acceptable level of approximation, leading us to choose the alternative approach of mapping chemical systems to approximate model Hamiltonians. The dynamics for such simplified models is much more tractable, and it is in fact possible to obtain

numerically exact populations from this approach. This approach also lends itself easily to non-adiabatic dynamics and allows us to average over all the modes associated with the condensed phase, as opposed to atomistic simulations that preserve extra information about modes needlessly. Admittedly, a large amount of information is also lost while mapping chemical systems to such simplified Hamiltonians but the success of Marcus theory (the simplest example of such a model) leads us to believe that it is a price worth paying.

In this chapter we begin by introducing the spin-boson model[17], which is the simplest possible two-state model Hamiltonian for condensed phase dynamics. Afterwards, we move on to a generalization called the linear vibronic coupling model[77–79], which permits relaxation by means of adiabatic surface crossings called conical intersections[19, 80], a phenomenon not permitted by the spin-boson model. We then describe the approach to obtain linear vibronic coupling model populations perturbatively via analytic closed form expressions (which also automatically gives us spin-boson populations if we neglect coupling fluctuations), and demonstrate how conical intersections alter dynamics. Finally, we return to the spin-boson model and present an exact solution in the slow bath limit, following which we try to generalize this model to multiple states.

3.2 The Spin-Boson Model

The spin-boson model assumes that the bath interacting with the system is purely harmonic and the system-bath coupling is linear in the bath coordinates. Devised in 1983 by Caldeira and Leggett[17], it is described by the Hamiltonian $\mathbf{H}_{SB}$ given by:

$$\mathbf{H}_{SB} = |1\rangle\langle 1| \otimes \mathbf{h_1} + |2\rangle\langle 2| \otimes \mathbf{h_2} + V\left(|1\rangle\langle 2| + |2\rangle\langle 1|\right) \otimes \mathbf{I} \tag{3.1}$$

$$\mathbf{h_1} = -\frac{\epsilon}{2} + \sum_i \left(\frac{p_{x_i}^2}{2m_i} + \frac{1}{2} m_i \omega_i^2 x_i^2 + c_i x_i \right) \tag{3.2}$$

$$\mathbf{h_2} = \frac{\epsilon}{2} + \sum_i \left(\frac{p_{x_i}^2}{2m_i} + \frac{1}{2} m_i \omega_i^2 x_i^2 - c_i x_i \right) \tag{3.3}$$

Here $|1\rangle, |2\rangle$ are the two orthogonal diabatic electronic states with an energy-bias ϵ and diabatic coupling V. $|1\rangle, |2\rangle$ are interacting with a harmonic bath with modes $\{x_i\}$, frequencies $\{\omega_i\}$ and masses $\{m_i\}$. $\{c_i\}$ are coupling constants that determine the strength of interaction between the electronic diabatic states and bath modes $\{x_i\}$. We define $\mathbf{h_{\{1,2\}}}$ to be compact descriptions for the bath hamiltonians associated with the diabatic electronic states $|1\rangle |2\rangle$. An useful way to think about $\mathbf{h_{\{1,2\}}}$ would be to consider them as representations of Marcus Theory parabolas while $|1\rangle, |2\rangle$ are the initial and final electronic states respectively. In fact it can easily be shown that the spin-boson model reduces to Marcus theory under appropriate limits(the proof is given in the Appendices), indicating that this model can be very useful for studying dynamics of electron transfer not only in Marcusian regimes, but also in cases where the assumptions behind Marcus theory break down. The spin-boson model can also be used to study photochemical processes or other chemical transformations that involve transitions between two electronic states, making it an useful starting point for developing quantum dynamics methods.

It might appear that the simple nature of the bath and system-bath coupling would allow this model to be solved relatively easily, but no exact analytic solution has yet been found for this model other than for the trivial case of $\{c_i\} = 0$. The cost for numerical evaluation of the propagator for determining time-evolution scales exponentially with number of bath modes, making it unsuitable for chemical systems where as many as Avogadro's number of modes might be involved.

In fact, the large number of bath modes in chemical systems indicates that is more practical to treat them as a continuum with spectral density $J(\omega)$ defined to be:

$$J(\omega) = \sum_i \frac{\pi c_i^2}{2m_i\omega_i}\delta(\omega - \omega_i) \rightarrow \frac{\pi\left(c(\omega)\right)^2}{2m(\omega)\omega}g(\omega) \tag{3.4}$$

(where $g(\omega)$ is the density of states) than to keep track of each separate mode (especially as our point of interest are the electronic states $|1\rangle, |2\rangle$, not the individual bath modes). It is known that the dynamics of the spin-boson model is completely specified by the energy-bias ϵ, diabatic coupling V and spectral density $J(\omega)$ (this is demon-

strated later, in Eqn. 3.61), although the exact nature of the expression continues to elude us. While essentially exact numeric methods based on hierarchical equations of motion exist for solving the problem for $J(\omega)$ of the Debye form $\frac{\eta\omega\omega_c}{\omega^2+\omega_c^2}$[81, 82], such methods are not readily generalizable to the more arbitrary $J(\omega)$ found in chemical systems.

Consequently, perturbative approaches represent the best way forward for this and related models. Classically, the Non-Interacting Blip Approximation (NIBA) [83, 84] has been one of the most widely used methods, but it is has certain limitations, being correct to only second order in V. Recent work[85–87] however indicates that resummation of perturbation theory terms to some small order (fourth, sixth or eighth) is sufficient to give a picture that is often numerically exact, and is at worst "merely" qualitatively accurate. This is the approach we shall persue for the most part, leading us to work on deriving the corresponding perturbation theory terms.

3.3 Linear Vibronic Coupling Model

The spin-boson model is a very good starting point for chemical systems, but it introduces too many simplifying assumptions. It is probably impossible to do due justice to some physical effects like bath anharmonicity with our analytic approach, but it is possible to relax certain other constraints of the model without compromising the effectiveness of our approach for computing dynamics.

In particular, it is not too difficult to abandon the condon approximation which assumes that electronic transitions are instantaneous compared to nuclear motion, leading to constant diabatic coupling V. This is especially important as adiabatic surface crossings are only allowed when $\mathbf{h_1} = \mathbf{h_2}$ and $\hat{V} = 0$ for the same set of bath coordinates, indicating that non-constant $\hat{V}$ is needed to have conical intersections in the model. Conical intersections are not only responsible for isomerization of DNA/RNA bases[68, 69] and rhodopsin the retina[88, 89], but they also play an important role in internal conversion and intersystem crossing[90], and thus are important for determining quantum yields of photovoltaics and LEDs[91]. We are therefore

interested in modeling systems with conical intersections, and spin-boson like models beyond the Condon approximation therefore represent a good starting point.
The linear vibronic coupling Hamiltonian is the simplest such extension of the spin-boson Hamiltonian, incorporating additional diabatic coupling terms that are linear in bath modes. Mathematically, we have:

$$\begin{aligned}\mathbf{H}_{LVC} = &|1\rangle\langle 1| \otimes (\mathbf{h_1} \otimes \mathbf{I} + \mathbf{I} \otimes \mathbf{h_3}) + |2\rangle\langle 2| \otimes (\mathbf{h_2} \otimes \mathbf{I} + \mathbf{I} \otimes \mathbf{h_3}) \\ &+ (|1\rangle\langle 2| + |2\rangle\langle 1|) \otimes \left(\left(V_0 + \sum_i V_{x_i} x_i\right) \otimes \mathbf{I} + \mathbf{I} \otimes \sum_j V_{y_j} y_j\right) \qquad (3.5)\end{aligned}$$

$$\mathbf{h_3} = \sum_j \left(\frac{p_{y_j}^2}{2m_j} + \frac{1}{2} m_j \omega_j^2 y_j^2\right) \qquad (3.6)$$

while $\mathbf{h}_{\{\mathbf{1,2}\}}$ is given by Eqns. 3.2 and 3.3. We have thus partitioned the bath into two fragments: one containing modes which couple to both the electronic states and the off-diagonal $\hat{V}$ (represented by modes $\{x_i\}$ and reduced Hamiltonians $\mathbf{h}_{\{\mathbf{1,2}\}}$) and the other containing modes that only couple to the off-diagonal $\hat{V}$ (represented by modes $\{y_j\}$ and reduced Hamiltonian $\mathbf{h_3}$). We felt that it was the best to partition the modes thus as we observed significantly different behavior between the two classes of modes, and because it allowed us to make some approximations that enabled derivation of a closed analytic representation of fourth order and beyond, while the non-partitioned model proved untractable beyond NIBA level of theory.

The dynamics for this model are completely specified by $\epsilon, V_0, J(\omega)$ and two additional spectral densities $J_{cross}(\omega)$ and $J_V(\omega)$ which are defined by:

$$J_{cross}(\omega) = \sum_{x_i} \frac{\pi c_i V_{x_i}}{2 m_i \omega_i} \delta(\omega - \omega_i) \rightarrow \frac{\pi c(\omega) V_x(\omega)}{2 m(\omega) \omega} g(\omega) \qquad (3.7)$$

$$J_V(\omega) = \frac{\pi}{2}\left(\sum_{x_i} \frac{V_{x_i}^2}{m_i \omega_i} \delta(\omega - \omega_i) + \sum_{y_j} \frac{V_{y_j}^2}{m_j \omega_j} \delta(\omega - \omega_j)\right) \rightarrow \frac{\pi\left(V_x^2(\omega) + V_y^2(\omega)\right)}{2 m(\omega) \omega} g(\omega) \qquad (3.8)$$

All further derivations will involve using the generalized $\mathbf{H}_{LVC}$ Hamiltonian, as it can be reduced to $\mathbf{H}_{SB}$ by merely setting $J_{cross}(\omega)$ and $J_V(\omega)$ to zero.

3.4 Mapping Chemical Systems to Models

Having defined our model Hamiltonians, we now describe our approach for mapping chemical systems to these models. We achieve this via classical molecular dynamics by sampling on a single surface. Let $E_{\{1,2\}}$ be the energy of states $\{1,2\}$ and V be the coupling for some bath configuration $\{\vec{p}_i, \vec{x}_i\}$, which is drawn from the canonical ensemble for the state 1 plus bath combination. $E_{\{1,2\}}$ is consequently just the value of $\mathbf{h_{\{1,2\}}}+\mathbf{h_3}$ for that bath configuration, allowing us to calculate correlation functions of fluctuations $\delta\Delta E(t)$ and $\delta V(t)$, which are defined to be:

$$\Delta E(t) \equiv E_1 - E_2 = -\epsilon + 2\sum_i c_i x_i(t) \tag{3.9}$$

$$\delta\Delta E(t) \equiv \Delta E(t) - \langle \Delta E(t) \rangle = 2\sum_i c_i \left(x_i(t) - \langle x_i(t) \rangle \right) \tag{3.10}$$

$$V = V_0 + \sum_i V_{x_i} x_i(t) + \sum_j V_{y_j} y_j(t) \tag{3.11}$$

$$\delta V(t) \equiv V(t) - \langle V(t) \rangle = \sum_i V_i \left(x_i(t) - \langle x_i(t) \rangle \right) + \sum_j V_{y_j} \left(y_j(t) - \langle y_j(t) \rangle \right) \tag{3.12}$$

where the averages are taken over the state 1 plus bath combination canonical ensemble. We then follow the procedure outlined in section 6.5.1 of Nitzan[92] to obtain:

$$\langle \delta\Delta E(t) \delta\Delta E(0) \rangle = \sum_i \frac{4c_i^2}{\beta m_i \omega_i^2} \cos \omega_i t \tag{3.13}$$

$$\implies \int_0^\infty \langle \delta\Delta E(t) \delta\Delta E(0) \rangle \cos \omega t dt = \sum_i \frac{4c_i^2}{\beta m_i \omega_i^2} \int_0^\infty \cos \omega_i t \cos \omega t dt \tag{3.14}$$

$$= \sum_i \frac{4c_i^2}{\beta m_i \omega_i^2} \left(\frac{\pi}{2} \delta(\omega - \omega_i) \right) = \frac{4}{\beta\omega} J(\omega) \tag{3.15}$$

leading to:

$$\therefore J(\omega) = \frac{\beta\omega}{4} \int_0^\infty \langle \delta\Delta E(t) \delta\Delta E(0) \rangle \cos \omega t dt \tag{3.16}$$

We similarly find that the other two correlation functions are:

$$J_{cross}(\omega) = \frac{\beta\omega}{2}\int_0^\infty \langle \delta\Delta E(t)\delta V(0)\rangle \cos\omega t dt \tag{3.17}$$

$$J_V(\omega) = \beta\omega\int_0^\infty \langle \delta V(t)\delta V(0)\rangle \cos\omega t dt \tag{3.18}$$

which can all be calculated from classical molecular dynamics.

3.5 Time Dependent Perturbation Theory

Having finally defined the chemical system to model Hamiltonian mapping, we can start working on calculating the dynamics for the LVC Hamiltonian. Treating the diabatic coupling (off-diagonal) terms of the LVC Hamiltonian as a perturbation, we obtain:

$$\mathbf{H}_{LVC} = \mathbf{H}_0 + \mathbf{H}_1 \tag{3.19}$$

$$\mathbf{H}_0 \equiv |1\rangle\langle 1| \otimes \mathbf{h_1} \otimes \mathbf{I} + |2\rangle\langle 2| \otimes \mathbf{h_2} \otimes \mathbf{I} + (|1\rangle\langle 1| + |2\rangle\langle 2|) \otimes \mathbf{I} \otimes \mathbf{h_3} \tag{3.20}$$

$$= |1\rangle\langle 1| \otimes \mathbf{h_1} \otimes \mathbf{I} + |2\rangle\langle 2| \otimes \mathbf{h_2} \otimes \mathbf{I} + \mathbf{I} \otimes \mathbf{I} \otimes \mathbf{h_3} \tag{3.21}$$

$$\mathbf{H}_1 \equiv (|1\rangle\langle 2| + |2\rangle\langle 1|) \otimes \left(\left(V_0 + \sum_i V_{x_i} x_i\right) \otimes \mathbf{I} + \mathbf{I} \otimes \sum_j V_{y_j} y_j\right) \tag{3.22}$$

In the interaction picture, we may define the operator:

$$\tilde{\mathbf{H}}_1(t) \equiv e^{it\mathbf{H}_0}\mathbf{H}_1 e^{-it\mathbf{H}_0} \tag{3.23}$$

Time-dependent perturbation then permits us to write the propagator $e^{-it\mathbf{H}_{LVC}}$ as the following power series:

$$\implies e^{-it\mathbf{H}_{LVC}} = e^{-it\mathbf{H}_0}\left(1 - i\int_0^t \tilde{\mathbf{H}}_1(t_1)dt_1 - \int_0^t dt_1 \int_0^{t_1} \tilde{\mathbf{H}}_1(t_1)\tilde{\mathbf{H}}_1(t_2)dt_2 \ldots\right) \tag{3.24}$$

We then utilize the orthogonality of $|1\rangle, |2\rangle$ to note that:

$$[|1\rangle\langle 1| \otimes \mathbf{h_1} \otimes \mathbf{I}, |2\rangle\langle 2| \otimes \mathbf{h_2} \otimes \mathbf{I}] = 0 \tag{3.25}$$

while it is trivially true that:

$$[|1\rangle\langle 1| \otimes \mathbf{h_1} \otimes \mathbf{I}, \mathbf{I} \otimes \mathbf{I} \otimes \mathbf{h_3}] = 0,\ [|2\rangle\langle 2| \otimes \mathbf{h_2} \otimes \mathbf{I}, \mathbf{I} \otimes \mathbf{I} \otimes \mathbf{h_3}] = 0 \tag{3.26}$$

This allows us to factorize $e^{-it\mathbf{H_0}}$ into:

$$e^{-it\mathbf{H_0}} = e^{-it|1\rangle\langle 1|\otimes\mathbf{h_1}\otimes\mathbf{I}} e^{-it|2\rangle\langle 2|\otimes\mathbf{h_2}\otimes\mathbf{I}} e^{-it\mathbf{I}\otimes\mathbf{I}\otimes\mathbf{h_3}} \tag{3.27}$$

and further simplify it by noting:

$$e^{-it|1\rangle\langle 1|\otimes\mathbf{h_1}\otimes\mathbf{I}} = \mathbf{1} + (-it\,|1\rangle\langle 1| \otimes \mathbf{I} \otimes \mathbf{h_3}) + \frac{(-it\,|1\rangle\langle 1| \otimes \mathbf{h_1} \otimes \mathbf{I})^2}{2!} \ldots \tag{3.28}$$

$$= \mathbf{1} + |1\rangle\langle 1| \otimes \left(-it\mathbf{h_1} + \frac{(-it\mathbf{h_1})^2}{2!} \ldots\right) \otimes \mathbf{I} \tag{3.29}$$

$$= |2\rangle\langle 2| \otimes \mathbf{I} \otimes \mathbf{I} + |1\rangle\langle 1| \otimes e^{-it\mathbf{h_1}} \otimes \mathbf{I} \tag{3.30}$$

Since $(|1\rangle\langle 1|)^n = |1\rangle(\langle 1|1\rangle)^n\langle 1| = |1\rangle\langle 1|\ \forall n \geq 1,\ n \in \mathbf{Z}^+$. Similarly we have:

$$e^{-it|2\rangle\langle 2|\otimes\mathbf{h_2}} = |1\rangle\langle 1| \otimes \mathbf{I} \otimes \mathbf{I} + |2\rangle\langle 2| \otimes e^{-it\mathbf{h_2}} \otimes \mathbf{I} \tag{3.31}$$

$$e^{-it\mathbf{I}\otimes\mathbf{I}\otimes\mathbf{h_3}} = \mathbf{I} \otimes \mathbf{I} \otimes e^{-it\mathbf{h_3}} \tag{3.32}$$

leading to

$$e^{-it\mathbf{H_0}} = |1\rangle\langle 1| \otimes e^{-it\mathbf{h_1}} \otimes e^{-it\mathbf{h_3}} + |2\rangle\langle 2| \otimes e^{-it\mathbf{h_2}} \otimes e^{-it\mathbf{h_3}} \tag{3.33}$$

$$\therefore \tilde{\mathbf{H}}_1(t) = e^{it\mathbf{H_0}} \left(|1\rangle\langle 2| \otimes \left(\left(V_0 + \sum_i V_{x_i} x_i\right) \otimes \mathbf{I} + \mathbf{I} \otimes \sum_j V_{y_j} y_j\right)\right) e^{-it\mathbf{H_0}} + \text{h.c.} \tag{3.34}$$

$$= |1\rangle\langle 2| \otimes O(t) + |2\rangle\langle 1| \otimes O^\dagger(t) \tag{3.35}$$

by defining:

$$O(t) \equiv e^{i\mathbf{th_1}} \left(V_0 + \sum_i V_{x_i} x_i \right) e^{-i\mathbf{th_2}} \otimes \mathbf{I} + e^{i\mathbf{th_1}} e^{-i\mathbf{th_2}} \otimes \left(\sum_j V_{y_j} y_j^H(t) \right) \tag{3.36}$$

$$y_j^H(t) = e^{i\mathbf{th_3}} y_j e^{-i\mathbf{th_3}} \tag{3.37}$$

$y_j^H(t)$ is just a standard Heisenberg representation of the coordinate y_j, and $O(t)$ represents a transition between $|1\rangle$ and $|2\rangle$. 3.35 also leads to:

$$\tilde{\mathbf{H}}_1(t_1)\tilde{\mathbf{H}}_1(t_2) = |1\rangle\langle 1| \otimes O(t_1)O^\dagger(t_2) + |2\rangle\langle 2| \otimes O^\dagger(t_1) \otimes O(t_2) \tag{3.38}$$

This immediately shows that multiplying an odd number of $\tilde{\mathbf{H}}_1$ terms will yield an electronically off-diagonal result (only $|1\rangle\langle 2|$ and $|2\rangle\langle 1|$ containing terms), while an even number of $\tilde{\mathbf{H}}_1$ will generate terms with only $|1\rangle\langle 1|$ and $|2\rangle\langle 2|$, which make contributions to populations. Thus, we will only concern ourselves with terms with an even number of $\tilde{\mathbf{H}}_1$ as the rest have zero trace. With this information, we are prepared to write the propagator down and obtain populations.

3.6 Perturbation Theory Populations

We are chiefly interested in initial density matrices of the form $|1\rangle\langle 1| \otimes \cdots$ (i.e. starting purely from state $|1\rangle$), as it is trivial to know what happens when we start from pure $|2\rangle$ via a simple inversion of labels. A more general density matrix of the form $p|1\rangle\langle 1| \ldots + (1-p)|2\rangle\langle 2| \ldots$ can be decomposed into pure $|1\rangle$ and $|2\rangle$ pieces that evolve independently in time and can be recombined to give the final population (from linearity of the time evolution of density matrices). We however avoid starting states with some coherence $|1\rangle\langle 2|$, as these are unlikely to occur in cases that we are interested in.

Therefore we restrict ourselves to $\rho(0) = |1\rangle\langle 1| \otimes \rho_{B_1} \otimes \rho_{B_2}$ where ρ_{B_1}, ρ_{B_2} are reduced initial density matrices for the two classes of modes $\{x_i\}$ and $\{y_i\}$. We then have

population in state $|1\rangle$, $p_1(t)$ be:

$$p_1(t) = \mathbf{Tr}\left[\rho(t)\left(|1\rangle\langle 1| \otimes \mathbf{I} \otimes \mathbf{I}\right)\right] \tag{3.39}$$

$$\rho(t) = e^{-it\mathbf{H}_{LVC}}\rho(0)e^{it\mathbf{H}_{LVC}} \tag{3.40}$$

$$= e^{-it\mathbf{H}_0}\left(1 - i\int_0^t \tilde{\mathbf{H}}_1(t_1)dt_1\ldots\right)\rho(0)\left(1 + i\int_0^t \tilde{\mathbf{H}}_1(t_1)dt_1\ldots\right)e^{it\mathbf{H}_0} \tag{3.41}$$

$$\therefore p_1(t) = \mathbf{Tr}\left[\left(e^{-it\mathbf{H}_0}\left(1 - i\ldots\right)\rho(0)\left(1 + i\ldots\right)e^{it\mathbf{H}_0}\right)\left(|1\rangle\langle 1| \otimes \mathbf{I} \otimes \mathbf{I}\right)\right] \tag{3.42}$$

$$= \mathbf{Tr}\left[\left(\left(1 - i\ldots\right)\rho(0)\left(1 + i\ldots\right)\right)e^{it\mathbf{H}_0}\left(|1\rangle\langle 1| \otimes \mathbf{I} \otimes \mathbf{I}\right)e^{-it\mathbf{H}_0}\right] \tag{3.43}$$

Now,

$$e^{it\mathbf{H}_0}\left(|1\rangle\langle 1| \otimes \mathbf{I} \otimes \mathbf{I}\right)e^{-it\mathbf{H}_0} = \left(|1\rangle\langle 1| \otimes \mathbf{I} \otimes \mathbf{I}\right) \tag{3.44}$$

from 3.33. Therefore we have:

$$p_1(t) = \mathbf{Tr}\left[\left(\left(1 - i\ldots\right)\rho(0)\left(1 + i\ldots\right)\right)\left(|1\rangle\langle 1| \otimes \mathbf{I} \otimes \mathbf{I}\right)\right] \tag{3.45}$$

$$= \mathbf{Tr}\left[\left(\left(1 - i\ldots\right)\left(|1\rangle\langle 1| \otimes \rho_{B_1} \otimes \rho_{B_2}\right)\left(1 + i\ldots\right)\right)\left(|1\rangle\langle 1| \otimes \mathbf{I} \otimes \mathbf{I}\right)\right] \tag{3.46}$$

We can immediately see that:

$$p_1^{(0)}(t) = \mathbf{Tr}\left[\left(|1\rangle\langle 1| \otimes \rho_{B_1} \otimes \rho_{B_2}\right)\left(|1\rangle\langle 1| \otimes \mathbf{I} \otimes \mathbf{I}\right)\right] = \mathbf{Tr}\left[\rho(0)\right] = 1 \tag{3.47}$$

$$\begin{aligned} p_1^{(2)}(t) =& \mathbf{Tr}\left[\left(\left(-\int_0^t dt_1 \int_0^{t_1} \tilde{\mathbf{H}}_1(t_1)\tilde{\mathbf{H}}_1(t_2)dt_2\right)\left(|1\rangle\langle 1| \otimes \rho_{B_1} \otimes \rho_{B_2}\right)\right)\left(|1\rangle\langle 1| \otimes \mathbf{I} \otimes \mathbf{I}\right)\right] \\ &+ \mathbf{Tr}\left[\left(\left(|1\rangle\langle 1| \otimes \rho_{B_1} \otimes \rho_{B_2}\right)\left(-\int_0^t dt_1 \int_0^{t_1} \tilde{\mathbf{H}}_1(t_2)\tilde{\mathbf{H}}_1(t_1)dt_2\right)\right)\left(|1\rangle\langle 1| \otimes \mathbf{I} \otimes \mathbf{I}\right)\right] \\ &+ \mathbf{Tr}\left[\left(\left(\int_0^t dt_1\tilde{\mathbf{H}}_1(t_1)\right)\left(|1\rangle\langle 1| \otimes \rho_{B_1} \otimes \rho_{B_2}\right)\left(\int_0^t dt_1\tilde{\mathbf{H}}_1(t_1)\right)\right)\left(|1\rangle\langle 1| \otimes \mathbf{I} \otimes \mathbf{I}\right)\right] \end{aligned} \tag{3.48}$$

and so on.

This is already becoming quite alarmingly complex, but it is possibly to simplify this by noting the following:

1. The second term is merely the complex conjugate of the first, as the operator being traced out is the hermitian conjugate of the operator being traced out in the first term.

2. The third term is zero. This is in fact an example of a more general case: whenever $\rho(0)$ is sandwiched between two chains of $\tilde{\mathbf{H}}_1$, the trace will be zero unless both sides have an even number of $\tilde{\mathbf{H}}_1$ terms. The case of one side being even and the other being odd is simple to see, it will become unbalanced and be reduced to an electronically off-diagonal term that leaves no trace. The case of both sides being odd is a bit more complex: this indicates both sides will have $|1\rangle\langle 2| \otimes \ldots + |2\rangle\langle 1| \otimes \ldots$ symmetry. Consequently the sandwich will reduce to:

$$\begin{aligned}&(|1\rangle\langle 2| \otimes \ldots + |2\rangle\langle 1| \otimes \ldots)(|1\rangle\langle 1| \otimes \rho_{B_1} \otimes \rho_{B_2})(|1\rangle\langle 2| \otimes \ldots + |2\rangle\langle 1| \otimes \ldots) \\ &= |2\rangle\langle 2| \ldots \end{aligned} \tag{3.49}$$

   Thus we have a product with $|2\rangle\langle 2| \ldots$ symmetry, which will cancel out with the final $|1\rangle\langle 1|$ term.

These simplifications make life significantly simple, and the second order term thus simply reduces to:

$$p_1^{(2)}(t) = -2\mathbf{Re}\left[\mathbf{Tr}\left[\left(\int_0^t dt_1 \int_0^{t_1} \tilde{\mathbf{H}}_1(t_1)\tilde{\mathbf{H}}_1(t_2)dt_2\right)(|1\rangle\langle 1| \otimes \rho_{B_1} \otimes \rho_{B_2})(|1\rangle\langle 1| \otimes \mathbf{I} \otimes \mathbf{I})\right]\right] \tag{3.50}$$

$$= -2\mathbf{Re}\left[\mathbf{Tr}\left[\left(\int_0^t dt_1 \int_0^{t_1} \tilde{\mathbf{H}}_1(t_1)\tilde{\mathbf{H}}_1(t_2)dt_2\right)(|1\rangle\langle 1| \otimes \rho_{B_1} \otimes \rho_{B_2})\right]\right] \tag{3.51}$$

$$= -2\int_0^t dt_1 \int_0^{t_1} \mathbf{Re}\left[\mathbf{Tr}\left[O(t_1)O^\dagger(t_2)(\rho_{B_1} \otimes \rho_{B_2})\right]\right] dt_2 \tag{3.52}$$

employing 3.38. In a similar fashion we have:

$$p_1^{(4)}(t) = 2\int_0^t dt_1 \int_0^{t_1} dt_2 \int_0^{t_2} dt_3 \int_0^{t_3} \mathbf{Re}\left[\mathbf{Tr}\left[O(t_1)O^\dagger(t_2)O(t_3)O^\dagger(t_4)\left(\rho_{B_1}\otimes\rho_{B_2}\right)\right]\right] dt_4$$
$$+\int_0^t dt_1 \int_0^{t_1} dt_2 \int_0^{t} dt_3 \int_0^{t_3} \mathbf{Re}\left[\mathbf{Tr}\left[O(t_3)O^\dagger(t_4)\left(\rho_{B_1}\otimes\rho_{B_2}\right)O(t_2)O^\dagger(t_1)\right]\right] dt_4 \tag{3.53}$$

$$=2\int_0^t dt_1 \int_0^{t_1} dt_2 \int_0^{t_2} dt_3 \int_0^{t_3} \mathbf{Re}\left[\mathbf{Tr}\left[O(t_1)O^\dagger(t_2)O(t_3)O^\dagger(t_4)\left(\rho_{B_1}\otimes\rho_{B_2}\right)\right]\right] dt_4$$
$$+\int_0^t dt_1 \int_0^{t_1} dt_2 \int_0^{t} dt_3 \int_0^{t_3} \mathbf{Re}\left[\mathbf{Tr}\left[O(t_2)O^\dagger(t_1)O(t_3)O^\dagger(t_4)\left(\rho_{B_1}\otimes\rho_{B_2}\right)\right]\right] dt_4 \tag{3.54}$$

using the fact that $\mathbf{Tr}\left[AB\right] = \mathbf{Tr}\left[BA\right]$ to group all the O operators together in the second term.

It immediately appears obvious that the crucial objective is to evaluate traces of the form $\mathbf{Tr}\left[O(t_1)O^\dagger(t_2)\ldots\left(\rho_{B_1}\otimes\rho_{B_2}\right)\right]$. For notational simplicity, we define:

$$F_{2n}(t_1,t_2,\ldots t_{2n}) = \mathbf{Tr}\left[O(t_1)O^\dagger(t_2)\ldots O(t_{2n-1})O^\dagger(t_{2n})\left(\rho_{B_1}\otimes\rho_{B_2}\right)\right] \tag{3.55}$$

and then use F_{2n} to calculate perturbation theory populations.

3.6.1 Traces within the Condon Approximation

Within the condon approximation $O(t) = Ve^{it\mathbf{h_1}}e^{-it\mathbf{h_2}} \otimes \mathbf{I}$, and so it makes sense to factor out the coupling V from the traces. Thus we use $f_{2n}(t_1, t_2, \ldots t_{2n})$ such that:

$$F_{2n}(t_1, t_2, \ldots t_{2n}) = V^{2n} f_{2n}(t_1, t_2, \ldots t_{2n}) \tag{3.56}$$

$$\implies f_{2n}(t_1, t_2, \ldots t_{2n}) = \mathbf{Tr}\left[\left(e^{it_1\mathbf{h_1}}e^{-it_1\mathbf{h_2}}e^{it_2\mathbf{h_2}}e^{-it_2\mathbf{h_1}} \ldots \otimes I\right)\left(\rho_{B_1} \otimes \rho_{B_2}\right)\right] \tag{3.57}$$

$$= \mathbf{Tr}\left[\left(e^{it_1\mathbf{h_1}}e^{-it_1\mathbf{h_2}}e^{it_2\mathbf{h_2}}e^{-it_2\mathbf{h_1}} \ldots\right)\rho_{B_1}\right]\mathbf{Tr}\left[\rho_{B_2}\right] \tag{3.58}$$

$$= \mathbf{Tr}\left[\left(e^{it_1\mathbf{h_1}}e^{-it_1\mathbf{h_2}}e^{it_2\mathbf{h_2}}e^{-it_2\mathbf{h_1}} \ldots\right)\rho_{B_1}\right] \tag{3.59}$$

as the trace of a density matrix is always one.

These traces f_{2n} may be analytically found in a variety of ways. We choose to evaluate them by employing the position representation of the harmonic oscillator coherent state basis $|\mathbf{p}, \mathbf{q}\rangle$. Using the resolution of identity we have:

$$\mathbf{Tr}\left[\left(e^{it_1\mathbf{h_1}}e^{-it_1\mathbf{h_2}}e^{it_2\mathbf{h_2}}e^{-it_2\mathbf{h_1}} \ldots e^{it_{2n}\mathbf{h_2}}e^{-it_{2n}\mathbf{h_1}}\right)\rho_{B_1}\right]$$
$$= \int d\mathbf{p}^{n+1}d\mathbf{q}^{n+1}d\mathbf{x}^{n+1}\left\langle \mathbf{x_1}|e^{it_1\mathbf{h_1}}|\mathbf{p_1}, \mathbf{q_1}\right\rangle\left\langle \mathbf{p_1}\mathbf{q_1}|e^{i(t_2-t_1)\mathbf{h_2}}|\mathbf{x_2}\right\rangle \ldots \left\langle \mathbf{p_{n+1}}, \mathbf{q_{n+1}}|\rho_{B_1}|\mathbf{x_1}\right\rangle \tag{3.60}$$

which could be evaluated by noting that $e^{it_1\mathbf{h_1}}$ etc. are the propagators for harmonic oscillator Hamiltonians. The position representation of a time-evolving coherent state is well-known to be Gaussian [93, 94], making this integral analytically tractable if the bath term $\left\langle \mathbf{p_{n+1}}, \mathbf{q_{n+1}}|\rho_{B_1}|\mathbf{x_1}\right\rangle$ follows a similar behavior.

Fortunately, the initial bath density matrix is unlikely to not be related to harmonic oscillators since that is the native state of the bath. ρ_{B_1} is often chosen to be of the "thermal form" $\dfrac{e^{-\beta\mathbf{h_1}}}{\mathbf{Tr}\left[e^{-\beta\mathbf{h_1}}\right]}$ $\left(\text{where } \beta = \dfrac{1}{k_B T}\right)$ since it indicates that the bath was originally in thermal equilibrium with the initial diabatic state $|1\rangle$, which is a natural starting point for studying electron-transfer dynamics. We are also interested ρ_{B_1} of the "photochemical form" $\dfrac{e^{-\beta\mathbf{h_2}}}{\mathbf{Tr}\left[e^{-\beta\mathbf{h_2}}\right]}$ due to our interest in the dynamics of excited states. This density matrix represents a case where the system was purely

in the thermal state $|2\rangle\langle 2| \otimes \frac{e^{-\beta \mathbf{h}_2}}{\mathbf{Tr}\left[e^{-\beta \mathbf{h}_2}\right]}$ before $t = 0$ but was electronically excited completely from state $|2\rangle$ to state $|1\rangle$ at $t = 0$, without giving the bath-modes an opportunity to respond. The bath-modes thus remained in thermal equilibrium with state $|2\rangle$, leading to a starting density matrix of the form $|1\rangle\langle 1| \otimes \frac{e^{-\beta \mathbf{h}_2}}{\mathbf{Tr}\left[e^{-\beta \mathbf{h}_2}\right]}$. Directly evaluating such traces for large $2n$ is especially tedious, but fortuitously we have:

$$\ln f_{2n}(t_1, t_2, t_3 \ldots t_{2n}) = \sum_{i=1}^{2n-1} \sum_{j=i+1}^{2n} (-1)^{i+j+1} \ln f_2(t_i, t_j) \tag{3.61}$$

Thus knowing f_2 is sufficient to determine behavior of these traces to arbitrary order. For thermal initial conditions we have (a complete derivation is given in appendix):

$$Q'(t) \equiv \frac{4}{\pi} \int_0^\infty \frac{J(\omega)}{\omega^2} (1 - \cos \omega t) \coth \frac{\beta \omega}{2} d\omega \tag{3.62}$$

$$Q''(t) \equiv \frac{4}{\pi} \int_0^\infty \frac{J(\omega)}{\omega^2} \sin \omega t d\omega \tag{3.63}$$

$$\ln f_2(t_1, t_2) = -i\epsilon(t_1 - t_2) - Q'(t_1 - t_2) - iQ''(t_1 - t_2) \tag{3.64}$$

while the photochemical initial conditions give:

$$\ln f_2(t_1, t_2) = -i\epsilon(t_1 - t_2) - Q'(t_1 - t_2) - iQ''(t_1 - t_2) + 2iQ''(t_1) - 2iQ''(t_2) \tag{3.65}$$

This shows that knowledge of ϵ and $J(\omega)$ is sufficient to completely specify f_{2n}. Together with V, these are thus all the parameters one needs to calculate the population dynamics of the spin-boson Hamiltonian (for the thermal and photochemical initial conditions at least).

We also note that 3.61 appears to be true in general for any $\rho_{B_1} = \frac{e^{-\kappa \mathbf{h}}}{\mathbf{Tr}\left[e^{-\kappa \mathbf{h}}\right]}$ if $\mathbf{h} = \sum_i \left(\frac{p_{x_i}^2}{2m_i} + \frac{1}{2} m_i \omega_i^2 x_i^2 + d_i x_i \right)$ is a harmonic oscillator Hamiltonian with same normal modes and frequencies as $\mathbf{h}_{\{1,2\}}$ but not necessarily same equilibrium positions and κ is an arbitrary positive real number. No deviation from this behavior

was observed numerically upto $2n = 20$ with randomly generated $\kappa, \mathbf{h}$. The thermal and photochemical starting states are special cases of this general ρ_{B_1} (albeit the only ones with obvious physical meaning).

3.6.2 Non-Condon Traces

Second Order

Non-Condon F_{2n} are substantially more complex than their Condon counterparts, not the least because the coupling is no longer constant and cannot be factored out.
As a first step we attempt to evaluate $F_2(t_1, t_2)$ to get a sense of the full-sense of the complexity. We have:

$$F_2(t_1, t_2) = \mathbf{Tr}\left[O(t_1)O^\dagger(t_2)\left(\rho_{B_1} \otimes \rho_{B_2}\right)\right] \tag{3.66}$$

Since the modes in ρ_{B_2} do not couple to the diabatic electronic states (only to couplings), we can conclude they are in thermal equilibrium, leading to $\rho_{B_2} = \frac{e^{-\beta \mathbf{h_3}}}{\mathbf{Tr}\left[e^{-\beta \mathbf{h_3}}\right]}$.
Consequently we may simplify F_2 down to:

$$\begin{aligned}
F_2(t_1, t_2) = &\left(V_0^2 + V_0 \mathbf{Tr}\left[\left(\sum_j V_{y_j} y_j^H(t_1) + \sum_j V_{y_j} y_j^H(t_2)\right)\rho_{B_2}\right]\right) \mathbf{Tr}\left[e^{it_1\mathbf{h_1}} e^{-it_1\mathbf{h_2}} e^{it_2\mathbf{h_2}} e^{-it_2\mathbf{h_1}} \rho_{B_1}\right] \\
&+ \mathbf{Tr}\left[\left(\sum_j V_{y_j} y_j^H(t_1)\right)\left(\sum_j V_{y_j} y_j^H(t_2)\right)\rho_{B_2}\right] \mathbf{Tr}\left[e^{it_1\mathbf{h_1}} e^{-it_1\mathbf{h_2}} e^{it_2\mathbf{h_2}} e^{-it_2\mathbf{h_1}} \rho_{B_1}\right] \\
&+ V_0 \mathbf{Tr}\left[e^{it_1\mathbf{h_1}}\left(\sum_i V_{x_i} x_i\right) e^{-it_1\mathbf{h_2}} e^{it_2\mathbf{h_2}} e^{-it_2\mathbf{h_1}} \rho_{B_1}\right] \\
&+ V_0 \mathbf{Tr}\left[e^{it_1\mathbf{h_1}} e^{-it_1\mathbf{h_2}} e^{it_2\mathbf{h_2}}\left(\sum_i V_{x_i} x_i\right) e^{-it_2\mathbf{h_1}} \rho_{B_1}\right] \\
&+ \mathbf{Tr}\left[e^{it_1\mathbf{h_1}} e^{-it_1\mathbf{h_2}}\left(\sum_i V_{x_i} x_i\right) e^{it_2\mathbf{h_2}}\left(\sum_i V_{x_i} x_i\right) e^{-it_2\mathbf{h_1}} \rho_{B_1}\right]
\end{aligned} \tag{3.67}$$

This is quite complex, and will have to be evaluated piecewise. From 3.59 we have:

$$\mathbf{Tr}\left[e^{it_1\mathbf{h_1}} e^{-it_1\mathbf{h_2}} e^{it_2\mathbf{h_2}} e^{-it_2\mathbf{h_1}} \rho_{B_1}\right] = f_2(t_1, t_2) \tag{3.68}$$

We also know that as $\rho_{B_2} = \frac{e^{-\beta \mathbf{h_3}}}{\mathbf{Tr}\left[e^{-\beta \mathbf{h_3}}\right]}$, we will have:

$$\mathbf{Tr}\left[\left(\sum_j V_{y_j} y_j^H(t_1)\right)\rho_{B_2}\right] = \sum_j V_{y_j}\left\langle y_j^H(t_1)\right\rangle = \sum_j V_{y_j} \times 0 = 0 \tag{3.69}$$

where the average is the thermal average. This results from the equilibrium position for $\mathbf{h_3}$ being $\{y_j\} = 0$ (3.6) as these modes are not coupled to the diabatic states. Similarly, we have:

$$\mathbf{Tr}\left[\left(\sum_j V_{y_j} y_j^H(t_1)\right)\left(\sum_j V_{y_j} y_j^H(t_2)\right)\rho_{B_2}\right] = \sum_j \sum_k V_{y_j} V_{y_k}\left\langle y_j^H(t_1) y_k^H(t_2)\right\rangle \tag{3.70}$$

$$= \sum_j V_{y_j}^2\left\langle y_j^H(t_1) y_j^H(t_2)\right\rangle + \sum_j \sum_{k\neq j} V_{y_j} V_{y_k}\left\langle y_j^H(t_1)\right\rangle\left\langle y_k^H(t_2)\right\rangle \tag{3.71}$$

as different modes are uncorrelated. However $\left\langle y_j^H(t_1)\right\rangle = 0$, leaving only:

$$\mathbf{Tr}\left[\left(\sum_j V_{y_j} y_j^H(t_1)\right)\left(\sum_j V_{y_j} y_j^H(t_2)\right)\rho_{B_2}\right] \tag{3.72}$$

$$= \sum_j V_{y_j}^2\left\langle y_j^H(t_1) y_j^H(t_2)\right\rangle \tag{3.73}$$

$$= \sum_j \frac{V_j^2}{2m_j\omega_j}\left(\cos\left(\omega_j(t_1-t_2)\right)\coth\frac{\beta\omega_j}{2} - i\sin\left(\omega_j(t_1-t_2)\right)\right)d\omega \tag{3.74}$$

from Eqn 6.97 of Nitzan[92].

We now focus on the more complex remaining terms. For these, it is convenient to decompose $\mathbf{h_{\{1,2\}}}$ into sums of single-mode Hamiltonians $\mathbf{h^i_{\{1,2\}}}$, which is to say:

$$\mathbf{h^i_{\{1,2\}}} \equiv \frac{p_{x_i}^2}{2m_i} + \frac{1}{2}m_i\omega_i^2 x_i^2 \pm c_i x_i \tag{3.75}$$

$$\mathbf{h_{\{1,2\}}} = \mp\frac{\epsilon}{2} + \sum_i \mathbf{h^i_{\{1,2\}}} \tag{3.76}$$

We may also similarly decompose starting density matrix $\rho_{B_1} = \prod_i \rho^i_{B_1}$ into a product of single-mode density matrices. This factorization is valid for any density matrix

of the general form $\frac{e^{-\kappa \mathbf{h}}}{\mathbf{Tr}\left[e^{-\kappa \mathbf{h}}\right]}$ where the hamiltonian $\mathbf{h}$ can be decomposed into a sum of single-mode hamiltonians, and is thus perfectly valid for both thermal and photochemical starting conditions.

Therefore we have:

$$\begin{aligned}
&\mathbf{Tr}\left[e^{it_1\mathbf{h_1}}x_i e^{-it_1\mathbf{h_2}}e^{it_2\mathbf{h_2}}e^{-it_2\mathbf{h_1}}\rho_{B_1}\right] \\
&= \mathbf{Tr}\left[e^{it_1\mathbf{h_1^i}}x_i e^{-it_1\mathbf{h_2^i}}e^{it_2\mathbf{h_2^i}}e^{-it_2\mathbf{h_1^i}}\rho^i_{B_1}\right]\prod_{j\neq i}\mathbf{Tr}\left[e^{it_1\mathbf{h_1^j}}e^{-it_1\mathbf{h_2^j}}e^{it_2\mathbf{h_2^j}}e^{-it_2\mathbf{h_1^j}}\rho^j_{B_1}\right]e^{-\epsilon(t_1-t_2)}
\end{aligned} \tag{3.77}$$

as all the modes are independent of each other, permitting this factorization.

$\mathbf{Tr}\left[e^{it_1\mathbf{h_1^i}}x_i e^{-it_1\mathbf{h_2^i}}e^{it_2\mathbf{h_2^i}}e^{-it_2\mathbf{h_1^i}}\rho^i_{B_1}\right]$ is basically $f_2(t_1,t_2)$ for a single mode, with $J(\omega)$ consequently being $\frac{\pi c_i^2}{2m_i\omega_i}\delta(\omega-\omega_i)$, and no energy gap. Therefore, we have:

$$f_2^i(t_1,t_2) = \mathbf{Tr}\left[e^{it_1\mathbf{h_1^i}}e^{-it_1\mathbf{h_2^i}}e^{it_2\mathbf{h_2^i}}e^{-it_2\mathbf{h_1^i}}\rho^i_{B_1}\right] \tag{3.78}$$

$$\implies \frac{d}{dt_1}f_2^i(t_1,t_2) = \frac{d}{dt_1}\mathbf{Tr}\left[e^{it_1\mathbf{h_1^i}}e^{-it_1\mathbf{h_2^i}}e^{it_2\mathbf{h_2^i}}e^{-it_2\mathbf{h_1^i}}\rho^i_{B_1}\right] \tag{3.79}$$

$$= \mathbf{Tr}\left[e^{it_1\mathbf{h_1^i}}\left(i\mathbf{h_1^i}-i\mathbf{h_2^i}\right)e^{-it_1\mathbf{h_2^i}}e^{it_2\mathbf{h_2^i}}e^{-it_2\mathbf{h_1^i}}\rho^i_{B_1}\right] \tag{3.80}$$

$$= \mathbf{Tr}\left[e^{it_1\mathbf{h_1^i}}\left(2ic_ix_i\right)e^{-it_1\mathbf{h_2^i}}e^{it_2\mathbf{h_2^i}}e^{-it_2\mathbf{h_1^i}}\rho^i_{B_1}\right] \tag{3.81}$$

$$\implies -\frac{i}{2c_i}\frac{d}{dt_1}f_2^i(t_1,t_2) = -\frac{i}{2c_i}\frac{d\ln f_2^i(t_1,t_2)}{dt_1}f_2^i(t_1,t_2) = \mathbf{Tr}\left[e^{it_1\mathbf{h_1^i}}x_i e^{-it_1\mathbf{h_2^i}}e^{it_2\mathbf{h_2^i}}e^{-it_2\mathbf{h_1^i}}\rho^i_{B_1}\right] \tag{3.82}$$

Similarly, we find that:

$$\frac{i}{2c_i}\frac{d}{dt_2}f_2^i(t_1,t_2) = \mathbf{Tr}\left[e^{it_1\mathbf{h_1^i}}e^{-it_1\mathbf{h_2^i}}e^{it_2\mathbf{h_2^i}}x_i e^{-it_2\mathbf{h_1^i}}\rho^i_{B_1}\right] \tag{3.83}$$

$$\frac{1}{4c_i^2}\frac{d^2}{dt_2dt_1}f_2^i(t_1,t_2) = \mathbf{Tr}\left[e^{it_1\mathbf{h_1^i}}e^{-it_1\mathbf{h_2^i}}x_i e^{it_2\mathbf{h_2^i}}x_i e^{-it_2\mathbf{h_1^i}}\rho^i_{B_1}\right] \tag{3.84}$$

Thus we have:

$$\mathbf{Tr}\left[e^{it_1\mathbf{h_1}}\left(\sum_i V_{x_i}x_i\right)e^{-it_1\mathbf{h_2}}e^{it_2\mathbf{h_2}}e^{-it_2\mathbf{h_1}}\rho_{B_1}\right] \tag{3.85}$$

$$=\left(\sum_i V_{x_i}\frac{i}{2c_i}\frac{d\ln f_2^i(t_1,t_2)}{dt_1}\right)f_2(t_1,t_2) \tag{3.86}$$

as multiplying all the single mode f_2^i (together with the energy bias ϵ) term gives $f_2(t_1,t_2)$ for the whole system. We also know that $\ln f_2^i(t_1,t_2) \propto J(\omega) \propto c_i^2$, and so the term will be some summation of c_iV_i (although the exact form depends on f_2^i and thus the starting conditions), allowing us to relate it to J_{cross}. We find $\mathbf{Tr}\left[e^{it_1\mathbf{h_1}}\left(\sum_i V_{x_i}x_i\right)e^{-it_1\mathbf{h_2}}e^{it_2\mathbf{h_2}}\left(\sum_i V_{x_i}x_i\right)e^{-it_2\mathbf{h_1}}\rho_{B_1}\right]$ similarly in terms of first and second derivatives of $f_2^i(t_1,t_2)$. With these we are able to write down $F_2(t_1,t_2)$ depending on the initial conditions. For the thermal case we have:

$$R'(t) \equiv \frac{2}{\pi}\int_0^\infty \frac{J_{cross}}{\omega}\cos\omega t d\omega \tag{3.87}$$

$$R''(t) \equiv \frac{2}{\pi}\int_0^\infty \frac{J_{cross}}{\omega}\sin\omega t\coth\frac{\beta\omega}{2}d\omega \tag{3.88}$$

$$S(t) \equiv \frac{1}{\pi}\int_0^\infty J_V(\omega)\left(\cos\omega t\coth\frac{\beta\omega}{2} - i\sin\omega t\right)d\omega \tag{3.89}$$

$$F_2(t_1,t_2) = \left((V_0 + iR''(t_1-t_2) - R'(t_1-t_2))^2 + S(t_1-t_2)\right)f_2(t_1,t_2) \tag{3.90}$$

The photochemical trace is even more complex, but can be worked out to be:

$$F_2(t_1,t_2) = ((V_0 + 2R'(t_1) - R'(t_1-t_2) + iR''(t_1-t_2))(V_0 + 2R'(t_2) - R'(t_1-t_2) + iR''(t_1-t_2)) + S(t_1-t_2))f_2(t_1,t_2) \tag{3.91}$$

Higher Orders

Most of the complexity of the non-condon traces stem from J_{cross} containing terms. However symmetry arguments can be made for a variety of systems of interest (such

as Fe(II)/Fe(III) self exchange) to show that J_{cross} is zero. Consequently, we decided to only evaluate higher-order traces after making the $J_{cross} = 0$ approximation (as they proved intractable otherwise). With this, we have:

$$F_{2n}(t_1, t_2, t_3, \ldots t_{2n}) = \mathbf{Tr}\left[\left(V_0 + \sum_j V_j y_j^H(t_1)\right)\left(V_0 + \sum_j V_j y_j^H(t_2)\right)\ldots \rho_{B_2}\right] f_{2n}(t_1, t_2, t_3, \ldots t_{2n}) \tag{3.92}$$

Since ρ_{B_2} is of the thermal form $\frac{e^{-\beta \mathbf{h_3}}}{\mathbf{Tr}\left[e^{-\beta \mathbf{h_3}}\right]}$, the first trace is merely a thermal average and can be simplified fairly easily. However, calculating all the traces directly is tedious, and so the following trace relationship proves useful:

$$T_{2n}(t_1, t_2, \ldots t_{2n}) \equiv \mathbf{Tr}\left[\left(\sum_j V_j y_j^H(t_1)\right)\left(\sum_j V_j y_j^H(t_2)\right)\ldots\left(\sum_j V_j y_j^H(t_{2n})\right)\rho_{B_2}\right] \tag{3.93}$$

$$T_2(t_1, t_2) = S(t_1 - t_2) \tag{3.94}$$

$$\begin{aligned} T_{2n}(t_1, t_2, \ldots t_{2n}) = {} & T_2(t_1, t_2) T_{2n-2}(t_3, t_4 \ldots, t_{2n}) + T_2(t_1, t_3) T_{2n-2}(t_2, t_4 \ldots, t_{2n}) \ldots \\ & + T_2(t_1, t_{2n}) T_{2n-2}(t_2, t_3 \ldots, t_{2n-1}) \end{aligned} \tag{3.95}$$

3.6.3 Populations from Traces

We have from Eqns. 3.46 and 3.55:

$$p_1^{(2)}(t) = -2\int_0^t dt_1 \int_0^{t_1} \mathbf{Re}\left[F_2(t_1, t_2)\right] dt_2 \tag{3.96}$$

$$\begin{aligned} p_1^{(4)}(t) = {} & 2\int_0^t dt_1 \int_0^{t_1} dt_2 \int_0^{t_2} dt_3 \int_0^{t_3} \mathbf{Re}\left[F_4(t_1, t_2, t_3, t_4)\right] dt_4 \\ & + \int_0^t dt_1 \int_0^{t_1} dt_2 \int_0^{t} dt_3 \int_0^{t_3} \mathbf{Re}\left[F_4(t_2, t_1, t_3, t_4)\right] dt_4 \end{aligned} \tag{3.97}$$

etc for population terms in the perturbation theory sequence.

A neat pattern is a bit hard to see, but differentiating with time, we obtain:

$$\frac{p_1^{(2)}(t)}{dt} = -2\int_0^t \mathbf{Re}\left[F_2(t,t_1)\right]dt_1 \tag{3.98}$$

$$\frac{p_1^{(4)}(t)}{dt} = 2\mathbf{Re}\left[\int_0^t dt_1\int_0^{t_1} dt_2\int_0^{t_2} F_4(t,t_1,t_2,t_3)dt_3 + \int_0^t dt_1\int_0^t dt_2\int_0^{t_2} F_4(t_1,t,t_2,t_3)dt_3\right] \tag{3.99}$$

allowing us to see a pattern a bit more clearly. Although mathematically hard to explain, we can obtain any $\frac{p^{(2n)}(t)}{dt}$ in the following fashion:

1. **Number of terms:** There will be n time-integrals of F_{2n} over $2n-1$ time indices. The first term will be $F_{2n}(t,t_1,t_2,\ldots t_{2n-1})$, the next $F_{2n}(t_1,t,t_2,\ldots t_{2n-1})$, then $F_{2n}(t_2,t_1,t,\ldots t_{2n-1})$ and so on. Essentially the index t translates down the argument lane, with time indices on the left going in strictly decreasing order and time indices on the right strictly increase along the sequence. The maximum index on the left however has to be less than the minimum on the right. The translation of t only stops once it reaches the nth argument position of F_{2n}, having begun moving from the first.

2. **Limits of integration:** Each of the extra $2n-1$ time indices of the F_{2n} are integrated over. The limits of integration for the time-indices adjacent to the t variable run from $0 \to t$. All other indices t_i are integrated from $0 \to t_{i-1}$.

3. **Final processing:** Finally, the real part of the sum of all these integrals is taken and multiplied by $2(-1)^n$.

Odd order terms ignored as the corresponding traces are zero, and thus we have closed form expressions for all perturbation theory population growth rates.

3.7 Memory Kernels

It is possible to obtain populations directly from summing the various $p^{(2n)}$s in the perturbation theory power series. However summing a finite number of terms is problematic as each individual $p^{(2n)}(t)$ diverges as $t \to \infty$, and none of the finite term sums are convergent. Therefore this approach ceases to be viable after very short times, and we are forced to seek alternative routes. One attractive approach is to use a memory kernel formalism in the style of Mukamel [95] and we choose to work with generalized master equations of the form:

$$\frac{dp_1}{dt} = -\int_0^t K_{11}(t,t_1)p_1(t_1)dt_1 + \int_0^t K_{22}(t,t_1)p_2(t_1)dt_1 \tag{3.100}$$

$$= -\int_0^t K_{11}(t,t_1)p_1(t_1)dt_1 + \int_0^t K_{22}(t,t_1)\left(1-p_1(t_1)\right)dt_1 \tag{3.101}$$

$$= -\int_0^t \left(K_{11}(t,t_1)+K_{22}(t,t_1)\right)p_1(t_1)dt_1 + \int_0^t K_{22}(t,t_1)dt_1 \tag{3.102}$$

$$= -\int_0^t K_{+}(t,t_1)p_1(t_1)dt_1 + \int_0^t K_{22}(t,t_1)dt_1 \tag{3.103}$$

where $K_+(t) \equiv K_{11}(t) + K_{22}(t)$.

This expression is similar to kinetic rates, and similarly prevents populations from diverging by making decay rates increase with increasing population. It must be noted however that the memory kernel formalism does not prevent unphysical populations greater than 1 or less than 0, which can only be prevented by having good quality K_{11} and K_{22} kernels.

Like the populations, the kernels $K(t)$ can be expanded into a power series in terms of the off-diagonal coupling, enabling us to define $K^{(n)}(t,t_1)$ such that $K(t,t_1) = \sum_{n=0}^{\infty} K^{(n)}(t,t_1)$. We can find $K^{(n)}$ by expanding K and p_1 into perturbation theory power series and matching all terms with same order on both sides of the equation. For a two level state we have $p_1^{(n)} = 0$ for odd n due to all traces being zero, leading

to $K^{(2n+1)} = 0 \; \forall \; n \in \mathbb{Z}$. Therefore we only focus on even orders and have:

$$\frac{dp_1^{(2n)}}{dt} = \int_0^t \left(K_{22}^{(2n)}(t,t_1) - \sum_{m=0}^{n} K_+^{(2n-2m)}(t,t_1) p_1^{(2m)}(t_1) \right) dt_1 \tag{3.104}$$

$$= -\int_0^t \left(K_{11}^{(2n)}(t,t_1) + \sum_{m=1}^{n} K_+^{(2n-2m)}(t,t_1) p_1^{(2m)}(t_1) \right) dt_1 \tag{3.105}$$

since $p_1^{(0)}(t) = 1$ (no population transfer sans coupling) and $K_+(t) \equiv K_{11}(t) + K_{22}(t)$. Reorganizing, we have:

$$\int_0^t K_{11}^{(2n)}(t,t_1) dt_1 = -\frac{dp_1^{(2n)}}{dt} - \int_0^t \sum_{m=1}^{n} K_+^{(2n-2m)}(t,t_1) p_1^{(2m)}(t_1) dt_1 \tag{3.106}$$

We know that $K_{11}^{(0)}(t,t_1) = 0$ as no population transfer happens without coupling. For the next few higher orders we have:

$$\int_0^t K_{11}^{(2)}(t,t_1) dt_1 = -\frac{dp_1^{(2)}}{dt} \tag{3.107}$$

$$\int_0^t K_{11}^{(4)}(t,t_1) dt_1 = -\frac{dp_1^{(4)}}{dt} - \int_0^t K_+^{(2)}(t,t_1) p_1^{(2)}(t_1) dt_1 \tag{3.108}$$

$$\int_0^t K_{11}^{(6)}(t,t_1) dt_1 = -\frac{dp_1^{(6)}}{dt} - \int_0^t \left(K_+^{(4)}(t,t_1) p_1^{(2)}(t_1) + K_+^{(2)}(t,t_1) p_1^{(4)}(t_1) \right) dt_1 \tag{3.109}$$

etc. We quickly see that sequential evaluation is required as each $K^{(2n)}$ requires knowledge of lower order kernels. $\frac{dp_1^{(2n)}}{dt}$ contains time integrals going from $0 \to t$, and we can compare LHS and RHS to obtain expressions for $K_{11}^{(2n)}(t,t_1)$ that are not necessarily unique, but yield populations correct to order $2n$ in perturbation theory. This is however only possible because $K_+^{(2n)}$ can be found by evaluating $K_{22}^{(2n)}$ similarly to $K_{11}^{(2n)}$ (it involves merely flipping the sign of ϵ).

3.7.1 Photochemical Kernels

Using this approach along with the rules for finding $\frac{dp_1^{(2n)}}{dt}$ outlined in the previous section, we have:

$$\int_0^t K_{11}^{(2)}(t,t_1)dt_1 = -\frac{dp_1^{(2)}}{dt} = 2\mathbf{Re}\left[\int_0^t F_2(t,t_1)dt_1\right] \implies K_{11}^{(2)}(t,t_1) = 2\mathbf{Re}\left[F_2(t,t_1)dt_1\right] \tag{3.110}$$

is a valid Kernel. Similarly, we have:

$$\int_0^t K_{11}^{(4)}(t,t_1)dt_1 = -\frac{dp_1^{(4)}}{dt} - \int_0^t K_+^{(2)}(t,t_1)p_1^{(2)}(t_1)dt_1 \tag{3.111}$$

$$= -2\mathbf{Re}\left[\int_0^t dt_1 \int_0^{t_1} dt_2 \int_0^{t_2} F_4(t,t_1,t_2,t_3)dt_3 + \int_0^t dt_1 \int_0^t dt_2 \int_0^{t_2} F_4(t_1,t,t_2,t_3)dt_3\right]$$

$$- \int_0^t K_+^{(2)}(t,t_1)p_1^{(2)}(t_1)dt_1 \tag{3.112}$$

$$\implies K_{11}^{(4)}(t,t_1) = -2\mathbf{Re}\left[\int_0^{t_1} dt_2 \int_0^{t_2} F_4(t,t_1,t_2,t_3)dt_3 + \int_0^t dt_2 \int_0^{t_2} F_4(t_1,t,t_2,t_3)dt_3\right]$$

$$- K_+^{(2)}(t,t_1)p_1^{(2)}(t_1) \tag{3.113}$$

and so on and so forth. These are the Kernels we use for problems with photochemical starting conditions, due to the simplicity in obtaining them.

3.7.2 Thermal Kernels

If F_2 is time-translationally invariant (as in the case with thermal initial conditions), we can go a step further and define $K(t,t_1) = K(t-t_1)$, reducing the kernel to a function of a single variable similar to the projector operator formalism of Nakajima[96] and Zwanzig[97–99]. This allows us to uniquely define the kernel by differentiating

Eqn. 3.106 to obtain:

$$K_{11}^{(2n)}(t) = -\frac{d^2 p_1^{(2n)}}{dt^2} - \int_0^t \sum_{m=1}^{n} K_+^{(2n-2m)}(t-t_1)\dot{p}_1^{(2m)}(t_1)dt_1 \tag{3.114}$$

where $\dot{p}_1^{(2m)}(t)$ is the time derivative $\frac{dp_1^{(2n)}}{dt}$.

The thermal kernels to second and fourth order are thus (derivation for $K^{(4)}(t)$ found in the appendices):

$$K_{11}^{(2)}(t) = 2\mathbf{Re}\left[F_2(t,0)\right] \tag{3.115}$$

$$K_{11}^{(4)}(t) = -2\mathbf{Re}\left[\int_0^t dt_1 \int_0^{t_1} \left(F_4(t,t_1,t_2,0) + F_4(0,t,t_1,t_2)\right) dt_2 + \int_0^t dt_1 \int_0^t F_4(t_1,t,t_2,0)dt_2\right]$$
$$- \int_0^t K_+^{(2)}(t-t_1)\dot{p}_1^{(2)}(t_1)dt_1 \tag{3.116}$$

We also note that the integral of a single time-index kernel (as in the thermal case) from $0 \rightarrow \infty$ gives the long-time rate constant for the reaction.

3.8 Photochemical Dynamics of Iron self exchange

Having derived closed form expressions for thermal and photochemical kernels, we proceed to employ them to study the dynamics of Fe(II)-Fe(III) self-exchange as a simple model system. Small V and $\epsilon = 0$ indicates that this system can be treated with $K^{(2)}$ alone, allowing us to avoid computing the multiple expensive integrals needed to obtain $K^{(4)}$.

We obtained the required correlation functions via classical molecular dynamics using the GROMACS 4.6.5 software package [100] and TIP3P water. V was assumed to be proportional to the t_{2g} orbital overlap between the two iron atoms (which was calculated with a STO-16G basis) and was then employed to calculate cross-correlation and coupling fluctuation autocorrelation. The symmetry of this problem

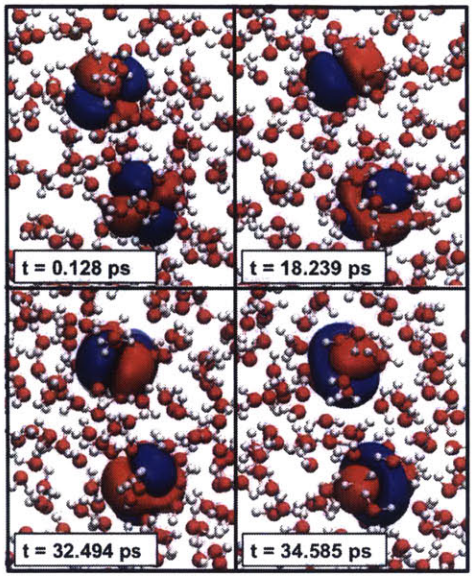

Figure 3-1: Change in orbital shapes (and consequently overlap) over the course of a single simulation. Figure taken from [5].

however led to cross-correlation being zero, which further simplified the problem. More details about the simulations may be found in our publication [5].

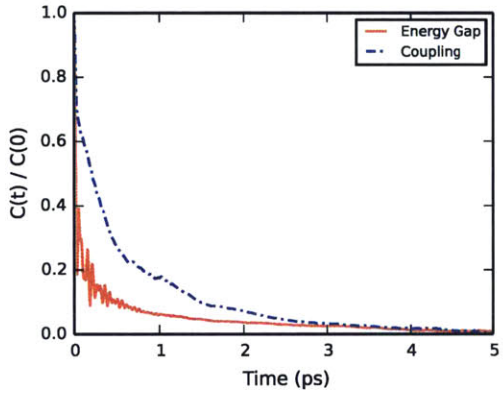

Figure 3-2: Correlation functions versus time. Figure taken from [5].

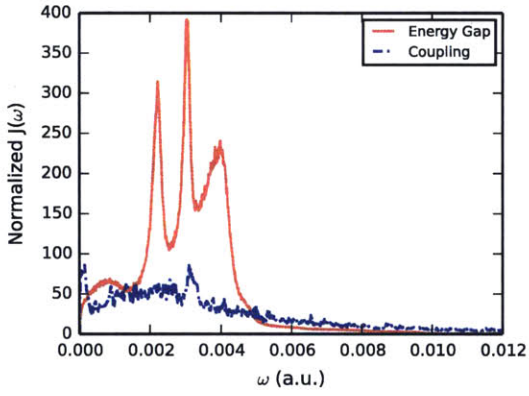

Figure 3-3: Spectral densities versus frequency. Figure taken from [5].

We observe substantial coupling fluctuation due to reorganization of the solvent sphere around the iron ions, which significantly affected orbital overlap (as shown in Fig. 3-1). This leads to a fairly large $\langle \delta V(t) \delta V(0) \rangle$ and correspondingly J_V, indicating that non-condon effects will play a major role in the dynamics.

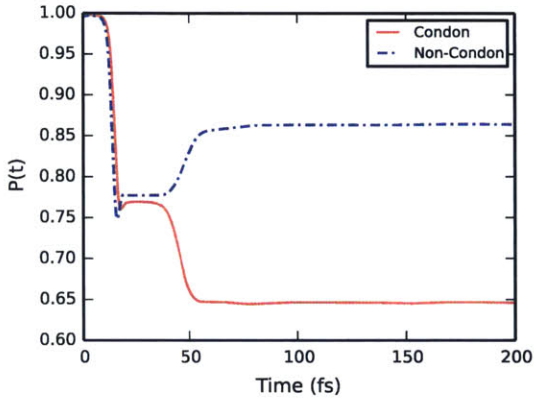

Figure 3-4: Dynamics with $V_{rms} = 573$ cm^{-1}.Figure taken from [5].

Our suspicions are proven correct as we observe a dramatic slowdown in diabatic population transfer on introducing non-condon effects (as show in in Fig. 3-4). This indicates that conical intersections play a major role in the dynamics, since the slowdown in diabatic population transfer implies a faster adiabatic population transfer, suggesting an adiabatic population "funnel" in the form of a conical intersection. We thus been able to obtain the impact of conical intersections on non-adiabatic dynamics with this simplified model, which can now be applied to more complex systems with confidence about its abilities to estimate the effect of such surface crossings.

3.9 Exact Solution for Slow Baths within the Condon Approximation

Having discussed the LVC model and procedures for solving it perturbatively in great details, we retreat back to the spin-boson model and attempt to figure out methods for solving it for large V, and potentially extend such methods to the LVC model by relaxing the Condon approximation. In the process we find that the spin-boson model can be exactly solved for very slow baths, and proceed to highlight the solution.

We have from 3.64 that for a thermal bath:

$$\ln f_2(t_1,t_2) = -i\epsilon(t_1-t_2) - \frac{4}{\pi}\int_0^\infty \frac{J(\omega)}{\omega^2}\left((1-\cos(\omega(t_1-t_2)))\coth\frac{\beta\omega}{2} + i\sin(\omega(t_1-t_2))\right)d\omega \tag{3.117}$$

For a very slow bath where $\omega \lll t$ for all ω with significant density of states, we may expand the sin and cos as Taylor series to obtain:

$$\ln f_2(t_1,t_2) = -a(t_1-t_2)^2 - i(\lambda+\epsilon)(t_1-t_2) \tag{3.118}$$

$$\lambda \equiv \frac{4}{\pi}\int_0^\infty \frac{J(\omega)}{\omega}d\omega, a \equiv \frac{2}{\pi}\int_0^\infty J(\omega)\coth\frac{\beta\omega}{2}d\omega \tag{3.119}$$

λ is the re-organization energy of the system as $\frac{4}{\pi}\int_0^\infty \frac{J(\omega)}{\omega}d\omega \equiv \sum \frac{2c_i^2}{m_i\omega_i^2}$, the potential energy stored in the modes of $\mathbf{h_2}$ when $\{x_i\}$ are at the equilibrium position of $\mathbf{h_1}$. The photochemical bath reduces to a similar gaussian form in the slow bath limit as well, and we believe that this is the case for all initial harmonic bath states.

Using 3.61 to calculate f_{2n}, we obtain:

$$f_{2n}(t_1,t_2,t_3\ldots t_{2n}) = f_2(t_1+t_3+t_5\ldots+t_{2n-1}, t_2+t_4\ldots+t_{2n}) \tag{3.120}$$

As a consequence of this we discover that perturbation theory population growth rate terms obey the following relationship:

$$\dot{p}^{(2n)}(t) = -\frac{2V^2}{n-1}\int_0^t t_1\dot{p}^{(2n-2)}(t_1)dt_1,\ \forall n>1, n\in\mathbb{Z}^+ \tag{3.121}$$

In Laplace space this becomes:

$$\dot{P}^{(2n)}(s) = \frac{2V^2}{n-1}\frac{1}{s}\frac{d}{ds}\dot{P}^{(2n-2)}(s) = \frac{1}{(n-1)!}\left(\frac{2V^2}{s}\frac{d}{ds}\right)^{n-1}\dot{P}^{(2)}(s) \tag{3.122}$$

We can now sum to infinite order easily and obtain:

$$\sum_{n=1}^{\infty} \dot{P}^{(2n)}(s) = \sum_{n=1}^{\infty} \frac{1}{(n-1)!} \left(\frac{2V^2}{s} \frac{d}{ds} \right)^{n-1} \dot{P}^{(2)}(s) = e^{\frac{2V^2}{s}\frac{d}{ds}} \dot{P}^{(2)}(s) \tag{3.123}$$

Now $e^{\frac{2V^2}{s}\frac{d}{ds}} = e^{4V^2\frac{d}{ds^2}}$ represents a translation in s^2. Therefore:

$$\dot{P}(s) = \sum_{n=1}^{\infty} \dot{P}^{(2n)}(s) = e^{4V^2\frac{d}{ds^2}} \dot{P}^{(2)}(\sqrt{s^2}) = \dot{P}^{(2)}(\sqrt{s^2 + 4V^2}) \tag{3.124}$$

In time domain this translates back to ([101]):

$$\dot{p}(t) = \sum_{n=1}^{\infty} \dot{p}^{(2n)}(t) = \dot{p}^{(2)}(t) - 2V \int_0^t J_1(2Vt_1)\dot{p}^{(2)}\left(\sqrt{t^2 - t_1^2}\right) dt_1 \tag{3.125}$$

Since f_2 itself is Gaussian, $\dot{p}_1^{(2)}(t) = -\mathbf{Re}\left[\frac{\sqrt{\pi}V^2 e^{-\frac{(\lambda+\epsilon)^2}{4a}} \mathrm{erf}\left(\frac{2at+i(\lambda+\epsilon)}{2\sqrt{a}}\right)}{\sqrt{a}}\right]$. Therefore we have:

$$\dot{p}_1(t) = V^2\sqrt{\frac{\pi}{a}} e^{-\frac{(\lambda+\epsilon)^2}{4a}} \mathbf{Re}\left[2V \int_0^t J_1(2Vt_1)\mathrm{erf}\left(\frac{2a\sqrt{t^2-t_1^2}+i(\lambda+\epsilon)}{2\sqrt{a}}\right) dt_1 - \mathrm{erf}\left(\frac{2at+i(\lambda+\epsilon)}{2\sqrt{a}}\right)\right] \tag{3.126}$$

We call this method GaussSB (Gaussian Spin-Boson).

3.9.1 Comparison to exact code

The accuracy of GaussSB populations were checked against numerically exact HEOM code for a Debye spectral density [81, 82, 102]. We also compare those to NIBA populations to see whether it can be applied in regimes where NIBA fails. Since $J(\omega) = \frac{\eta\omega_c\omega}{\omega_c^2 + \omega^2}$, the cutoff frequency ω_c controls the bath time-scale and is chosen to be 10^{-4} a.u. C++ code was written by the author employing the error function implementation by Johnson [103] and the GSL implementation of Quadpack integration routines [104, 105] to give the populations predicted by 3.126. While it is impossible

to achieve agreement to doubles precision on account of errors in the erf function [103] and HEOM truncation errors, we obtain essentially exact visual agreement.

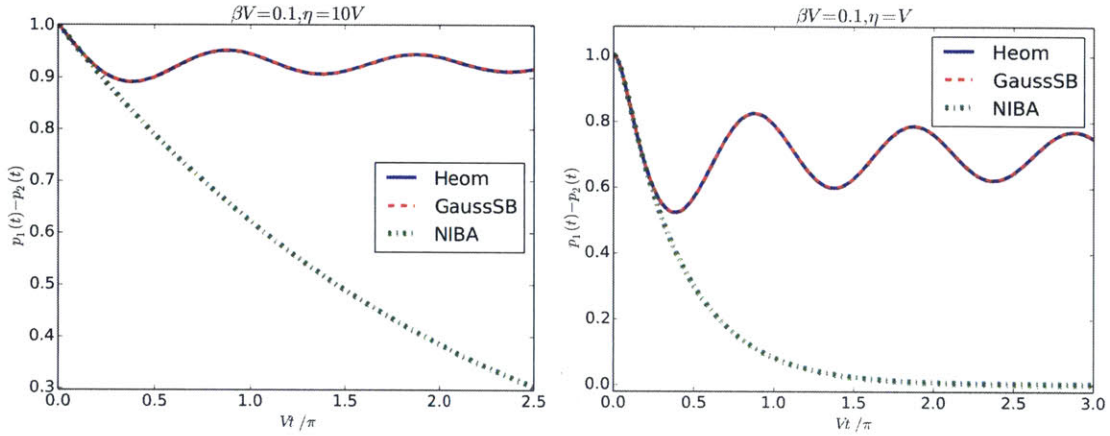

(a) High T, large λ. (b) High T, intermediate λ.

Figure 3-5: Comparison of HEOM, GaussSB and NIBA: I.

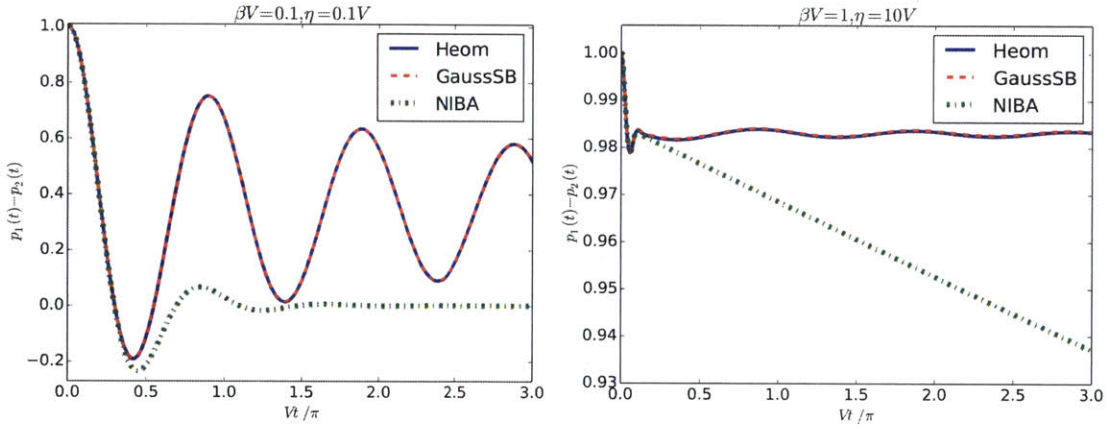

(a) High T, small λ. (b) Intermediate T, large λ.

Figure 3-6: Comparison of HEOM, GaussSB and NIBA: II.

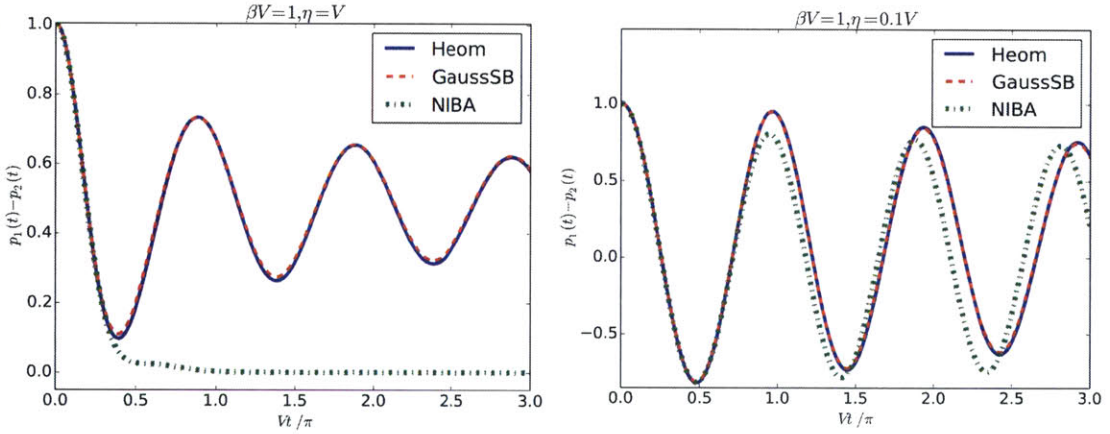

(a) Intermediate T and λ. (b) Intermediate T, small λ.

Figure 3-7: Comparison of HEOM, GaussSB and NIBA: III.

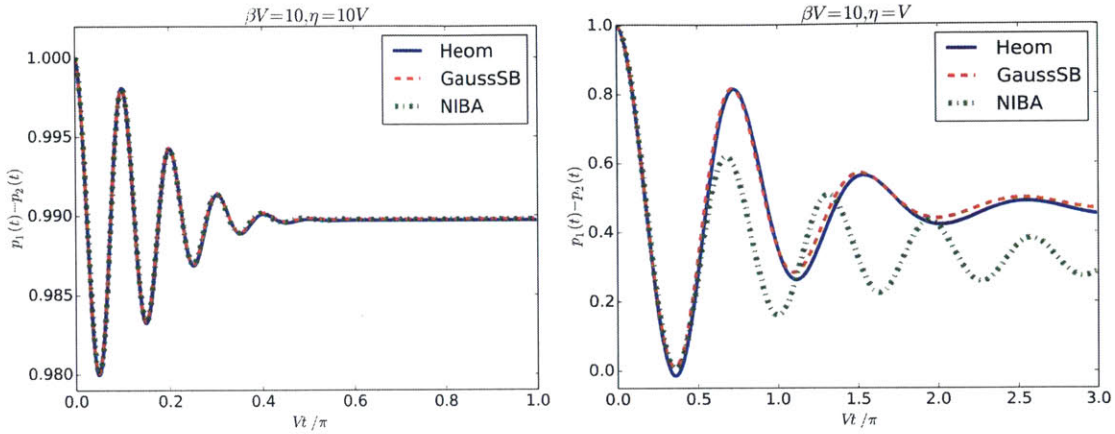

(a) Low T, large λ. (b) Low T, intermediate λ.

Figure 3-8: Comparison of HEOM, GaussSB and NIBA: IV.

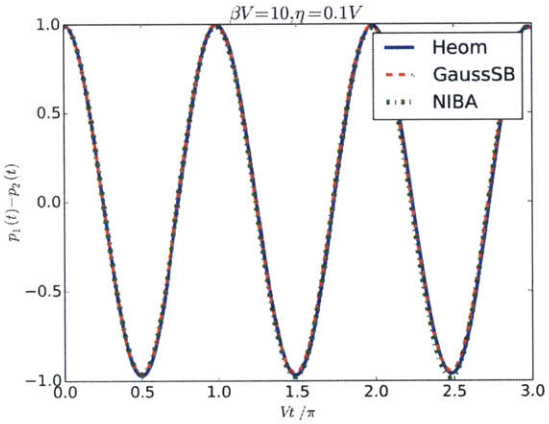

(a) Low T, small λ.

Figure 3-9: Comparison of HEOM, GaussSB and NIBA: V.

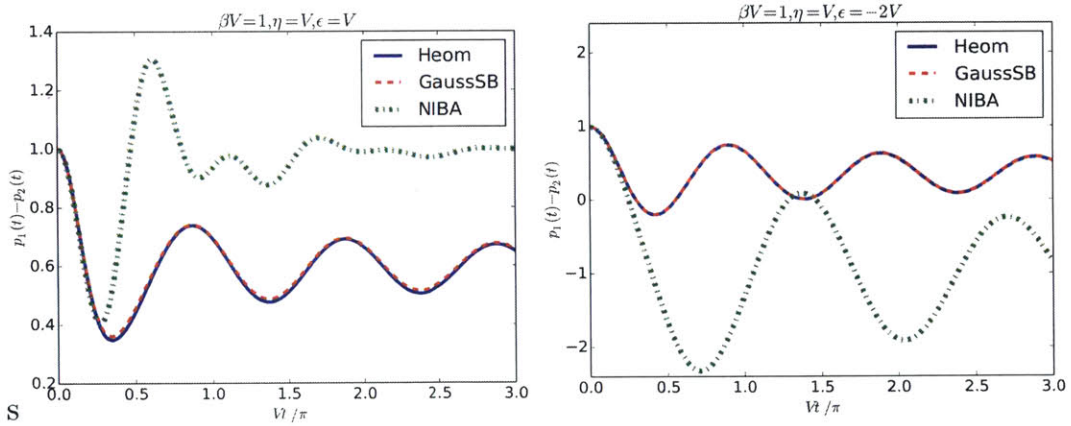

(a) Positive bias. (b) Negative bias.

Figure 3-10: Comparison of HEOM, GaussSB and NIBA: VI.

We also check cases with non-zero energy bias (where NIBA is prone to catas-

trophic failure) and obtain visual agreement there as well.

3.9.2 Non-exponential relaxation

In the event of zero energy bias ϵ, we have $K_{11}(t) = K_{22}(t)$ from symmetry. Consequently we have:

$$\frac{dp_1}{dt} = -\int_0^{t_1} K_{11}(t-t_1)\left(p_1(t_1) - p_2(t_1)\right) dt_1 \tag{3.127}$$

$$= -\int_0^{t_1} K_{11}(t-t_1)\left(2p_1(t_1) - 1\right) dt_1 \tag{3.128}$$

$$\implies \mathcal{L}\left[\frac{dp_1}{dt}\right] = \dot{P}_1(s) = -k_{11}(s)\left(2P_1(s) - \frac{1}{s}\right) \tag{3.129}$$

after taking a Laplace transform on both sides of the equation ($k(s)$ is the Laplace transform of $K(t)$).

From properties of Laplace transforms we also know that:

$$\dot{P}_1(s) = sP_1(s) - p_1(0) = sP_1(s) - 1 \implies P_1(s) = \frac{\dot{P}_1(s) + 1}{s} \tag{3.130}$$

Therefore, we have:

$$k_{11}(s) = \frac{\dot{P}_1(s)}{\frac{1}{s} - 2P_1(s)} = -\frac{s\dot{P}_1(s)}{1 + 2\dot{P}_1(s)} \tag{3.131}$$

The rate constant is the time-integral of $K_{11}(t)$ from $0 \to \infty$, and is thus $k(0)$, which is zero unless the denominator also goes to zero permitting some limit to be taken. This is in-fact what happens in real systems. However, for very slow baths we have from Eqns. 3.124 and 3.126 that

$$\dot{P}_1(s) = \dot{P}_1^{(2)}(\sqrt{s^2+4V^2}) = -\mathbf{Re}\left[\frac{\sqrt{\pi}V^2 e^{-\frac{(b-i\sqrt{s^2+4V^2})^2}{4a}}\left(1 - i\mathrm{erfi}\left(\frac{b-i\sqrt{s^2+4V^2}}{2\sqrt{a}}\right)\right)}{\sqrt{a(s^2+4V^2)}}\right] \tag{3.132}$$

$$\therefore \dot{P}_1(0) = -\mathbf{Re}\left[\frac{\sqrt{\pi}V^2 e^{-\frac{(b-2iV)^2}{4a}}\left(1 - i\mathrm{erfi}\left(\frac{b-2iV}{2\sqrt{a}}\right)\right)}{2V\sqrt{a}}\right] \neq -\frac{1}{2} \tag{3.133}$$

for arbitrary a, b, V. Therefore, the formal rate constant for the Gaussian bath system is zero, indicating non-exponential relaxation. This is interesting, but not particularly surprising, as a slow bath would take an enormous amount of time to relax to equilibrium, and can thus have a formal rate constant of near zero.

3.10 Many Level Systems

The LVC and spin-boson models suffer from a major drawback in that they are two level models while most excited state dynamics processes involve multiple levels. TADF itself involves no less than five for instance, encouraging us to attempt to generalize our results to many level problems.

We begin with the basic generalization of the spin-boson model, where:

$$\mathbf{H} = \sum_{\alpha=1}^{n} |\alpha\rangle\langle\alpha| \otimes \mathbf{h}_\alpha + \sum_{\alpha=1}^{n-1}\sum_{\beta=\alpha+1}^{n} V_{\alpha\beta}\left(|\alpha\rangle\langle\beta| + |\beta\rangle\langle\alpha|\right) \otimes \mathbf{I} \tag{3.134}$$

$$\mathbf{h}_\alpha = \epsilon_\alpha + \sum_i \left(\frac{\hat{p}_i^2}{2m_i} + \frac{1}{2}m_i\omega_i^2\left(\hat{x}_i + \frac{c_i^\alpha}{m_i\omega_i^2}\right)^2\right) \tag{3.135}$$

$\mathbf{h}_\alpha$ is the harmonic oscillator Hamiltonian associated with diabatic state α. We further define:

$$c_i^{\alpha\beta} \equiv c_i^\alpha - c_i^\beta \tag{3.136}$$

$$O_{\alpha\beta}(t) \equiv e^{i\mathbf{h}_\alpha t}e^{-i\mathbf{h}_\beta t} \tag{3.137}$$

$$F_n(t_1, t_2, t_3 \ldots t_n, \alpha_1, \alpha_2 \ldots \alpha_n, \alpha_{n+1}) \equiv \mathbf{Tr}\left[\rho_B \prod_{k=1}^{n} O_{\alpha_k\alpha_{k+1}}(t_k)\right] \tag{3.138}$$

Population current only flows if $\alpha_{n+1} = \alpha_1$, which by our convention about starting electronic state must be $|1\rangle$. With thermal initial conditions $\rho_B = \frac{e^{-\beta\mathbf{h}_1}}{\mathbf{Tr}\left[e^{-\beta\mathbf{h}_1}\right]}$,we

have:

$$F_n(t_1,t_2,t_3\ldots t_n,\alpha_1=1,\alpha_2\ldots\alpha_n,\alpha_{n+1}=1)=\frac{\mathbf{Tr}\left[e^{-\beta\mathbf{h}_1}e^{i\mathbf{h}_1 t_1}\left(\prod_{k=1}^{n-1}e^{i\mathbf{h}_{\alpha_{k+1}}(t_{k+1}-t_k)}\right)e^{-i\mathbf{h}_1 t_n}\right]}{\mathbf{Tr}\left[e^{-\beta\mathbf{h}_1}\right]} \tag{3.139}$$

We then have the following trace relationship:

$$\ln F_n=-\underbrace{\sum_i}_{\text{modes}}\sum_{k=1}^{n-1}\sum_{l=k+1}^{n}\frac{c_i^{\alpha_k\alpha_{k+1}}c_i^{\alpha_l\alpha_{l+1}}}{2m_i\omega_i^3}\left(\left(-1+\cos\left(\omega_i(t_k-t_l)\right)\right)\coth\frac{\beta\omega_i}{2}-i\sin\left(\omega_i(t_k-t_l)\right)\right) \tag{3.140}$$

$$=-\frac{4}{\pi}\sum_{k=1}^{n-1}\sum_{l=k+1}^{n}\int_0^\infty\frac{J_{kl}(\omega)}{\omega^2}\left(\left(-1+\cos\left(\omega(t_k-t_l)\right)\right)\coth\frac{\beta\omega}{2}-i\sin\left(\omega(t_k-t_l)\right)\right)d\omega \tag{3.141}$$

$$J_{kl}(\omega)=\frac{\beta\omega}{4}\int_0^\infty\langle\delta\Delta E_{\alpha_k\alpha_{k+1}}(t),\delta\Delta E_{\alpha_l\alpha_{l+1}}\cos\omega t\rangle dt \tag{3.142}$$

$$\delta\Delta E_{\alpha_i\beta_i}(t)=\Delta E_{\alpha_i\beta_i}(t)-\langle\Delta E_{\alpha_i\beta_i}(t)\rangle \tag{3.143}$$

$$\Delta E_{\alpha_i\beta_i}(t)=E_{\alpha_i}(t)-E_{\beta_i}(t) \tag{3.144}$$

In other words, $\ln F_n$ is a sum of all pairs of possible bath correlation functions with two time-ordered time indices. The weights of each of these functions depend on the energy-gap cross-correlation between the respective Hamiltonian pairs. This may be interpreted as follows: $O_{\alpha_i\alpha_{i+1}}(t_i)$ represents a "hop" from $|\alpha_i\rangle\rightarrow|\alpha_{i+1}\rangle$ in time t_i. Population current can only flow if we have a closed path of the form $|1\rangle\rightarrow|n\rangle\ldots\rightarrow|1\rangle$, otherwise all we will have is coherence. Thus, the traces are basically an expectation value of all the hops needed along that path. It therefore not unsurprising that we obtain an expression that is effectively the product of correlations between two hops, over all such possible pairs of hops. The correlation between hops depends on how the normal modes responsible couple, resulting the expression with spectral densities that tie it to the energy gap cross-correlation over each hop pairs.

While there is a great level of semblance, Eqn. 3.141 is however not strictly speaking a generalization of Eqn. 3.61 as it only holds for thermal conditions, while the more general Eqn. 3.61 holds for any harmonic initial conditions for systems with only two states. The photochemical conditions are trickier, and have so far not been amenable to such a closed form relationship, although we believe that one exists and will be discovered.

One final note is that with multiple levels in the picture, odd ordered kernels and populations are no longer zero beyond the first order (where they remain zero). Thus the complexity of the problem increases significantly, but not insurmountably. We are currently attempting to extend GaussSB for such systems with so far little success, but we hope that it will not be so for long.

3.11 Conclusion and Future Directions

In this chapter we described an approach for perturbatively solving spin-boson and LVC type systems and provided closed form expressions which can easily be generalized and applied to as high an order in perturbation theory as desired (or possible based on computing power). This enabled us to discover conical intersections in a model Fe(II)-Fe(III) self-exchange electron transfer, and also study effects of such surface crossings on the dynamics of the system. The obvious next step will be to apply this to larger chemical systems where conical intersections are observed in real life. Members of our group are already attempting to employ this method to study the effect of conical intersections on the keto-enol tautomerism of nucleic-acid bases, and we hope to study larger systems in the future.

We have also proposed a simple analytic exact solution to the spin-boson problem in the slow bath regime, which we have verified against HEOM. However this solution does not work for fast baths for timescales beyond the characteristic bath response time, and we now seek to adjust this method to handle moderately fast baths. We have noted that one of the issues with the GaussSB solution is that the memory kernel is too long lived, and we are currently exploring avenues to ensure that the kernel

decays at approximately the right rate at long times, using what we already know about perturbative solutions. Various interpolations and resummation techniques are currently under consideration, but we are yet to find an approach that will be satisfactory for fast baths in thr strong V regime.

Finally, we hope to extent GaussSB to the LVC model and to many level systems. We have been able to determine a trace relationship for many level systems (with thermal initial conditions) that allow us to write down simple closed form expressions for the populations, but an analytic solution still lies beyond reach. We hope to work out such an expression soon, and use it to study dynamics of organic semiconductor materials, and especially TADF.

Chapter 4

Conclusions and Future Directions

In the two preceding chapters we have explored how approximate quantum chemistry methods may be employed to determine properties and dynamics of electronic excited states. In particular, we discovered that while LR-TDDFT is not particularly effective for studying charge-transfer excited states, ROKS can give reasonably accurate numbers for such states with semi-local-hybrid functionals. This enables use of ROKS to study materials proposed as candidates for fabricating TADF OLEDs, and thus assist computational design of materials. However, we need to explicitly account for the effect of the condensed phase (solvent or host material) into our calculations, for even though experimental data indicates that they do not affect the stationary properties of the material all that much, we know from other dynamics studies that they will play a major role in dynamics and related parameters like quantum yields and energy efficiency.

We have also worked on developing quantum dynamics methods in order to be able to calculate such properties cheaply in condensed phases. Currently we are able to compute dynamics for the LVC model perturbatively to fourth order, which we then can resum to approximate higher orders. This has enabled us to determine the effect of conical intersections on non-adiabatic dynamics for a model Fe(II)-Fe(III) self-exchange reaction, indicating that non-Condon effects play a major role even in outer sphere electron transfer dynamics, even if they do not affect long term rates as much. We now hope to use our method on more complex systems, such as photochemistry of

DNA bases and potentially dynamics of electron transfer for organic semiconductors, where coupling is expected to fluctuate significantly based on conformations.

At the other limit we have attempted to solve the spin-boson model exactly for arbitrary coupling strengths. We have succeeded exactly in the slow bath limit, where we have obtained an exact analytic form for the population that is consistent with HEOM for Debye spectral densities. In future, we hope to generalize this solution to faster baths and other models like LVC, bringing us a step closer to obtaining numerically exact quantum dynamics for such models.

We have also begun working on extending our approaches to many-state problems, where we have already found a general form for the relevant traces, and can connect them together to obtain Kernels as well as potentially an exact slow bath solution. All these in combination would enable us to solve difficult problems regarding behavior of excited states, where we would be able to use ROKS to obtain the energy surfaces for each state, and then be able to witness their dynamics. This method can be employed to study TADF, exciton dynamics, conical intersections in photochemistry, photosynthesis and other processes of experiment, hopefully helping us design new material. Even if we are rather unfortunate and these methods fail to have sufficient predictive power, we would still be able to understand what phenomenon are consequential at the microscopic level, by recognizing the places where our approximations missed the mark. This is a long way off from "solving" all of chemistry, but it is a baby step in that direction, to be extended and refined over the years.

Appendix A

TADF Test-Set

A.1 Molecules Tested

The effectiveness of the four devised protocols were determined by comparison to experimental data for the following compounds (structures given in Figure A-1): 2CzPN[1], 4CzPN[1], 4CzTPN-Me[1], 4CzTPN[1], PIC-TRZ[1], ACRFLCN[1], α-NPD[1], PXZ-TAZ[2], DPA-DPS[1], PXZ-OXD[2], DTC-DPS[1, 4], CBP[1], CC2TA[1], DMAC-DPS[3], 2PXZ-OXD[2], DTPA-DPS[1], NPh3[1], PhCz[1], 4CzIPN[1], 2PXZ-TAZ[2], PXZ-DPS[3], PPZ-4TPT[3], DMOC-DPS[4], PPZ-DPS[3], PXZ-TRZ[1], PPZ-DPO[3] and PPZ-3TPT[3]. The calculated equilibrium geometries are provided in the associated geometry.zip file. Convergence failure prevented a couple of S_1 optimizations with the LC-ωPBE functional (specific instances are noted in the data tables below), and thus the provided geometry corresponds to the final structure before the calculations crashed.

A.2 Structures of tested molecules

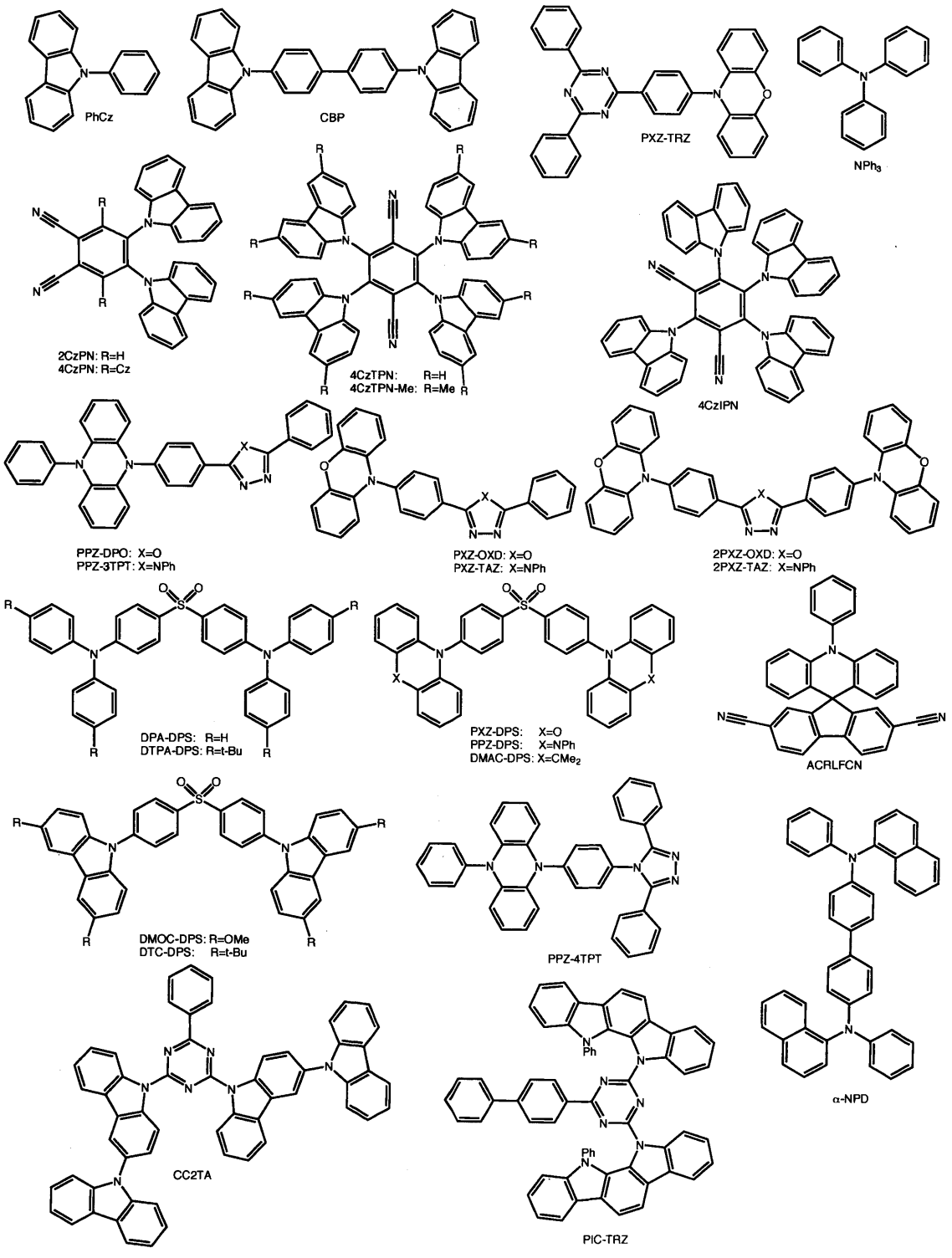

Figure A-1: Structures of all the molecules in the test-set[1–4].

A.3 PBE Functional Calculations

Compound	Expt.	Prot. A/B	Prot. C/D
2CzPN	3.19	2.01	2.68
4CzPN	2.82	1.61	2.23
4CzTPN-Me	2.49	1.40	2.09
4CzTPN	2.61	1.49	1.97
PIC-TRZ	3.35	1.90	2.54
ACRFLCN	3.05	1.71	3.01
a-NPD	3.31	2.26	2.46
PXZ-TAZ	3.33	1.85	2.73
DPA-DPS	3.53	2.80	2.78
PXZ-OXD	3.18	1.36	2.59
DTC-DPS	3.62	2.47	2.87
CBP	3.80	2.70	3.54
CC2TA	3.64	1.79	2.76
DMAC-DPS	3.38	1.88	2.61
2PXZ-OXD	3.12	1.19	2.05
DTPA-DPS	3.47	2.75	2.71
NPh3	3.74	3.30	3.36
PhCz	3.66	3.39	3.49
4CzIPN	2.85	1.66	2.16
2PXZ-TAZ	3.30	1.70	2.64
PXZ-DPS	3.13	1.54	2.29
PPZ-4TPT	3.34	1.68	2.42
DMOC-DPS	3.35	2.20	2.60
PPZ-DPS	2.76	1.20	1.92
PXZ-TRZ	2.73	1.13	2.65
PPZ-DPO	2.78	0.96	2.17
PPZ-3TPT	3.34	1.47	2.33

Table A.1: E_{abs} from PBE functional in eV. For Protocols A/B, RMS error is 1.38 eV and mean error -1.31 eV, while Protocols C/D have RMS error 0.69 eV and mean error -0.64 eV.

Table A.2: E_{em} from PBE functional in eV. Protocol A has RMS error 0.81 eV and mean error −0.75 eV; Protocol B has RMS error 1.48 eV and mean error −1.45 eV; Protocol C has RMS error 0.53 eV and mean error −0.49 eV; and Protocol D has RMS error 0.52 eV and mean error −0.48 eV.

Compound	Expt.	Prot. A	Prot. B	Prot. C	Prot. D
2CzPN	2.63	2.01	1.06	2.35	2.38
4CzPN	2.38	1.61	0.80	1.81	1.81
4CzTPN-Me	2.22	1.40	0.77	1.56	1.80
4CzTPN	2.32	1.49	0.85	1.55	1.56
PIC-TRZ	2.52	1.90	1.14	2.12	2.14
ACRFLCN	2.55	1.71	1.42	2.49	2.35
a-NPD	2.87	2.26	1.44	2.10	2.09
PXZ-TAZ	2.72	1.85	1.19	2.18	2.15
DPA-DPS	3.09	2.80	1.62	2.50	2.50
PXZ-OXD	2.50	1.36	0.97	2.09	2.07
DTC-DPS	3.07	2.47	1.49	2.62	2.59
CBP	3.40	2.70	2.09	2.50	2.47
CC2TA	2.63	1.79	1.13	2.30	2.35
DMAC-DPS	2.70	1.88	1.26	2.28	2.29
2PXZ-OXD	2.47	1.19	0.81	1.78	1.77
DTPA-DPS	2.96	2.75	1.52	2.41	2.41
NPh3	3.46	3.30	2.43	3.05	3.14
PhCz	3.43	3.39	3.18	3.26	3.21
4CzIPN	2.48	1.66	1.00	1.81	1.80
2PXZ-TAZ	2.68	1.70	1.05	1.91	1.89
PXZ-DPS	2.45	1.54	0.81	1.96	1.97
PPZ-4TPT	2.50	1.68	0.97	2.05	2.05
DMOC-DPS	2.79	2.20	1.04	2.42	2.42
PPZ-DPS	2.15	1.20	0.46	1.61	1.61
PXZ-TRZ	2.27	1.13	0.79	2.11	2.12
PPZ-DPO	2.15	0.96	0.56	1.84	1.83
PPZ-3TPT	2.35	1.47	0.77	1.97	1.96

Table A.3: E_{0-0} from PBE functional in eV. Experimental data was unavailable for a few of the molecules, and thus the corresponding slots have been left blank. Protocol A has RMS error 1.00 eV and mean error −0.95 eV; Protocol B has RMS error 1.30 eV and mean error −1.25 eV; Protocol C has RMS error 0.56 eV and mean error −0.54 eV; and Protocol D has RMS error 0.55 eV and mean error −0.52 eV.

Compound	Expt.	Prot. A	Prot. B	Prot. C	Prot. D
2CzPN	2.94	2.01	1.55	2.54	2.57
4CzPN	2.60	1.61	1.40	2.03	2.02
4CzTPN-Me	2.33	1.40	1.13	1.72	1.96
4CzTPN	2.43	1.49	1.26	1.75	1.75
PIC-TRZ	2.91	1.90	1.55	2.36	2.39
ACRFLCN	2.83	1.71	1.59	2.67	2.55
a-NPD	3.10	2.26	1.84	2.29	2.30
PXZ-TAZ		1.85	1.48	2.42	2.42
DPA-DPS	3.28	2.80	2.28	2.64	2.65
PXZ-OXD		1.36	1.18	2.26	2.27
DTC-DPS	3.34	2.47	2.08	2.75	2.74
CBP	3.54	2.70	2.43	2.73	2.76
CC2TA	3.15	1.79	1.52	2.55	2.57
DMAC-DPS	3.00	1.88	1.63	2.45	2.47
2PXZ-OXD		1.19	1.04	1.92	1.93
DTPA-DPS	3.19	2.75	2.18	2.56	2.56
NPh3	3.60	3.30	2.96	3.20	3.35
PhCz	3.58	3.39	3.40	3.36	3.45
4CzIPN	2.63	1.66	1.48	2.00	1.97
2PXZ-TAZ		1.70	1.34	2.11	2.11
PXZ-DPS	2.73	1.54	1.26	2.15	2.15
PPZ-4TPT	2.80	1.68	1.31	2.23	2.24
DMOC-DPS	3.12	2.20	1.69	2.52	2.51
PPZ-DPS	2.40	1.20	0.87	1.77	1.76
PXZ-TRZ	2.53	1.13	0.97	2.23	2.25
PPZ-DPO	2.40	0.96	0.77	2.00	2.00
PPZ-3TPT	2.65	1.47	1.07	2.14	2.15

Table A.4: ΔE_{ST} from PBE functional in meV. Experimental data was unavailable for a few of the molecules, and thus the corresponding slots have been left blank. Some of the calculated numbers were negative, and thus were excluded from the log error calculation. Protocol A has log RMS error is 0.92 and log mean error -0.74; Protocol B has log RMS error 1.45 and log mean error -1.34; Protocol C has log RMS error 0.73 and log mean error -0.55; and Protocol D has log RMS error 0.49 and log mean error -0.34.

Compound	Expt.	Prot. A	Prot. B	Prot. C	Prot. D
2CzPN	310	163	9	202	225
4CzPN	150	81	8	13	-1
4CzTPN-Me	90	50	9	-18	223
4CzTPN	90	71	11	-10	-8
PIC-TRZ	180	34	26	64	92
ACRFLCN	240	6	8	342	228
a-NPD	730	140	15	124	136
PXZ-TAZ		6	4	167	173
DPA-DPS	520	295	26	114	117
PXZ-OXD		5	4	178	192
DTC-DPS	360	119	2	81	76
CBP	710	177	118	248	276
CC2TA	200	13	23	62	81
DMAC-DPS	90	6	2	1	25
2PXZ-OXD		4	3	80	95
DTPA-DPS	460	278	32	80	83
NPh3	570	400	171	228	383
PhCz	550	402	466	291	382
4CzIPN	100	69	11	14	-16
2PXZ-TAZ		4	3	76	77
PXZ-DPS	80	5	2	6	10
PPZ-4TPT	420	10	3	142	149
DMOC-DPS	240	109	1	63	57
PPZ-DPS	90	5	2	-5	-17
PXZ-TRZ	60	4	4	94	109
PPZ-DPO	90	4	3	106	108
PPZ-3TPT	270	5	3	122	126

A.4 B3LYP Functional Calculations

Table A.5: E_{abs} from B3LYP functional in eV. The numbers in brackets for Protocols C/D are from the cc-pVTZ basis set (some calculations crashed for a few of the larger molecules, leading to blanks). The larger basis introduces an RMS red-shift of about 0.08 eV for both protocols, which however does not affect the overall conclusions. For Protocols A/B, RMS error is 0.57 eV and mean error −0.45 eV, while Protocols C/D have RMS error 0.18 eV and mean error −0.06 eV. All the reported errors correspond to the 6-31G* calculations alone.

Compound	Expt.	Prot. A/B	Prot. C/D
2CzPN	3.19	2.84	3.16 (3.14)
4CzPN	2.82	2.47	2.74 (2.72)
4CzTPN-Me	2.49	2.21	2.44 (2.40)
4CzTPN	2.61	2.26	2.47 (2.43)
PIC-TRZ	3.35	2.82	3.24
ACRFLCN	3.05	2.55	3.25 (3.17)
a-NPD	3.31	3.07	3.22 (3.14)
PXZ-TAZ	3.33	2.74	3.33 (3.27)
DPA-DPS	3.53	3.53	3.52 (3.42)
PXZ-OXD	3.18	2.31	3.12 (3.07)
DTC-DPS	3.62	3.31	3.55
CBP	3.80	3.56	3.68 (3.60)
CC2TA	3.64	2.92	3.45
DMAC-DPS	3.38	2.75	3.27 (3.19)
2PXZ-OXD	3.12	2.21	2.79 (2.77)
DTPA-DPS	3.47	3.47	3.48
NPh3	3.74	3.93	3.92 (3.69)
PhCz	3.66	4.04	4.02 (3.89)
4CzIPN	2.85	2.50	2.65 (2.64)
2PXZ-TAZ	3.30	2.63	3.28 (3.22)
PXZ-DPS	3.13	2.46	2.96 (2.89)
PPZ-4TPT	3.34	2.53	2.95 (2.85)
DMOC-DPS	3.35	3.10	3.34 (3.26)
PPZ-DPS	2.76	2.05	2.75
PXZ-TRZ	2.73	2.10	2.97 (2.93)
PPZ-DPO	2.78	1.90	2.68 (2.63)
PPZ-3TPT	3.34	2.34	2.89 (2.81)

Table A.6: E_{em} from B3LYP functional in eV. The labels R and U for Protocol D describes whether the triplet geometries were obtained via RODFT or UODFT respectively. The numbers in brackets for Protocols C and D are from the cc-pVTZ basis set (some calculations crashed for a few of the larger molecules, leading to blanks). The larger basis introduces an RMS red-shift of about 0.07 eV for both protocols, which however does not affect the overall conclusions. Protocol A has RMS error 0.25 eV and mean error 0.11 eV; Protocol B has RMS error 0.65 eV and mean error −0.62 eV; Protocol C has RMS error 0.19 eV and mean error −0.001 eV; and Protocol D has RMS error 0.22 eV and mean error 0.02 eV with RODFT; and RMS error 0.23 eV with mean error 0.01 eV when used with UODFT. All the reported errors correspond to the 6-31G* calculations alone.

Compound	Expt.	Prot. A	Prot. B	Prot. C	Prot. D (R)	Prot. D (U)
2CzPN	2.63	2.84	1.85	2.66 (2.65)	2.79 (2.76)	2.78
4CzPN	2.38	2.47	1.55	2.11 (2.10)	2.25 (2.24)	2.25
4CzTPN-Me	2.22	2.21	1.41	1.87	2.07 (2.03)	2.00
4CzTPN	2.32	2.26	1.50	1.98 (1.96)	2.01 (1.99)	2.00
PIC-TRZ	2.52	2.82	1.79	2.54 (2.52)	2.70	2.72
ACRFLCN	2.55	2.55	2.12	2.77 (2.71)	2.83 (2.76)	2.82
a-NPD	2.87	3.07	2.19	2.72 (2.64)	2.62 (2.55)	2.62
PXZ-TAZ	2.72	2.74	2.10	2.72 (2.66)	2.63 (2.57)	2.62
DPA-DPS	3.09	3.53	2.59	3.11 (3.02)	3.10 (3.01)	3.10
PXZ-OXD	2.5	2.31	1.82	2.58 (2.53)	2.49 (2.44)	2.47
DTC-DPS	3.07	3.31	2.52	3.21	3.17	3.17
CBP	3.40	3.56	2.87	2.99 (2.91)	2.87 (2.79)	2.85
CC2TA	2.63	2.92	1.87	2.66	2.74	2.69
DMAC-DPS	2.70	2.75	2.27	2.90 (2.84)	3.27 (3.18)	3.29
2PXZ-OXD	2.47	2.21	1.70	2.37 (2.35)	2.28 (2.26)	2.26
DTPA-DPS	2.96	3.47	2.46	3.03	3.04	3.04
NPh3	3.46	3.93	3.13	3.56 (3.39)	3.51 (3.40)	3.51
PhCz	3.43	4.04	3.74	3.75 (3.65)	3.75 (3.64)	3.68
4CzIPN	2.48	2.50	1.70	2.20 (2.19)	2.26 (2.25)	2.25
2PXZ-TAZ	2.68	2.63	1.99	2.54 (2.51)	2.47 (2.43)	2.46
PXZ-DPS	2.45	2.46	1.81	2.52 (2.46)	2.53 (2.46)	2.53
PPZ-4TPT	2.50	2.53	1.88	2.50 (2.42)	2.49 (2.40)	2.49
DMOC-DPS	2.79	3.10	2.16	3.00 (2.91)	3.00 (2.92)	3.00
PPZ-DPS	2.15	2.05	1.45	2.23	2.29	2.29
PXZ-TRZ	2.27	2.10	1.62	2.51 (2.47)	2.51 (2.46)	2.50
PPZ-DPO	2.15	1.90	1.38	2.25 (2.21)	2.25 (2.21)	2.25
PPZ-3TPT	2.35	2.34	1.66	2.43 (2.37)	2.43 (2.37)	2.43

Table A.7: E_{0-0} from B3LYP functional in eV. Experimental data was unavailable for a few of the molecules, and thus the corresponding slots have been left blank. The labels R and U for Protocol D describes whether the triplet geometries were obtained via RODFT or UODFT respectively. The numbers in brackets for Protocols C and D are from the cc-pVTZ basis set (some calculations crashed for a few of the larger molecules, leading to blanks). The larger basis introduces an RMS shift of about 0.05 eV for both protocols, which however does not affect the overall conclusions. Protocol A has RMS error 0.26 eV and mean error −0.10 eV; Protocol B has RMS error 0.52 eV and mean error −0.46 eV; Protocol C has RMS error 0.14 eV and mean error 0.02 eV; Protocol D has RMS error 0.23 eV and mean error 0.10 eV with RODFT; and RMS error 0.24 eV with mean error 0.09 eV when used with UODFT. All the reported errors correspond to the 6-31G* calculations alone.

Compound	Expt.	Prot. A	Prot. B	Prot. C	Prot. D (R)	Prot. D (U)
2CzPN	2.94	2.84	2.28	2.95 (2.96)	3.03 (3.04)	3.04
4CzPN	2.60	2.47	2.04	2.46 (2.45)	2.49 (2.51)	2.49
4CzTPN-Me	2.33	2.21	1.81	2.20	2.26	2.22
4CzTPN	2.43	2.26	1.9	2.24 (2.23)	2.24 (2.25)	2.24
PIC-TRZ	2.91	2.82	2.35	2.91	3.09	3.16
ACRFLCN	2.83	2.55	2.34	3.02 (2.97)	3.17 (3.12)	3.19
a-NPD	3.10	3.07	2.65	2.97 (2.90)	3.01 (2.94)	3.02
PXZ-TAZ		2.74	2.41	3.03 (3.01)	3.06 (3.05)	3.07
DPA-DPS	3.28	3.53	3.11	3.33 (3.26)	3.39 (3.33)	3.39
PXZ-OXD		2.31	2.07	2.82 (2.81)	2.85 (2.85)	2.86
DTC-DPS	3.34	3.31	2.91	3.41	3.48	3.49
CBP	3.54	3.56	3.24	3.30 (3.24)	3.41 (3.26)	3.32
CC2TA	3.15	2.92	2.43	3.09	3.09	3.08
DMAC-DPS	3.00	2.75	2.54	3.11 (3.06)	3.66 (3.63)	3.69
2PXZ-OXD		2.21	1.95	2.58 (2.59)	2.61 (2.63)	2.61
DTPA-DPS	3.19	3.47	3.02	3.27	3.32	3.33
NPh3	3.60	3.93	3.65	3.74 (3.60)	3.86 (3.78)	3.86
PhCz	3.58	4.04	3.9	3.88 (3.81)	4.14 (4.05)	4.08
4CzIPN	2.63	2.5	2.12	2.46 (2.45)	2.46 (2.47)	2.45
2PXZ-TAZ		2.63	2.31	2.84 (2.85)	2.88 (2.89)	2.89
PXZ-DPS	2.73	2.46	2.17	2.78 (2.75)	2.78 (2.76)	2.78
PPZ-4TPT	2.80	2.53	2.22	2.73 (2.66)	2.74 (2.66)	2.74
DMOC-DPS	3.12	3.1	2.59	3.21 (3.13)	3.27 (3.21)	3.27
PPZ-DPS	2.40	2.05	1.78	2.51	2.52	2.52
PXZ-TRZ	2.53	2.1	1.87	2.73 (2.71)	2.76 (2.75)	2.76
PPZ-DPO	2.40	1.9	1.65	2.47 (2.44)	2.47 (2.44)	2.47
PPZ-3TPT	2.65	2.34	1.99	2.66 (2.61)	2.67 (2.62)	2.67

Table A.8: ΔE_{ST} from B3LYP functional in eV. The labels R and U for Protocols C and D describes whether the T_1 state was obtained via RODFT or UODFT respectively. Experimental data was unavailable for a few of the molecules, and thus the corresponding slots have been left blank. Some of the calculated numbers were negative, and thus were excluded from the log error calculation. The numbers in brackets for Restricted calculations with Protocols C and D are from the cc-pVTZ basis set (some calculations crashed for a few of the larger molecules, leading to blanks). The larger basis introduces some shift which however does not affect the overall conclusions. Protocol A has log RMS error is 0.68 and log mean error −0.37; Protocol B has log RMS error 1.04 and log mean error −0.85; Protocol C has log RMS error 0.35 and log mean error −0.20 with RODFT; and log RMS error 0.16 and log mean error 0.00 with UODFT. Finally, Protocol D has log RMS error 0.35 and log mean error −0.03 with RODFT, and log RMS error 0.31 and log mean error 0.12 with UODFT. All the reported errors correspond to the 6-31G* calculations alone.

Compound	Expt.	Prot. A	Prot. B	Prot. C (R)	Prot. C (U)	Prot. D (R)	Prot. D (U)
2CzPN	310	340	10	284 (274)	394	357 (352)	477
4CzPN	150	179	10	13 (-26)	71	48 (41)	105
4CzTPN-Me	90	107	10	-13	49	47	64
4CzTPN	90	129	-3	52 (50)	108	44 (67)	99
PIC-TRZ	180	78	28	129	198	308	448
ACRFLCN	240	8	10	354 (313)	439	500 (468)	613
a-NPD	730	582	513	370 (365)	430	411 (408)	479
PXZ-TAZ		11	7	353 (333)	413	382 (372)	447
DPA-DPS	520	636	395	341 (320)	403	407 (397)	472
PXZ-OXD		8	6	324 (304)	387	356 (347)	424
DTC-DPS	360	337	80	265	324	341	404
CBP	710	596	753	497 (487)	570	610 (505)	597
CC2TA	200	66	55	53	139	53	135
DMAC-DPS	90	9	9	79 (53)	146	631 (614)	727
2PXZ-OXD		20	6	175 (167)	224	202 (208)	259
DTPA-DPS	460	606	338	307	369	363	428
NPh3	570	745	699	460 (359)	540	582 (536)	661
PhCz	550	852	1007	599 (571)	702	863 (813)	908
4CzIPN	100	126	10	35 (23)	92	27 (42)	83
2PXZ-TAZ		9	6	215 (211)	267	247 (255)	315
PXZ-DPS	80	38	8	20 (-21)	66	18 (-11)	62
PPZ-4TPT	420	57	6	239 (244)	289	254 (244)	306
DMOC-DPS	240	280	6	177 (162)	232	239 (244)	301
PPZ-DPS	90	7	7	131	178	134	181
PXZ-TRZ	60	6	5	197 (176)	255	228 (220)	287
PPZ-DPO	90	6	5	135 (132)	179	141 (140)	185
PPZ-3TPT	270	8	5	195 (196)	241	207 (205)	255

A.5 PBE0 Functional Calculations

Table A.9: E_{abs} from PBE0 functional in eV. For Protocols A/B, RMS error is 0.43 eV and mean error −0.28 eV, while Protocols C/D have RMS error 0.28 eV and mean error 0.11 eV.

Compound	Expt.	Prot. A/B	Prot. C/D
2CzPN	3.19	3.03	3.31
4CzPN	2.82	2.66	2.83
4CzTPN-Me	2.49	2.41	2.61
4CzTPN	2.61	2.45	3.31
PIC-TRZ	3.35	3.03	3.35
ACRFLCN	3.05	2.73	3.29
a-NPD	3.31	3.22	3.36
PXZ-TAZ	3.33	2.90	3.41
DPA-DPS	3.53	3.63	3.63
PXZ-OXD	3.18	2.50	3.20
DTC-DPS	3.62	3.47	3.67
CBP	3.80	3.73	4.73
CC2TA	3.64	3.16	3.66
DMAC-DPS	3.38	2.91	3.35
2PXZ-OXD	3.12	2.39	3.12
DTPA-DPS	3.47	3.57	3.56
NPh3	3.74	4.05	4.04
PhCz	3.66	4.16	4.16
4CzIPN	2.85	2.70	2.78
2PXZ-TAZ	3.30	2.81	3.38
PXZ-DPS	3.13	2.65	3.04
PPZ-4TPT	3.34	2.69	3.04
DMOC-DPS	3.35	3.29	3.47
PPZ-DPS	2.76	2.20	2.80
PXZ-TRZ	2.73	2.28	3.02
PPZ-DPO	2.78	2.09	2.76
PPZ-3TPT	3.34	2.51	2.97

Table A.10: E_{em} from PBE0 functional in eV. Protocol A has RMS error 0.35 eV and mean error 0.28 eV; Protocol B has RMS error 0.49 eV and mean error −0.44 eV; Protocol C has RMS error 0.20 eV and mean error 0.10 eV; and Protocol D has RMS error 0.23 eV and mean error 0.11 eV.

Compound	Expt.	Prot. A	Prot. B	Prot. C	Prot. D
2CzPN	2.63	3.03	2.00	2.73	2.89
4CzPN	2.38	2.66	1.80	2.36	2.45
4CzTPN-Me	2.22	2.41	1.57	2.09	2.13
4CzTPN	2.32	2.45	1.66	2.09	2.12
PIC-TRZ	2.52	3.03	2.03	2.62	2.88
ACRFLCN	2.55	2.73	2.28	2.94	2.84
a-NPD	2.87	3.22	2.40	2.83	2.74
PXZ-TAZ	2.72	2.90	2.29	2.84	2.74
DPA-DPS	3.09	3.63	2.77	3.21	3.20
PXZ-OXD	2.50	2.50	2.01	2.68	2.59
DTC-DPS	3.07	3.47	2.63	3.32	3.29
CBP	3.40	3.73	3.10	3.13	2.99
CC2TA	2.63	3.16	2.11	2.83	2.83
DMAC-DPS	2.70	2.91	2.39	2.94	2.91
2PXZ-OXD	2.47	2.39	1.90	2.49	2.39
DTPA-DPS	2.96	3.57	2.57	3.11	3.13
NPh3	3.46	4.05	3.32	3.51	3.62
PhCz	3.43	4.16	3.94	3.88	3.91
4CzIPN	2.48	2.70	1.86	2.37	2.43
2PXZ-TAZ	2.68	2.81	2.18	2.67	2.62
PXZ-DPS	2.45	2.65	1.95	2.59	2.60
PPZ-4TPT	2.50	2.69	2.05	2.57	2.57
DMOC-DPS	2.79	3.29	2.35	3.11	3.30
PPZ-DPS	2.15	2.20	1.55	2.21	2.18
PXZ-TRZ	2.27	2.28	1.79	2.55	2.57
PPZ-DPO	2.15	2.09	1.57	2.31	2.32
PPZ-3TPT	2.35	2.51	1.84	2.50	2.51

Table A.11: E_{0-0} from PBE0 functional in eV. Experimental data was unavailable for a few of the molecules, and thus the corresponding slots have been left blank. Protocol A has RMS error 0.23 eV and mean error 0.07 eV; Protocol B has RMS error 0.37 eV and mean error −0.28 eV; Protocol C has RMS error 0.17 eV and mean error 0.11 eV; and Protocol D has RMS error 0.27 eV and mean error 0.19 eV.

Compound	Expt.	Prot. A	Prot. B	Prot. C	Prot. D
2CzPN	2.94	3.03	2.48	3.05	3.14
4CzPN	2.60	2.66	2.29	2.63	2.69
4CzTPN-Me	2.33	2.41	1.99	2.33	2.33
4CzTPN	2.43	2.45	2.10	2.34	2.36
PIC-TRZ	2.91	3.03	2.55	2.99	3.32
ACRFLCN	2.83	2.73	2.51	3.20	3.22
a-NPD	3.10	3.22	2.83	3.10	3.15
PXZ-TAZ		2.90	2.59	3.12	3.17
DPA-DPS	3.28	3.63	3.26	3.43	3.51
PXZ-OXD		2.50	2.26	2.90	2.96
DTC-DPS	3.34	3.47	3.09	3.51	3.64
CBP	3.54	3.73	3.46	3.44	3.46
CC2TA	3.15	3.16	2.66	3.21	3.21
DMAC-DPS	3.00	2.91	2.67	3.16	3.32
2PXZ-OXD		2.39	2.14	2.69	2.74
DTPA-DPS	3.19	3.57	3.15	3.35	3.43
NPh3	3.60	4.05	3.84	3.84	3.99
PhCz	3.58	4.16	4.09	4.01	4.31
4CzIPN	2.63	2.70	2.35	2.60	2.62
2PXZ-TAZ		2.81	2.48	2.95	3.03
PXZ-DPS	2.73	2.65	2.30	2.84	2.85
PPZ-4TPT	2.80	2.69	2.37	2.80	2.83
DMOC-DPS	3.12	3.29	2.77	3.31	3.51
PPZ-DPS	2.40	2.20	1.90	2.45	2.44
PXZ-TRZ	2.53	2.28	2.04	2.76	2.81
PPZ-DPO	2.40	2.09	1.83	2.53	2.55
PPZ-3TPT	2.65	2.51	2.16	2.73	2.77

Table A.12: ΔE_{ST} from PBE0 functional in meV. Experimental data was unavailable for a few of the molecules, and thus the corresponding slots have been left blank. Protocol A has log RMS error is 0.45 and log mean error −0.09; Protocol B has log RMS error 0.85 and log mean error −0.60; Protocol C has log RMS error 0.27 and log mean error −0.07; and Protocol D has log RMS error 0.32 and log mean error 0.04.

Compound	Expt.	Prot. A	Prot. B	Prot. C	Prot. D
2CzPN	310	477	12	316	410
4CzPN	150	276	51	130	190
4CzTPN-Me	90	154	60	65	71
4CzTPN	90	177	58	92	105
PIC-TRZ	180	215	38	158	486
ACRFLCN	240	134	13	468	483
a-NPD	730	805	814	445	496
PXZ-TAZ		144	203	388	438
DPA-DPS	520	767	587	423	504
PXZ-OXD		11	9	349	403
DTC-DPS	360	460	255	332	457
CBP	710	785	1028	573	599
CC2TA	200	181	66	81	82
DMAC-DPS	90	13	14	141	294
2PXZ-OXD		10	8	204	249
DTPA-DPS	460	727	510	386	465
NPh3	570	936	960	529	679
PhCz	550	1062	1278	676	980
4CzIPN	100	213	29	76	92
2PXZ-TAZ		45	9	261	344
PXZ-DPS	80	98	11	29	40
PPZ-4TPT	420	243	9	270	304
DMOC-DPS	240	397	9	318	517
PPZ-DPS	90	10	10	12	11
PXZ-TRZ	60	8	8	202	254
PPZ-DPO	90	9	7	136	153
PPZ-3TPT	270	51	8	213	245

A.6 LC-ωPBE Functional Calculations

Table A.13: E_{abs} from LC-ωPBE functional in eV. For Protocols A/B, RMS error is 0.74 eV and mean error 0.72 eV, while Protocols C/D have RMS error 0.82 eV and mean error 0.75 eV.

Compound	Expt.	Prot. A/B	Prot. C/D
2CzPN	3.19	3.98	3.85
4CzPN	2.82	3.65	3.52
4CzTPN-Me	2.49	3.45	3.45
4CzTPN	2.61	3.36	3.44
PIC-TRZ	3.35	4.13	4.22
ACRFLCN	3.05	4.21	3.74
a-NPD	3.31	4.01	4.64
PXZ-TAZ	3.33	4.02	4.06
DPA-DPS	3.53	4.22	4.80
PXZ-OXD	3.18	3.80	3.54
DTC-DPS	3.62	4.34	4.35
CBP	3.80	4.47	4.93
CC2TA	3.64	4.34	4.38
DMAC-DPS	3.38	4.02	4.48
2PXZ-OXD	3.12	3.74	3.47
DTPA-DPS	3.47	4.19	4.76
NPh3	3.74	4.59	4.81
PhCz	3.66	4.48	4.76
4CzIPN	2.85	3.58	3.58
2PXZ-TAZ	3.30	4.08	3.84
PXZ-DPS	3.13	3.81	3.59
PPZ-4TPT	3.34	3.58	3.58
DMOC-DPS	3.35	4.09	4.17
PPZ-DPS	2.76	3.47	3.16
PXZ-TRZ	2.73	3.71	3.34
PPZ-DPO	2.78	3.49	3.15
PPZ-3TPT	3.34	3.58	3.58

Table A.14: E_{em} from LC-ωPBE functional in eV. A few of the S_1 optimizations for Protocol C failed to converge, and the corresponding spaces have been left blank. Protocol A has RMS error 1.28 eV and mean error 1.29 eV; Protocol B has RMS error 0.66 eV and mean error 0.63 eV; Protocol C has RMS error 0.79 eV and mean error 0.45 eV; and Protocol D has RMS error 0.85 eV and mean error 0.79 eV.

Compound	Expt.	Prot. A	Prot. B	Prot. C	Prot. D
2CzPN	2.63	3.98	3.32	3.10	3.43
4CzPN	2.38	3.65	3.15		3.10
4CzTPN-Me	2.22	3.45	2.82		2.87
4CzTPN	2.32	3.36	2.86		2.90
PIC-TRZ	2.52	4.13	3.75	2.91	2.99
ACRFLCN	2.55	4.21	3.56	3.17	3.13
a-NPD	2.87	4.01	3.49	3.75	3.52
PXZ-TAZ	2.72	4.02	3.19	3.24	3.34
DPA-DPS	3.09	4.22	3.82	3.67	3.85
PXZ-OXD	2.50	3.80	3.30	3.02	3.16
DTC-DPS	3.07	4.34	3.54	3.80	4.39
CBP	3.4	4.47	3.76	3.93	4.80
CC2TA	2.63	4.34	3.12		4.19
DMAC-DPS	2.70	4.02	3.30	3.14	3.77
2PXZ-OXD	2.47	3.74	3.24	3.63	3.46
DTPA-DPS	2.96	4.19	3.45	3.66	3.78
NPh3	3.46	4.59	4.09	1.14	4.13
PhCz	3.43	4.48	4.23	4.43	4.43
4CzIPN	2.48	3.58	3.06	2.95	3.17
2PXZ-TAZ	2.68	4.08	3.17	3.83	3.30
PXZ-DPS	2.45	3.81	2.88	2.71	3.48
PPZ-4TPT	2.50	3.58	2.82	2.60	2.92
DMOC-DPS	2.79	4.09	3.31	3.53	4.08
PPZ-DPS	2.15	3.47	2.65	2.30	2.30
PXZ-TRZ	2.27	3.71	3.12	2.72	3.00
PPZ-DPO	2.15	3.49	2.93	2.53	2.53
PPZ-3TPT	2.35	3.58	2.93	2.75	2.92

Table A.15: E_{0-0} from LC-ωPBE functional in eV. The blanks in the Experimental column correspond to cases where data was unavailable, while the blanks in column C resulted from convergence failure in S_1 optimization. Protocol A has RMS error 1.04 eV and mean error 1.03 eV; Protocol B has RMS error 0.82 eV and mean error 0.81 eV; Protocol C has RMS error 0.70 eV and mean error 0.66 eV; and Protocol D has RMS error 1.09 eV and mean error 1.03 eV.

Compound	Expt.	Prot. A	Prot. B	Prot. C	Prot. D
2CzPN	2.94	3.98	3.74	3.54	3.43
4CzPN	2.60	3.65	3.51		3.10
4CzTPN-Me	2.33	3.45	3.07		2.87
4CzTPN	2.43	3.36	3.13		2.90
PIC-TRZ	2.91	4.13	4.09	3.51	2.99
ACRFLCN	2.83	4.21	3.90	3.46	3.13
a-NPD	3.10	4.01	3.76	4.15	3.52
PXZ-TAZ		4.02	3.79	3.57	3.34
DPA-DPS	3.28	4.22	4.04	4.40	3.85
PXZ-OXD		3.80	3.56	3.29	3.16
DTC-DPS	3.34	4.34	4.19	4.09	4.39
CBP	3.54	4.47	4.17	4.37	4.80
CC2TA	3.15	4.34	3.96		4.19
DMAC-DPS	3.00	4.02	3.74	3.53	3.77
2PXZ-OXD		3.74	3.49	3.90	3.46
DTPA-DPS	3.19	4.19	4.03	3.98	3.78
NPh3	3.60	4.59	4.58	4.16	4.13
PhCz	3.58	4.48	4.36	4.59	4.43
4CzIPN	2.63	3.58	3.42	3.31	3.17
2PXZ-TAZ		4.08	3.75	4.25	3.30
PXZ-DPS	2.73	3.81	3.44	3.19	3.48
PPZ-4TPT	2.80	3.58	3.44	3.15	2.92
DMOC-DPS	3.12	4.09	3.96	3.90	4.08
PPZ-DPS	2.40	3.47	3.12	2.78	2.30
PXZ-TRZ	2.53	3.71	3.42	3.03	3.00
PPZ-DPO	2.40	3.49	3.21	2.84	2.53
PPZ-3TPT	2.65	3.58	3.47	3.13	2.92

Table A.16: ΔE_{ST} from LC-ωPBE functional in meV. The blanks in the Experimental column correspond to cases where data was unavailable, while the blanks in column C resulted from convergence failure in S_1 optimization. Some of the calculated numbers were negative, and thus were excluded from the log error calculation. Protocol A has log RMS error is 0.76 and log mean error 0.71; Protocol B has log RMS error 0.74 and log mean error 0.69; Protocol C has log RMS error 0.58 and log mean error −0.06; and Protocol D has log RMS error 0.65 and log mean error 0.25.

Compound	Expt.	Prot. A	Prot. B	Prot. C	Prot. D
2CzPN	310	1187	1292	-9	349
4CzPN	150	990	696		764
4CzTPN-Me	90	774	442		392
4CzTPN	90	698	443		496
PIC-TRZ	180	1290	1703	25	79
ACRFLCN	240	1538	1673	438	690
a-NPD	730	1562	1242	1118	1176
PXZ-TAZ		1229	1272	459	850
DPA-DPS	520	1235	1321	1204	1087
PXZ-OXD		1003	1030	324	730
DTC-DPS	360	1297	902	617	1478
CBP	710	1386	1725	1145	2123
CC2TA	200	1305	1174		1232
DMAC-DPS	90	857	512	220	1067
2PXZ-OXD		934	698	958	1014
DTPA-DPS	460	1215	1318	577	808
NPh3	570	1432	1725	731	1200
PhCz	550	1396	1586	1053	1432
4CzIPN	100	879	976	346	688
2PXZ-TAZ		1235	1223	1142	805
PXZ-DPS	80	938	903	46	734
PPZ-4TPT	420	1040	1206	257	403
DMOC-DPS	240	1113	1305	559	1163
PPZ-DPS	90	917	883	2	6
PXZ-TRZ	60	910	900	-339	11
PPZ-DPO	90	947	974	7	7
PPZ-3TPT	270	1045	1244	252	408

Appendix B

Explicit derivation of photochemical $f_2(t_1, t_2)$ from populations

Under thermal initial conditions we have $f_2(t_1, t_2)$ defined to be:

$$f_2(t_1, t_2) = \mathbf{Tr}\left[e^{it_1\mathbf{h_1}}e^{-it_1\mathbf{h_2}}e^{it_2\mathbf{h_2}}e^{-it_2\mathbf{h_1}}\frac{e^{-\beta\mathbf{h_2}}}{\mathbf{Tr}\left[e^{-\beta\mathbf{h_2}}\right]}\right] \tag{B.1}$$

$$\mathbf{h_1} = -\frac{\epsilon}{2} + \sum_i \left(\frac{p_{x_i}^2}{2m_i} + \frac{1}{2}m_i\omega_i^2 x_i^2 + c_i x_i\right) \tag{B.2}$$

$$\mathbf{h_2} = \frac{\epsilon}{2} + \sum_i \left(\frac{p_{x_i}^2}{2m_i} + \frac{1}{2}m_i\omega_i^2 x_i^2 - c_i x_i\right) \tag{B.3}$$

Since all the modes are independent, we can first calculate the one mode trace (using the one-mode Hamiltonians defined by Eqns. 3.75 and 3.76), multiply them together and finally add in the energy bias.

We begin by calculating:

$$\mathbf{Tr}\left[e^{it_1\mathbf{h_1^i}}e^{-it_1\mathbf{h_2^i}}e^{it_2\mathbf{h_2^i}}e^{-it_2\mathbf{h_1^i}}e^{-\beta\mathbf{h_2^i}}\right] \tag{B.4}$$

$$= \int_{-\infty}^{\infty} dp_1 \int_{-\infty}^{\infty} dq_1 \left\langle p_1, q_1 | e^{it_1\mathbf{h_1^i}}e^{-it_1\mathbf{h_2^i}}e^{it_2\mathbf{h_2^i}}e^{-it_2\mathbf{h_1^i}}e^{-\beta\mathbf{h_2^i}} | p_1 q_1 \right\rangle \tag{B.5}$$

Using the coherent state basis $|p_1, q_1\rangle$-which is a coherent state of a harmonic oscillator (with mass m_i and frequency ω_i) hamiltonian with initial position q_1 and initial

momentum p_1. These form an overcomplete basis when p_1, q_1 span the whole of phase space.

We know from Tannor[94] that for a harmonic oscillator hamiltonian with mass m_i and frequency ω_i will have their position and momentum evolve with classical equations of motion. Specifically we have in the position representation:

$$\mathbf{h} = \frac{p^2}{2m_i} + \frac{1}{2}m_i\omega_i^2 x^2 + \kappa x = \frac{p^2}{2m_i} + \frac{1}{2}m_i\omega_i^2\left(x + \frac{\kappa}{m_i\omega_i^2}\right)^2 - \frac{\kappa^2}{2m_i\omega_i^2} \tag{B.6}$$

$$\implies \left\langle x_1|e^{-it\mathbf{h}}|p_1, q_1\right\rangle = e^{-\frac{m_i\omega_i}{2}(x_1-q_1(t))^2+ip_1(t)(x_1-q_1(t))+\frac{i}{2}\left(p_1(t)\left(q_1(t)+\frac{\kappa}{m_i\omega_i^2}\right)-p_1\left(q_1+\frac{\kappa}{m_i\omega_i^2}\right)\right)-it\frac{\kappa^2}{2m_i\omega_i^2}} \tag{B.7}$$

This is a gaussian in terms of x_1, p_1, q_1 and can thus be integrated over analytically. We may factorize the whole trace into products like this, having:

$$\mathbf{Tr}\left[e^{it_1\mathbf{h_1^i}}e^{-it_1\mathbf{h_2^i}}e^{it_2\mathbf{h_2^i}}e^{-it_2\mathbf{h_1^i}}e^{-\beta\mathbf{h_2^i}}\right] \tag{B.8}$$

$$= \int_{-\infty}^{\infty} dp_1 \int_{-\infty}^{\infty} dq_1 \left\langle p_1, q_1|e^{it_1\mathbf{h_1^i}}e^{-it_1\mathbf{h_2^i}}e^{it_2\mathbf{h_2^i}}e^{-it_2\mathbf{h_1^i}}e^{-\beta\mathbf{h_2}}|p_1q_1\right\rangle \tag{B.9}$$

$$= \int_{-\infty}^{\infty} dp_1 \int_{-\infty}^{\infty} dq_1 \int_{-\infty}^{\infty} dx_1 \int_{-\infty}^{\infty} dp_2 \int_{-\infty}^{\infty} dq_2 \int_{-\infty}^{\infty} dx_2$$

$$\left\langle p_1, q_1|e^{it_1\mathbf{h_1^i}}|x_1\right\rangle \left\langle x_1|e^{-i(t_1-t_2)\mathbf{h_2^i}}|p_2q_2\right\rangle \left\langle p_2q_2|e^{-it_2\mathbf{h_1^i}}|x_2\right\rangle \left\langle x_2|e^{-i(i\beta)\mathbf{h_2}}|p_1q_1\right\rangle \tag{B.10}$$

by treating $i\beta$ as a "time" as well. Eqn. B.7 then enables us to write down the argument of the integrand as a product of gaussians (which itself is a gaussian) in $x_1, x_2, p_1, p_2, p_3, p_4$ (as changing $\kappa \to \pm c_i$ gives us $\mathbf{h} = \mathbf{h^i_{\{1,2\}}}$). Integrating the gaussian via Mathematica, we analytically obtain:

$$\mathbf{Tr}\left[e^{it_1\mathbf{h_1^i}}e^{-it_1\mathbf{h_2^i}}e^{it_2\mathbf{h_2^i}}e^{-it_2\mathbf{h_1^i}}e^{-\beta\mathbf{h_2^i}}\right] \tag{B.11}$$

$$= \mathbf{Tr}\left[e^{-\beta\mathbf{h_2^i}}\right] e^{-\frac{2c_i^2}{m_i\omega_i^3}\left((1-\cos(\omega_i(t_1-t_2)))\coth\frac{\beta\omega_i}{2}+i\sin(\omega_i(t_1-t_2))-2i\sin\omega_i t_1+2i\sin\omega_i t_2\right)} \tag{B.12}$$

Therefore:

$$f_2(t_1,t_2) = \frac{\mathbf{Tr}\left[e^{it_1\mathbf{h_1}}e^{-it_1\mathbf{h_2}}e^{it_2\mathbf{h_2}}e^{-it_2\mathbf{h_1}}e^{-\beta\mathbf{h_2}}\right]}{\mathbf{Tr}\left[e^{-\beta\mathbf{h_2}}\right]} \tag{B.13}$$

$$= e^{-i\epsilon(t_1-t_2)}\frac{\prod_i \mathbf{Tr}\left[e^{it_1\mathbf{h_1^i}}e^{-it_1\mathbf{h_2^i}}e^{it_2\mathbf{h_2^i}}e^{-it_2\mathbf{h_1^i}}e^{-\beta\mathbf{h_2^i}}\right]}{\prod_i \mathbf{Tr}\left[e^{-\beta\mathbf{h_2^i}}\right]} \tag{B.14}$$

$$= e^{-i\epsilon(t_1-t_2)}\prod_i e^{-\frac{2c_i^2}{m_i\omega_i^3}\left((1-\cos(\omega_i(t_1-t_2)))\coth\frac{\beta\omega_i}{2}+i\sin(\omega_i(t_1-t_2))-2i\sin\omega_i t_1+2i\sin\omega_i t_2\right)} \tag{B.15}$$

$$= e^{-i\epsilon(t_1-t_2)}e^{-\sum_i \frac{2c_i^2}{m_i\omega_i^3}\left((1-\cos(\omega_i(t_1-t_2)))\coth\frac{\beta\omega}{2}+i\sin(\omega_i(t_1-t_2))-2i\sin\omega_i t_1+2i\sin\omega_i t_2\right)} \tag{B.16}$$

$$= e^{-i\epsilon(t_1-t_2)}e^{-\frac{4}{\pi}\int_0^\infty \frac{J(\omega)}{\omega^2}\left((1-\cos(\omega(t_1-t_2)))\coth\frac{\beta\omega}{2}+i\sin(\omega(t_1-t_2))-2i\sin\omega t_1+2i\sin\omega t_2\right)} \tag{B.17}$$

$$= e^{-i\epsilon(t_1-t_2)-Q'(t_1-t_2)-iQ''(t_1-t_2)+2iQ''(t_1)-2iQ''(t_2)} \tag{B.18}$$

which is what we found earlier. This same procedure could be in principle generalized to find higher order traces, but Eqn. 3.61 already does that for us.

Appendix C

Marcus Theory from Spin-Boson Model

For electron-transfer in outer-sphere complexes we have V sufficiently small that NIBA is adequate. Therefore we may assume that $K(t) \approx K^{(2)}(t)$.

We have from 3.118 that

$$\ln f_2(t_1, t_2) = -a(t_1 - t_2)^2 - i(\lambda + \epsilon)(t_1 - t_2) \tag{C.1}$$

$$a \equiv \frac{2}{\pi} \int_0^\infty J(\omega) \coth \frac{\beta\omega}{2} d\omega = \frac{4}{\pi\beta} \int_0^\infty \frac{J(\omega)}{\omega} d\omega = \frac{\lambda}{\beta} \tag{C.2}$$

$$f_2(t_1, t_2) = e^{-\frac{\lambda}{\beta}(t_1 - t_2)^2 - i(\lambda+\epsilon)(t_1 - t_2)} \tag{C.3}$$

at high-temperature ($\beta\omega \lll 1$). We thus have:

$$K(t) = K^{(2)}(t) = 2V^2 \mathbf{Re}\left[f_2(t, 0)\right] = 2V^2 e^{-\frac{\lambda}{\beta}t^2} \cos\left((\lambda + \epsilon)t\right) \tag{C.4}$$

Integrating we get the rate constant

$$k = \int_0^t K(t)dt = 2V^2 \int_0^\infty e^{-\frac{\lambda}{\beta}t^2} \cos\left((\lambda + \epsilon)t\right) = V^2 \sqrt{\frac{\pi\beta}{\lambda}} e^{-\frac{\beta(\epsilon+\lambda)^2}{4\lambda}} \tag{C.5}$$

which is the Marcus rate-law!

Appendix D

Explicit derivation of thermal $K^{(4)}(t)$ from populations

$F_4(t_1, t_2, t_3, t_4)$ and $F_2(t_1, t_2)$ exhibit time-translation invariance due to thermal starting conditions, allowing us to obtain an unique one time index kernel. However, this derivation is slightly more involved than the arguments by analogy used for the two time index photochemical kernel, and thus we choose to describe this derivation exactly. $K^{(2)}(t)$ is trivial and $K^{(6)}$ onwards can be found similarly to this, making it a perfect example.

We have from Eqn. 3.99 that:

$$\dot{p}_1^{(4)}(t) = 2\mathbf{Re}\left[\int_0^t dt_1 \int_0^{t_1} dt_2 \int_0^{t_2} dt_3 F_4(t, t_1, t_2, t_3) + \int_0^t dt_1 \int_0^t dt_2 \int_0^{t_2} dt_3 F_4(t_1, t, t_2, t_3)\right] \tag{D.1}$$

$$= 2\mathbf{Re}\left[\int_0^t dt_1 \int_0^{t_1} dt_2 \int_0^{t_2} dt_3 F_4(0, t_1 - t, t_2 - t, t_3 - t) + \int_0^t dt_1 \int_0^t dt_2 \int_0^{t_2} dt_3 F_4(t_1 - t, 0, t_2 - t, t_3 - t)\right] \tag{D.2}$$

from time translation invariance. Therefore we can differentiate to obtain:

$$\therefore \ddot{p}^{(4)}(t) = 2\frac{d}{dt}\mathbf{Re}\left[\int_0^t dt_1 \int_0^{t_1} dt_2 \int_0^{t_2} dt_3 F_4(0, t_1 - t, t_2 - t, t_3 - t) + \int_0^t dt_1 \int_0^t dt_2 \int_0^{t_2} dt_3 F_4(t_1 - t, 0, t_2 - t, t_3 - t)\right] \tag{D.3}$$

We can simplify piecewise in the following manner:

$$\frac{d}{dt}\int_0^t dt_1 \int_0^{t_1} dt_2 \int_0^{t_2} dt_3 F_4(0, t_1 - t, t_2 - t, t_3 - t) \tag{D.4}$$

$$= \int_0^t dt_2 \int_0^{t_2} dt_3 F_4(0, 0, t_2 - t, t_3 - t) - \int_0^t dt_1 \int_0^{t_1} dt_2 \int_0^{t_2} dt_3 \frac{d}{dt_1} F_4(0, t_1 - t, t_2 - t, t_3 - t)$$
$$- \int_0^t dt_1 \int_0^{t_1} dt_2 \int_0^{t_2} dt_3 \frac{d}{dt_2} F_4(0, t_1 - t, t_2 - t, t_3 - t)$$
$$- \int_0^t dt_1 \int_0^{t_1} dt_2 \int_0^{t_2} dt_3 \frac{d}{dt_3} F_4(0, t_1 - t, t_2 - t, t_3 - t) \tag{D.5}$$

$$\int_0^t dt_1 \int_0^{t_1} dt_2 \int_0^{t_2} dt_3 \frac{d}{dt_3} F_4(0, t_1 - t, t_2 - t, t_3 - t)$$

$$= \int_0^t dt_1 \int_0^{t_1} dt_2 F_4(0, t_1 - t, t_2 - t, t_2 - t) - \int_0^t dt_1 \int_0^{t_1} dt_2 F_4(0, t_1 - t, t_2 - t, -t) \tag{D.6}$$

$$\int_0^t dt_1 \int_0^{t_1} dt_2 \int_0^{t_2} dt_3 \frac{d}{dt_2} F_4(0, t_1 - t, t_2 - t, t_3 - t) \tag{D.7}$$

$$= \int_0^t dt_1 \int_0^{t_1} dt_3 \int_{t_3}^{t_1} dt_2 \frac{d}{dt_2} F_4(0, t_1 - t, t_2 - t, t_3 - t) \text{ (Integration limits switched)}$$

(D.8)

$$= \int_0^t dt_1 \int_0^{t_1} dt_3 \left(F_4(0, t_1 - t, t_1 - t, t_3 - t) - F_4(0, t_1 - t, t_3 - t, t_3 - t)\right) \tag{D.9}$$

Similarly:

$$\int_0^t dt_1 \int_0^{t_1} dt_2 \int_0^{t_2} dt_3 \frac{d}{dt_1} F_4(0, t_1 - t, t_2 - t, t_3 - t) \tag{D.10}$$

$$= \int_0^t dt_3 \int_{t_3}^t dt_2 \int_{t_2}^t dt_1 \frac{d}{dt_1} F_4(0, t_1 - t, t_2 - t, t_3 - t) \tag{D.11}$$

$$= \int_0^t dt_3 \int_{t_3}^t dt_2 \left(F_4(0, 0, t_2 - t, t_3 - t) - F_4(0, t_2 - t, t_2 - t, t_3 - t)\right) \tag{D.12}$$

Adding Eqns. D.6, D.9 and D.12 we have:

$$\begin{aligned}
&\int_0^t dt_1 \int_0^{t_1} dt_2 \left(F_4(0, t_1 - t, t_2 - t, t_2 - t) - F_4(0, t_1 - t, t_2 - t, -t)\right) \\
&+ \int_0^t dt_1 \int_0^{t_1} dt_3 \left(F_4(0, t_1 - t, t_1 - t, t_3 - t) - F_4(0, t_1 - t, t_3 - t, t_3 - t)\right) \\
&+ \int_0^t dt_3 \int_{t_3}^t dt_2 \left(F_4(0, 0, t_2 - t, t_3 - t) - F_4(0, t_2 - t, t_2 - t, t_3 - t)\right) \qquad \text{(D.13)} \\
&= \int_0^t dt_1 \int_0^{t_1} dt_2 \left(F_4(0, t_1 - t, t_2 - t, t_2 - t) - F_4(0, t_1 - t, t_2 - t, -t)\right. \\
&\quad \left. + F_4(0, t_1 - t, t_1 - t, t_2 - t) - F_4(0, t_1 - t, t_2 - t, t_2 - t)\right) \\
&\quad + \int_0^t dt_2 \int_0^{t_2} dt_3 \left(F_4(0, 0, t_2 - t, t_3 - t) - F_4(0, t_2 - t, t_2 - t, t_3 - t)\right) \qquad \text{(D.14)} \\
&= \int_0^t dt_1 \int_0^{t_1} dt_2 \left(F_4(0, 0, t_1 - t, t_2 - t)\right) - F_4(0, t_1 - t, t_2 - t, -t)) \qquad \text{(D.15)}
\end{aligned}$$

by reorganizing the dummy time indices and reswitching integration limits. Therefore,

we have:

$$\frac{d}{dt}\int_0^t dt_1 \int_0^{t_1} dt_2 \int_0^{t_2} dt_3 F_4(0, t_1 - t, t_2 - t, t_3 - t) = \int_0^t dt_1 \int_0^{t_1} F_4(0, t_1 - t, t_2 - t, -t) dt_2 \tag{D.16}$$

by inserting Eqn. D.15 into Eqn. D.5.

Next we proceed to attack the other term and have:

$$\frac{d}{dt}\int_0^t dt_1 \int_0^t dt_2 \int_0^{t_2} dt_3 F_4(t_1 - t, 0, t_2 - t, t_3 - t) \tag{D.17}$$

$$= \int_0^t dt_2 \int_0^{t_2} dt_3 F_4(0, 0, t_2 - t, t_3 - t) + \int_0^t dt_1 \int_0^t dt_3 F_4(t_1 - t, 0, 0, t_3 - t)$$

$$+ \int_0^t dt_1 \int_0^t dt_2 \int_0^{t_2} dt_3 \frac{d}{dt} F_4(t_1 - t, 0, t_2 - t, t_3 - t) \tag{D.18}$$

where

$$\int_0^t dt_1 \int_0^t dt_2 \int_0^{t_2} dt_3 \frac{d}{dt} F_4(t_1 - t, 0, t_2 - t, t_3 - t) \tag{D.19}$$

$$= -\int_0^t dt_1 \int_0^t dt_2 \int_0^{t_2} dt_3 \left(\frac{d}{dt_1} F_4(t_1 - t, 0, t_2 - t, t_3 - t) + \frac{d}{dt_2} F_4(t_1 - t, 0, t_2 - t, t_3 - t) \right)$$

$$- \int_0^t dt_1 \int_0^t dt_2 \int_0^{t_2} dt_3 \frac{d}{dt_3} F_4(t_1 - t, 0, t_2 - t, t_3 - t) \tag{D.20}$$

Thus:

$$\int_0^t dt_1 \int_0^t dt_2 \int_0^{t_2} dt_3 \frac{d}{dt_3} F_4(t_1 - t, 0, t_2 - t, t_3 - t) \tag{D.21}$$

$$= \int_0^t dt_1 \int_0^t dt_2 \left(F_4(t_1 - t, 0, t_2 - t, t_2 - t) - F_4(t_1 - t, 0, t_2 - t, -t) \right) \tag{D.22}$$

$$\int_0^t dt_1 \int_0^t dt_2 \int_0^{t_2} dt_3 \frac{d}{dt_1} F_4(t_1 - t, 0, t_2 - t, t_3 - t) \tag{D.23}$$

$$= \int_0^t dt_2 \int_0^{t_2} dt_3 \left(F_4(0, 0, t_2 - t, t_3 - t) - F_4(-t, 0, t_2 - t, t_3 - t)\right) \tag{D.24}$$

$$= \int_0^t dt_1 \int_0^{t_1} dt_2 \left(F_4(0, 0, t_1 - t, t_2 - t) - F_4(-t, 0, t_1 - t, t_2 - t)\right) \tag{D.25}$$

$$\int_0^t dt_1 \int_0^t dt_2 \int_0^{t_2} dt_3 \frac{d}{dt_2} F_4(t_1 - t, 0, t_2 - t, t_3 - t) \tag{D.26}$$

$$= \int_0^t dt_1 \int_0^t dt_3 \int_{t_3}^t dt_2 \frac{d}{dt_2} F_4(t_1 - t, 0, t_2 - t, t_3 - t) \tag{D.27}$$

$$= \int_0^t dt_1 \int_0^t dt_3 \left(F_4(t_1 - t, 0, 0, t_3 - t) - F_4(t_1 - t, 0, t_3 - t, t_3 - t)\right) \tag{D.28}$$

Combining we have:

$$-\int_0^t dt_1 \int_0^t dt_2 \int_0^{t_2} dt_3 \frac{d}{dt} F_4(t_1 - t, 0, t_2 - t, t_3 - t) \tag{D.29}$$

$$= \int_0^t dt_1 \int_0^{t_1} dt_2 \left(F_4(0, 0, t_1 - t, t_2 - t) - F_4(-t, 0, t_1 - t, t_2 - t)\right)$$

$$+ \int_0^t dt_1 \int_0^t dt_2 \left(F_4(t_1 - t, 0, 0, t_2 - t) - F_4(t_1 - t, 0, t_2 - t, -t)\right) \tag{D.30}$$

Therefore from Eqns. D.18 and D.30:

$$\frac{d}{dt} \int_0^t dt_1 \int_0^t dt_2 \int_0^{t_2} dt_3 F_4(t_1 - t, 0, t_2 - t, t_3 - t) \tag{D.31}$$

$$= \int_0^t dt_1 \int_0^{t_1} dt_2 F_4(-t, 0, t_1 - t, t_2 - t) + \int_0^t dt_1 \int_0^t dt_2 F_4(t_1 - t, 0, t_2 - t, -t) \tag{D.32}$$

The total expression is:

$$\ddot{p}_1^{(4)}(t) = 2\mathbf{Re}\left[\int_0^t dt_1 \int_0^{t_1} dt_2 \left(F_4(0, t_1 - t, t_2 - t, -t) + F_4(-t, 0, t_1 - t, t_2 - t)\right)\right.$$
$$\left. + \int_0^t dt_1 \int_0^t dt_2 F_4(t_1 - t, 0, t_2 - t, -t)\right] \tag{D.33}$$
$$= 2\mathbf{Re}\left[\int_0^t dt_1 \int_0^{t_1} dt_2 \left(F_4(t, t_1, t_2, 0) + F_4(0, t, t_1, t_2)\right) + \int_0^t dt_1 \int_0^t dt_2 F_4(t_1, t, t_2, 0)\right] \tag{D.34}$$

from time-translation invariance.

Therefore we have from Eqn. 3.114:

$$K_{11}^{(4)}(t) = -\ddot{p}_1^{(4)}(t) - \int_0^t K_+^{(2)}(t - t_1)\dot{p}_1^{(2)}(t_1)dt_1 \tag{D.35}$$
$$= -2\mathbf{Re}\left[\int_0^t dt_1 \int_0^{t_1} \left(F_4(t, t_1, t_2, 0) + F_4(0, t, t_1, t_2)\right) dt_2 + \int_0^t dt_1 \int_0^t F_4(t_1, t, t_2, 0) dt_2\right]$$
$$- \int_0^t K_+^{(2)}(t - t_1)\dot{p}_1^{(2)}(t_1)dt_1 \tag{D.36}$$

Bibliography

[1] Huang, S.; Zhang, Q.; Shiota, Y.; Nakagawa, T.; Kuwabara, K.; Yoshizawa, K.; Adachi, C. *J. Chem. Theory Comput.* **2013**, *9*, 3872–3877.

[2] Lee, J.; Shizu, K.; Tanaka, H.; Nomura, H.; Yasuda, T.; Adachi, C. *J. Mater. Chem. C* **2013**, *1*, 4599–4604.

[3] Zhang, Q.; Li, B.; Huang, S.; Nomura, H.; Tanaka, H.; Adachi, C. *Nature Photon.* **2014**, *8*, 326–332.

[4] Wu, S.; Aonuma, M.; Zhang, Q.; Huang, S.; Nakagawa, T.; Kuwabara, K.; Adachi, C. *J. Mater. Chem. C* **2014**, *2*, 421–424.

[5] Mavros, M. G.; Hait, D.; Van Voorhis, T. *J. Chem. Phys.* Submitted.

[6] Dirac, P. A. Quantum mechanics of many-electron systems. Proc. R. Soc. A. 1929; pp 714–733.

[7] Knowles, P.; Handy, N. *Chem. Phys. Lett.* **1984**, *111*, 315–321.

[8] Szabo, A.; Ostlund, N. S. *Modern Quantum Chemistry: Introduction to Advanced Electronic Structure Theory*; Dover Publications, Inc.: Mineola, New York, 1996; pp 286–296.

[9] Hohenberg, P.; Kohn, W. *Phys. Rev.* **1964**, *136*, B864–871.

[10] Kohn, W.; Sham, L. J. *Phys. Rev.* **1965**, *140*, A1133–1138.

[11] Runge, E.; Gross, E. K. U. *Phys. Rev. Lett.* **1984**, *52*, 997–1000.

[12] Dreuw, A.; Weisman, J. L.; Head-Gordon, M. *J. Chem. Phys.* **2003**, *119*, 2943–2946.

[13] Sobolewski, A. L.; Domcke, W. *Chem. Phys.* **2003**, *294*, 73 – 83.

[14] Dreuw, A.; Fleming, G. R.; Head-Gordon, M. *Phys. Chem. Chem. Phys.* **2003**, *5*, 3247–3256.

[15] Ziegler, T.; Rauk, A.; Baerends, E. *Theor. Chim. Acta* **1977**, *43*, 261–271.

[16] Kowalczyk, T.; Tsuchimochi, T.; Chen, P. T.; Top, L.; Van Voorhis, T. *J. Chem. Phys.* **2013**, *138*, 164101.

[17] Caldeira, A.; Leggett, A. *Ann. Phys.* **1983**, *149*, 374 – 456.

[18] Marcus, R. A. *J. Chem. Phys.* **1956**, *24*, 966–978.

[19] Von Neumann, J.; Wigner, E. *Z. Phys* **1929**, *30*, 467–470.

[20] Yamamoto, T.; Zhou, Z. H.; Kanbara, T.; Shimura, M.; Kizu, K.; Maruyama, T.; Nakamura, Y.; Fukuda, T.; Lee, B. L.; Ooba, N.; Tomaru, S.; Kurihara, T.; Kaino, T.; Kubota, K.; Sasaki, S. *J. Am. Chem. Soc.* **1996**, *118*, 10389–10399.

[21] Lima, I. T.; Risko, C.; Aziz, S. G.; da Silva Filho, D. A.; Brédas, J.-L. *J. Mater. Chem. C* **2014**, *2*, 8873–8879.

[22] Brédas, J. L. *Science* **1994**, *263*, 487–488.

[23] Yu, G.; Gao, J.; Hummelen, J. C.; Wudl, F.; Heeger, A. J. *Science* **1995**, *270*, 1789–1791.

[24] Tseng, H. R.; Ying, L.; Hsu, B. B. Y.; Perez, L. A.; Takacs, C. J.; Bazan, G. C.; Heeger, A. J. *Nano Lett.* **2012**, *12*, 6353–6357.

[25] Köhler, A.; Bässler, H. *Mater. Sci. Eng. R-Rep.* **2009**, *66*, 71 – 109.

[26] Méhes, G.; Nomura, H.; Zhang, Q.; Nakagawa, T.; Adachi, C. *Angew. Chem. Int. Ed.* **2012**, *51*, 11311–11315.

[27] Uoyama, H.; Goushi, K.; Shizu, K.; Nomura, H.; Adachi, C. *Nature* **2012**, *492*, 234–238.

[28] Tanaka, H.; Shizu, K.; Miyazaki, H.; Adachi, C. *Chem. Commun.* **2012**, *48*, 11392–11394.

[29] Penfold, T. J. *J. Phys. Chem. C* **2015**, *119*, 13535–13544.

[30] Sun, H.; Zhong, C.; Brédas, J. L. *J. Chem. Theory Comput.* **2015**, *11*, 3851–3858.

[31] Parker, C. A.; Hatchard, C. G. *Trans. Faraday Soc.* **1961**, *57*, 1894–1904.

[32] Valeur, B. *Molecular Fluorescence: Principles and Applications*; Wiley-VCH Verlag GmbH: Weinheim, 2001; Chapter 3, p 41.

[33] Endo, A.; Ogasawara, M.; Takahashi, A.; Yokoyama, D.; Kato, Y.; Adachi, C. *Adv. Mater.* **2009**, *21*, 4802–4806.

[34] Endo, A.; Sato, K.; Yoshimura, K.; Kai, T.; Kawada, A.; Miyazaki, H.; Adachi, C. *Appl. Phys. Lett.* **2011**, *98*, 083302.

[35] Zhang, Q.; Li, J.; Shizu, K.; Huang, S.; Hirata, S.; Miyazaki, H.; Adachi, C. *J. Am. Chem. Soc.* **2012**, *134*, 14706–14709.

[36] Nakagawa, T.; Ku, S. Y.; Wong, K. T.; Adachi, C. *Chem. Commun.* **2012**, *48*, 9580–9582.

[37] Lee, S. Y.; Yasuda, T.; Nomura, H.; Adachi, C. *Appl. Phys. Lett.* **2012**, *101*, 093306.

[38] Hachmann, J.; Olivares-Amaya, R.; Atahan-Evrenk, S.; Amador-Bedolla, C.; Sánchez-Carrera, R. S.; Gold-Parker, A.; Vogt, L.; Brockway, A. M.; Aspuru-Guzik, A. *J. Phys. Chem. Lett.* **2011**, *2*, 2241–2251.

[39] Baumeier, B.; May, F.; Lennartz, C.; Andrienko, D. *J. Mater. Chem.* **2012**, *22*, 10971–10976.

[40] Andersson, K.; Malmqvist, P. Å.; Roos, B. O.; Sadlej, A. J.; Wolinski, K. *J. Phys. Chem.* **1990**, *94*, 5483–5488.

[41] Andersson, K.; Malmqvist, P. Å.; Roos, B. O. *J. Chem. Phys.* **1992**, *96*, 1218–1226.

[42] Schreiber, M.; Silva-Junior, M. R.; Sauer, S. P. A.; Thiel, W. *J. Chem. Phys.* **2008**, *128*, 134110.

[43] Kánnár, D.; Szalay, P. G. *J. Chem. Theory Comput.* **2014**, *10*, 3757–3765.

[44] Parr, R. G.; Yang, W. *Density-functional theory of atoms and molecules*; Oxford university press: New York, 1989.

[45] Marques, M.; Gross, E. *Annu. Rev. Phys. Chem.* **2004**, *55*, 427–455.

[46] Becke, A. D. *J. Chem. Phys.* **1993**, *98*, 5648–5652.

[47] Perdew, J. P.; Ernzerhof, M.; Burke, K. *J. Chem. Phys.* **1996**, *105*, 9982–9985.

[48] Dreuw, A.; Head-Gordon, M. *Chem. Rev.* **2005**, *105*, 4009–4037.

[49] Stein, T.; Kronik, L.; Baer, R. *J. Am. Chem. Soc.* **2009**, *131*, 2818–2820.

[50] Salzner, U.; Aydin, A. *J. Chem. Theory Comput.* **2011**, *7*, 2568–2583.

[51] Yanai, T.; Tew, D. P.; Handy, N. C. *Chem. Phys. Lett.* **2004**, *393*, 51 – 57.

[52] Vydrov, O. A.; Heyd, J.; Krukau, A. V.; Scuseria, G. E. *J. Chem. Phys.* **2006**, *125*, 074106.

[53] Körzdörfer, T.; Sears, J. S.; Sutton, C.; Brédas, J. L. *J. Chem. Phys.* **2011**, *135*, 204107.

[54] Sun, H.; Autschbach, J. *J. Chem. Theory Comput.* **2014**, *10*, 1035–1047.

[55] Baer, R.; Livshits, E.; Salzner, U. *Annu. Rev. Phys. Chem.* **2010**, *61*, 85–109.

[56] Frank, I.; Hutter, J.; Marx, D.; Parrinello, M. *J. Chem. Phys.* **1998**, *108*, 4060–4069.

[57] Okazaki, I.; Sato, F.; Yoshihiro, T.; Ueno, T.; Kashiwagi, H. *J. Mol. Struc. : THEOCHEM* **1998**, *451*, 109 – 119.

[58] Filatov, M.; Shaik, S. *Chem. Phys. Lett.* **1999**, *304*, 429 – 437.

[59] Shao, Y. et al. *Mol. Phys.* **2015**, *113*, 184–215.

[60] Perdew, J. P.; Burke, K.; Ernzerhof, M. *Phys. Rev. Lett.* **1996**, *77*, 3865–3868.

[61] Hariharan, P.; Pople, J. *Theor. Chim. Acta* **1973**, *28*, 213–222.

[62] Dunning, T. H. *J. Chem. Phys.* **1989**, *90*, 1007–1023.

[63] Tamm, I. *J. Phys. (U.S.S.R.)* **1945**, *9*, 449.

[64] Dancoff, S. *Phys. Rev.* **1950**, *78*, 382.

[65] Hirata, S.; Head-Gordon, M. *Chem. Phys. Lett.* **1999**, *314*, 291–299.

[66] Kaduk, B.; Kowalczyk, T.; Van Voorhis, T. *Chem. Rev.* **2012**, *112*, 321–370.

[67] Haynes, W. M., Ed. *CRC Handbook of Chemistry and Physics*; CRC press: Boca Raton, Florida, 2013.

[68] Canuel, C.; Mons, M.; Piuzzi, F.; Tardivel, B.; Dimicoli, I.; Elhanine, M. *J. Chem. Phys.* **2005**, *122*.

[69] Matsika, S. *J. Phy. Chem. A* **2004**, *108*, 7584–7590.

[70] Marcus, R. A. *J. Chem. Phys.* **1965**, *43*, 679–701.

[71] Marcus, R. A. *Angew. Chem. Int. Ed. (English)* **1993**, *32*, 1111–1121.

[72] Barbara, P. F.; Meyer, T. J.; Ratner, M. A. *J. Phys. Chem.* **1996**, *100*, 13148–13168.

[73] Newton, M. D.; Sutin, N. *Annu.l Rev. Phys. Chem.* **1984**, *35*, 437–480.

[74] Car, R.; Parrinello, M. *Phys. Rev. Lett.* **1985**, *55*, 2471–2474.

[75] Tully, J. C. *J. Chem. Phys.* **1990**, *93*.

[76] Landry, B. R.; Subotnik, J. E. *The Journal of chemical physics* **2011**, *135*, 191101.

[77] Domcke, W.; Yarkony, D. R. *Annu. Rev. Phys.* **2012**, *63*, 325–352.

[78] Borrelli, R.; Peluso, A. *J. Chem. Theory Comput.* **2015**, *11*, 415–422.

[79] Izmaylov, A. F.; Mendive-Tapia, D.; Bearpark, M. J.; Robb, M. A.; Tully, J. C.; Frisch, M. J. *J. Chem. Phys.* **2011**, *135*, 234106.

[80] Domcke, W.; Yarkony, D. R.; Köppel, H. *Conical intersections: theory, computation and experiment*; World Scientific, 2011; Vol. 17.

[81] Ishizaki, A.; Tanimura, Y. *J. Phys. Soc. Jpn.* **2005**, *74*, 3131–3134.

[82] Tanimura, Y. *J. Phys. Soc. Jpn.* **2006**, *75*, 082001.

[83] Chakravarty, S.; Leggett, A. J. *Phys. Rev. Lett.* **1984**, *52*, 5.

[84] Leggett, A. J.; Chakravarty, S.; Dorsey, A.; Fisher, M. P.; Garg, A.; Zwerger, W. *Rev. Mod. Phys.* **1987**, *59*, 1.

[85] Mavros, M. G.; Van Voorhis, T. *The Journal of Chemical Physics* **2014**, *141*.

[86] Gong, Z.; Tang, Z.; Mukamel, S.; Cao, J.; Wu, J. *J. Chem. Phys.* **2015**, *142*.

[87] Chen, H.-T.; Berkelbach, T. C.; Reichman, D. R. *J. Chem. Phys.* **2016**, *144*.

[88] Florean, A. C.; Cardoza, D.; White, J. L.; Lanyi, J.; Sension, R. J.; Bucksbaum, P. H. *Proc. Natl. Acad. Sci. USA* **2009**, *106*, 10896–10900.

[89] Polli, D.; Altoè, P.; Weingart, O.; Spillane, K. M.; Manzoni, C.; Brida, D.; Tomasello, G.; Orlandi, G.; Kukura, P.; Mathies, R. A.; Garavelli, M.; Cerullo, G. *Nature* **2010**, *467*, 440–443.

[90] Bernardi, F.; Olivucci, M.; Robb, M. A. *Chem. Soc. Rev.* **1996**, *25*, 321–328.

[91] Brédas, J.-L.; Norton, J. E.; Cornil, J.; Coropceanu, V. *Accounts Chem. Res.* **2009**, *42*, 1691–1699.

[92] Nitzan, A. *Chemical Dynamics in Condensed Phases: Relaxation, Transfer and Reactions in Condensed Molecular Systems: Relaxation, Transfer and Reactions in Condensed Molecular Systems*; OUP Oxford, 2006.

[93] Heller, E. J. *J. Chem. Phys.* **1981**, *75*, 2923–2931.

[94] Tannor, D. J. *Introduction to Quantum Mechanics: A Time-Dependent Perspective*; University Science Books, 2007.

[95] Sparpaglione, M.; Mukamel, S. *J. Chem. Phys.* **1988**, *88*, 3263–3280.

[96] Nakajima, S. *Progr. Theor. Exp. Phys.* **1958**, *20*, 948–959.

[97] Zwanzig, R. *J. Chem. Phys.* **1960**, *33*, 1338–1341.

[98] Zwanzig, R. *Phys. Rev.* **1961**, *124*, 983.

[99] Zwanzig, R. *Physica* **1964**, *30*, 1109–1123.

[100] Hess, B.; Kutzner, C.; Van Der Spoel, D.; Lindahl, E. *J. Chem. Theory Comput.* **2008**, *4*, 435–447.

[101] Erdélyi, A.; Bateman, H. *Tables of Integral Transforms: Based in Part on Notes Left by Harry Bateman and Compiled by the Staff of the Bateman Manuscript Project*; McGraw-Hill, 1954.

[102] Strümpfer, J.; Schulten, K. *J. Chem. Theory Comput.* **2012**, *8*, 2808–2816.

[103] Johnson, S. Faddeeva Package. 2012.

[104] Gough, B. *GNU scientific library reference manual*; Network Theory Ltd., 2009.

[105] Piessens, R.; de Doncker-Kapenga, E.; Überhuber, C. W.; Kahaner, D. K. *Quadpack: a subroutine package for automatic integration*; Springer Science & Business Media, 2012; Vol. 1.